Master's thesis

NTNU
Norwegian University of Science and Technology
Faculty of Natural Sciences
Department of Physics

Alexander Edin Varegg

A Study of Chemical Potential Influenced by Parametric Pumping of Antiferromagnetic Magnons

Master's thesis in Applied Physics and Mathematics
Supervisor: Arne Bratass & Roberto E. Troncoso
July 2019

NTNU
Norwegian University of
Science and Technology

Alexander Edin Varegg

A Study of Chemical Potential Influenced by Parametric Pumping of Antiferromagnetic Magnons

Master's thesis in Applied Physics and Mathematics
Supervisor: Arne Bratass & Roberto E. Troncoso
July 2019

Norwegian University of Science and Technology
Faculty of Natural Sciences
Department of Physics

NTNU
Norwegian University of
Science and Technology

Abstract

A flourishing research field of late concerns Bose-Einstein condensation (BEC) of magnons in antiferromagnets. One promising technique of manipulating magnon excitation is parametric parallel pumping (PPP). By applying a sufficiently large oscillating magnetic field in parallel to the static magnetization, one allows for mode- and frequency-selective amplification of spin waves. In this thesis we study the influence of PPP on the chemical potential of a coupled system of condensate- and thermal antiferromagnetic magnons modelled by a generalized Gross-Pitaevskii equation and the Boltzmann equation.

We examine the theoretical framework of a hard-axis collinear antiferromagnet, while treating the Zeeman coupling from the parametric pumping as a perturbation. We diagonalize a Hamiltonian with exchange interaction, out-of-plane and in-plane magnetocrystalline anisotropies and a time-independent Zeeman coupling. The dispersion relation is plotted, examined in the center of the Brillouin zone and compared to the known frequencies of the hard-axis antiferromagnet Nickel Oxide. The physical nature of the effect of PPP is discussed and by using the Heisenberg equation, an equation of motion is derived describing the growth of thermal magnons due to PPP. In the two-fluid model, we describe the condensate magnons by the Gross-Pitaevskii (GP) equation for the Bose macroscopic wavefunction, which accounts for collisions with thermal magnons and assumes Gilbert damping as the only relaxation mechanism. We write the generalized GP on a hydrodynamic form, rendering the equations of motion for the condensate density and velocity. To describe the thermal cloud we derive a quantum kinetic equation for the thermal magnons, a.k.a. the Boltzmann equation for a single-particle local equilibrium Bose distribution function. The contributions in the Boltzmann equation describes the coupling with the phonon bath, the PPP and the contribution from magnon collisions. By assuming zero condensate velocity and a high temperature in a constant and homogeneous system, we develop an equation of motion for the thermal density.

In the steady state limit we combine the equations of motion to express the pumping field amplitude and the chemical potential as functions of the condensate density. Without pertaining to a specific material, a set of general magnitudes for the variables based on prior experimental measurements is used to illustrate the behaviour of the chemical potential. Due to the default magnitudes yielding a zero-valued thermal density and pumping of magnons exclusively in the center of the Brillouin zone, a discussion is held regarding the analytical consistency of the chosen parameter magnitudes. Finally, we evaluate the derivation of the thermal density in order to provide more insight in future studies of the chemical potential.

Sammendrag

Et blomstrende forskningsfelt i nyere tid omfatter Bose-Einstein kondensasjon (BEC) av magnoner i antiferromagneter. En lovende metode for å manipulere eksitasjon av magnoner er parametrisk parallell pumping (PPP). Ved å påføre et tilstrekkelig sterkt oscillerende magnetisk felt parallelt den statiske magnetiseringen, tillater man modus- og frekvens-selektiv oppfostring av spinnbølger. I denne avhandlingen studerer vi hvordan PPP påvirker det kjemiske potensialet i et koblet system av antiferromagnetiske kondensat- og termiske magnoner modellert av en generalisert 'Gross-Pitaevskii'-ligning og Boltzmann-ligningen.

Vi undersøker det teoretiske rammeverket for en hard-akset kollinær antiferomagnet, hvor Zeeman-koblingen fra den parametriske pumpingen behandles som en perturbasjon. Vi diagonaliser en Hamiltonian med vesklings-interaksjon, megnetokrystallinske anisotropier både i og ut av baseplanet, og en tidsuavhengig Zeeman-kobling. Dispersjonsrelasjonen plottes, undersøkes i sentrum av Brillouin-sonen, og sammenlignes med kjente frekvenser av den hard-aksede antiferromagneten nikkeloksid. Den fysiske naturen av effekten av PPP diskuteres, og ved å bruke Heisenberg-ligningen utledes en bevegelsesligning som beskriver veksten av termiske magnoner forårsaket av PPP. I modellen for to fluidum beskriver vi kondensat-magnoner ved 'Gross-Pitaevskii'-ligningen (GP) for den makroskopiske Bose-bølgefunksjonen som tar høyde for kollisjoner med termiske magnoner og antar Gilbert-demping som den eneste relaksasjonsmekanismen. Vi skriver den generaliserte GP-en på en hydrodynamisk form som tilsvarer bevgelsesligningene for tettheten av kondensat-magnoner og kondensat-hastigheten. For å beskrive den termiske skyen utleder vi en kvantemekanisk kinetisk ligning for de termiske magnonene, m.a.o. Boltzmann-ligningen for en enkelt-partikkel Bose distribusjonsfunksjon ved lokalt ekvilibrium. Bidragene i Boltzmann-ligningen beskriver koblingen med fononbadet, PPP-en og bidraget fra kollisjonene mellom magnonene. Ved å anta null kondensat-hastighet og høy temperatur i et konstant og homogent system utvikler vi en bevegelsesligning for tettheten av termiske magnoner.

I 'steady state'-grensen kombinerer vi bevegelsesligningene for å uttrykke amplituden til pumpefeltet og det kjemiske potensialet som funksjoner av tettheten av kondensat-magnoner. Med formål om å ikke referere til et spesifikt material, brukes et sett med generelle størrelser basert på tidligere eksperimentelle målinger for å illustrere hvordan det kjemiske potensialet utarter seg. Siden standard-størrelsene resulterte i en nullverdig tetthet for termisk magnoner og pumping av magnoner kun i sentrum av Brillouin-sonen, holdes en diskusjon rundt hvorvidt de valgte størrelsene av parameterene er analytisk konsekvente. Til slutt evaluerer vi utledningen av tettheten for termiske magnoner med formål om å gi mer innsikt i fremtidige studier av det kjemiske potensialet.

Preface

This thesis completes a five-year master's degree programme in Applied Physics and Mathematics at the Norwegian University of Science and Technology. It was written during the spring semester of 2019 and builds on my project assignment written during the fall semester of 2018, see [1]. A sizeable portion of chapter 1-4 and appendix A is more or less identical to the project assignment, with some structural alternations and improvements.

I thank my supervisors Postdoc. Roberto E. Troncoso and Prof. Arne Brataas for giving me the opportunity to work on this project. The material was fascinating and enjoyable from day one, and I am grateful for this opportunity to interact with the Center for Quantum Spintronics (QuSpin) at NTNU. I graciously thank the student organization Nabla with all its components for making my studying years some of the best years of my life. Without this creative outlet, I can not imagine how these years would be anything other than mediocre in comparison. Finally, I would like to thank my mother and father for the unwavering support you have given me throughout these years.

Alexander Edin Varegg
Trondheim, Norway
July 2019

Nomenclature

Symbols

α	The Gilbert damping parameter
γ	Gyromagnetic ratio
μ_e	Magnetic moment of electron
ω_E	The antiferromagnetic resonance frequency
ρ	Condensate magnon density
c_l	Lattice parameter of a cubic 3D lattice
D_x	Magnetocrystalline anisotropy constant in the x-direction
J	Heisenberg exchange constant
N	Number of spins in an antiferromagnetic sublattice
n	Thermal magnon density
z	Number of nearest neighbours in a cubic 3D lattice

Physical Constants

$\hbar$	Reduced Planck's Constant
μ_0	Vacuum permeability
μ_B	Bohr magneton
k_B	Boltzmann constant

Conventions

- **Bold text** and $\overrightarrow{\text{arrows}}$ implies vectors.

Table of Contents

Abstract **i**

Sammendrag **iii**

Preface **v**

Nomenclature **vii**

Table of Contents **x**

List of Figures **xiii**

List of Tables **xv**

1 Introduction **1**
1.1 Structure of the thesis 2

2 Antiferromagnetic free energy **3**
2.1 The Heisenberg Exchange Hamiltonian 4
2.2 Magnetocrystalline anisotropy 4
2.3 Demagnetization 5
2.4 Zeeman interaction 5

3 Low-energy antiferromagnetic fluctuations **7**
3.1 Magnetic excitation and the Holstein-Primakoff representation 8
3.2 Ground State for a collinear antiferromagnet 9
3.3 The antiferromagnetic Hamiltonian 10
3.4 Dispersion relation 13

4 Parallel Parametric Pumping **15**
4.1 Parallel pumping in an antiferromagnet 16
4.2 Magnon growth due to PPP 18

5 The magnon condensate and the thermal cloud **21**
5.1 Bose-Einstein Condensation 22
5.1.1 The Bose macroscopic wavefunction and the single-particle distribution function 24
5.2 The equations of motion for the condensate density 25
5.3 Equation of motion for the thermal magnon density 29

6 The chemical potential in the steady state limit **37**
6.1 The steady state limit 37
6.2 Computations of the chemical potential 41
6.2.1 Pumping frequency $\omega_p/\mathrm{kOe} = 100\,\mathrm{THz}$ 44
6.2.2 Pumping frequency $\omega_p/\mathrm{kOe} = 150\,\mathrm{THz}$ 47
6.2.3 Pumping frequency $\omega_p/\mathrm{kOe} = 200\,\mathrm{THz}$ 49
6.3 Discussion 51

7 Conclusion **53**
7.1 Outlook 54

Appendices **55**

A Bogoliubov coefficients **57**

B Hydrodynamic form of the generalized Gross-Pitaevskii equation **61**

C Collision integral contributions in a strong magnetic field **63**

Bibliography **67**
References 67

List of Figures

2.1 Average relative spin directions in a two-dimensional lattice with (a) ferromagnetic and (b) antiferromagnetic order. (The ordering direction is arbitrary.) 3

3.1 One-dimensional spin chain with a spin wave propagating from left to right. The black arrow denotes the direction of the spin vector for each electron. 8

3.2 Spin-wave dispersion relations in the antiferromagnet NiO at $T = 300\,\mathrm{K}$. (a) Curves showing both magnon frequencies computed with Eqs. (3.41) and (3.42). (b) Display of the separation of the magnon modes α (upper blue curve) and β (lower red curve) in the Brillouin zone center. 13

4.1 Elliptical precession of local magnetization caused from elliptically precessing spin vectors. The precession is driven by a parametric pumping field parallel to the z-axis. The dotted circle is the initial stable spin orbit. 15

4.2 A photon from the oscillating pumping field with frequency $\omega = 2\omega_{\pm\boldsymbol{k}}$ directly excites two magnons of wave numbers $\pm\boldsymbol{k}$. 16

5.1 Illustrative renditions of the fractions of condensate magnons (red particles) compared to thermal magnons (green particles). The left plot illustrates the high concentration of condensate magnons in the center of the Brilluoin zone compared to the thermal cloud. The right plot illustrates the spatial regions the thermal and condensate magnons occupy with notably different densities. 22

5.2 A four-stage illustration of Bose-Einstein condensation. At a high temperature, particles move freely. As the temperature sinks, so does the energy of the particles and they develop wave-like behaviour. As the temperature continues to sink, the waves continue to expand, and at a sufficient temperature, T_{BEC}, the particles condense into a collective wave known as a Bose-Einstein condensate. 23

5.3 Illustration of C_{12}-collisions (left) between one condensate- and one thermal magnon resulting in two thermal magnons, and C_{22}-collisions (right) between two thermal magnons resulting in two thermal magnons. 33

6.1 Left plot: Measured relaxation rates displayed as the critical field $h_c \sim \eta$ in comparison with theoretical rates as a function of temperature for $\mathrm{MnF_2}$ magnons. Right plot: Variation of relaxation rates vs wave-vector amplitude at several temperatures. Both plots are from Barak *et al.* [74]. . 41

6.2 The chemical potential, μ given in Eq. (6.4), as a function of the pumping field strength, h given in Eq. (6.5), at $T = 1\,\mathrm{K}$ and room temperature. The lines are presented separately to avoid complete overlap. 42

6.3 The chemical potential, μ given in Eq. (6.4), plotted logarithmically as a function of the pumping field strength, h given in Eq. (6.5), at different spin numbers, $2N_1 = 10^8$, $2N_2 = 10^6$ and $2N_3 = 10^4$. 43

6.4 The chemical potential, μ given in Eq. (6.4), plotted as a function of the total spin number N, plotted logarithmically. 43

6.5 Computations at $\omega_p/\mathrm{kOe} = 100\,\mathrm{THz}$. (a) The chemical potential, Eq. (6.4), as a function of the pumping field amplitude, Eq. (6.5). (b) The simplified chemical potential, Eq. (6.19), as a function of the simplified pumping field amplitude, Eq. (6.16) (c) The pumping field amplitude, Eq. (6.5), as a function of the condensate density. (d) The simplified pumping field amplitude, Eq. (6.5), as a function of the condensate density. (e) The difference between the unaltered chemical potential in (a) and the simplified chemical potential in (b) as a function of the pumping field amplitude. (f) The difference between the unaltered pumping field amplitude in (c) and the simplified pumping field amplitude in (d) as a function of the condensate density. 45

6.6 A closer inspection of plot (e) from Fig. 6.5. The six discrete values of $\mu - \mu_s$ are outlined by horizontal translucent orange lines. 46

6.7 Computations at $\omega_p/\mathrm{kOe} = 150\,\mathrm{THz}$. (a) The chemical potential, Eq. (6.4), as a function of the pumping field amplitude, Eq. (6.5). (b) The simplified chemical potential, Eq. (6.19), as a function of the simplified pumping field amplitude, Eq. (6.16) (c) The pumping field amplitude, Eq. (6.5), as a function of the condensate density. (d) The simplified pumping field amplitude, Eq. (6.5), as a function of the condensate density. (e) The difference between the unaltered chemical potential in (a) and the simplified chemical potential in (b) as a function of the pumping field amplitude. (f) The difference between the unaltered pumping field amplitude in (c) and the simplified pumping field amplitude in (d) as a function of the condensate density. 48

6.8 Computations at $\omega_p/\mathrm{kOe} = 200\,\mathrm{THz}$. (a) The chemical potential, Eq. (6.4), as a function of the pumping field amplitude, Eq. (6.5). (b) The simplified chemical potential, Eq. (6.19), as a function of the simplified pumping field amplitude, Eq. (6.16) (c) The pumping field amplitude, Eq. (6.5), as a function of the condensate density. (d) The simplified pumping field amplitude, Eq. (6.5), as a function of the condensate density. (e) The difference between the unaltered chemical potential in (a) and the simplified chemical potential in (b) as a function of the pumping field amplitude. (f) The difference between the unaltered pumping field amplitude in (c) and the simplified pumping field amplitude in (d) as a function of the condensate density. 50

List of Tables

6.1 A list of parameters and their magnitudes necessary in the computation of the chemical potential of an antiferromagnet influenced by parallel pumping, given by Eq. (6.4). The magnitudes are chosen based on experimental studies with similar theoretical frameworks with the intention of being analytically consistent. The magnitudes were chosen with the aim to not pertain to any specific material. 39
6.2 The structure factors, given by Eq. (6.12), corresponding to pumping frequencies in Figs. 6.5, 6.7 and 6.8. 47

Chapter 1

Introduction

The nonlinear kinetics and dynamics of magnetically ordered dielectrics have gained massive attention at present [2]. Ferro- and antiferromagnetic systems under the external action of an electromagnetic field explore the behaviour of quasiparticles (magnons, phonons, etc.) and their interactions [2]. One especially popular research field of late is Bose-Einstein condensation (BEC) of magnons [3–11]. The quantum phenomenon in a magnetically ordered body dictates the condensation of magnons into a singular Bose quantum state at a certain density [12–14]. To achieve BEC, one either increases the density of bosons or lowers the temperature [7]. However, magnon condensates have been observed in ferrimagnetic insulators at room temperature [7]. This supports the potential for utilization of BEC without advanced cooling equipment. There are predictions of electrically induced magnon condensation in ferromagnets [15,16], but antiferromagnets remain much less explored for spintronics purposes. Yet, spin dynamics of antiferromagnets tend to be a thousand times more rapid than the magnetization dynamics in ferromagnets [17].

BEC of magnons might also open the possibility of executing and controlling spin superfluidity [18–27], i.e. the possibility of spin transport without dissipation. Compared with conventional electric currents, logic circuits based on nonlinear wave interaction and wave interference can be designed with magnon-based currents to carry, process and transport information with much smaller footprint [28]. As spin superfluidity already has been observed in Bose-Einstein condensates of cold atoms [19], one might realize dissipationless spin transport if one were able to electrically drive BEC of magnons. One approach to spin-wave amplification is parallel parametric pumping (PPP). An applied sufficiently large oscillating magnetic field interacts with selected spin waves at half the frequency of the pumping field and acts in parallel to the static magnetization. Parallel pumping allows mode- and frequency-selective amplification of spin waves and is one of the more promising techniques of parametric excitation [29]. PPP is proven superior to among others STT (the reduction of spin-wave damping by spin transfer torque) [30–33]. Naturally, a prerequisite to induce Bose-Einstein condensation, is to properly control the chemical potential of the material. Therefore, we aim in this thesis to study how the chemical potential of an antiferromagnet in a state of BEC is influenced by PPP. More specifically, we will ex-

plore how the chemical potential can be manipulated by the field strength of the parametric pumping field.

1.1 Structure of the thesis

The organization of the thesis is as follows. In chapter 2, we start by dissecting the antiferromagnetic free energy and explore the components of the antiferromagnetic Hamiltonian. A phenomenological description and an analytical representation will be provided of the Heisenberg Exchange Hamiltonian, magnetocrystalline anisotropy, demagnetization and the Zeeman interaction. Afterwards, we discuss the physical picture of low-energy antiferromagnetic fluctuations, magnetic excitation and the ground state for a collinear antiferromagnet in chapter 3. We also compute and analyze the dispersion relation in a generic hard-axis antiferromagnet and demonstrate our theoretical work with the experimental work of Rezende *et al.* with Nickel Oxide in the absence of an external magnetic field [34]. Next, we describe the effect of parallel parametric pumping on our Hamiltonian in chapter 4 and compute the equation of motion for the system. In chapter 5, we establish a phenomenological description of Bose-Einstein condensation and derive equations of motion for the condensate density, the condensate velocity and thermal cloud density. In chapter 6, we examine the steady state limit and combine the aforementioned equations of motion to acquire the means to plot how the pumping field amplitude affects the chemical potential of the system. Without pertaining to a specific material, we choose a set of default magnitudes for the parameters the chemical potential consists of, in order to compute its behaviour. We discuss the results and evaluate the default magnitudes and some of the approximations made in the derivation of the equations of motion. Finally, we conclude the thesis in chapter 7 and provide a short discussion of the outlook. The Appendices supply the more tedious calculations of this thesis in full detail.

Chapter 2

Antiferromagnetic free energy

Para-, dia-, ferri-, ferro- and antiferromagnetic materials are variants of substances characterized by their magnetic properties. In this chapter, we will elaborate on the characteristics and energy contributions of a generic antiferromagnet. In addition to illustrating antiferromagnetic spin alignment, the Heisenberg exchange interaction, magnetocrystalline anisotropy, demagnetization and Zeeman couplings will be introduced.

As shown in Fig. 2.1, the magnetic moments in a ferromagnet follow parallel alignment to their neighbouring moments. In an antiferromagnet the alignment is antiparallel. The antiferromagnetic lattice is easily divided into two sublattices A and B, where each contain the magnetic moments with equal magnetization pointing either up (A) or down (B). The prevalent convention is to label the lattice sites of the magnetic moments according to the their residing sublattices (lattice sites $i \in A$ and $j \in B$). The symmetric alignment and the resulting zero bulk magnetization is expected in the absence of an external magnetic field and below the critical Néel temperature T_N [35]. The antiferromagnetic arrangement becomes disordered by strong thermal fluctuations above this temperature [35].

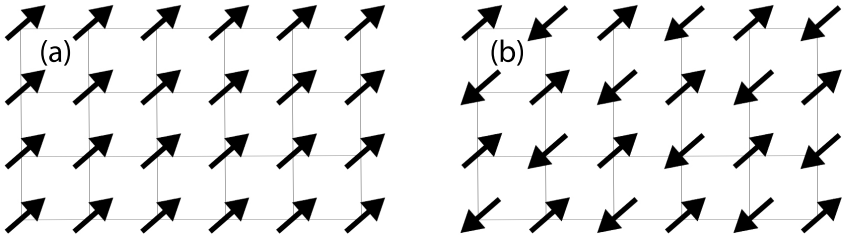

Figure 2.1: Average relative spin directions in a two-dimensional lattice with (a) ferromagnetic and (b) antiferromagnetic order. (The ordering direction is arbitrary.)

The antiferromagnetic free energy is defined by several interaction mechanisms. The

contributions will be represented semi-classically with spin Hamiltonians localized at lattice sites. We start with the most significant energy; the Heisenberg Exchange Hamiltonian.

2.1 The Heisenberg Exchange Hamiltonian

The exchange interaction is a quantum mechanical effect related to the Pauli exclusion principle. As a consequence of the spin-statistics theorem, two electrons (fermions) cannot occupy the same spatial state if they have the same spin. The energy of the exchange interaction between two electrons was pointed out by Paul Dirac [36] to be the potential between the coupled spins of the electrons. The energy term could be described by their spin momenta and in the classical Heisenberg model, the Heisenberg Exchange Hamiltonian is given by

$$H = \sum_{\langle i<j \rangle} 2J\vec{S}_i \cdot \vec{S}_j \tag{2.1}$$

where the summation is over the nearest-neighbour lattice sites i and j and J is the exchange constant. We have assumed that the potentials between spins that are not nearest-neighbours are negligible (which is often realistic) and that the system is in an isotropic material where the exchange constant J is equal for every interaction between nearest-neighbours spins [34]. The factor 2 appears because the summation avoids double counting due to the summation convention $i < j$. If the exchange constant is negative (positive), the system promotes adjacent spins with parallel (antiparallel) alignment. In the free magnetic energy, the exchange energy will ordinarily be the dominating term in comparison with other sources of magnetic energies [2].

2.2 Magnetocrystalline anisotropy

A material is said to have magnetocrystalline anisotropy if the energy necessary to magnetize it vary in certain directions. These directions usually relate to the principal axes of the materials crystal lattice [37]. The primary source of magnetocrystalline anisotropies is the spin-orbit coupling between the magnetic moment of the electrons and the electric field induced by the ions. The anisotropy is introduced in the occupation of the electrons, and through the spin-orbit coupling, the electrons experience the anisotropy in their orbital angular momentum [37]. This interaction gives rise to the first order contribution to the anisotropy H_A which is given by [38]

$$H_A = \sum_i D_x (S_i^x)^2, \tag{2.2}$$

where D_x is the anisotropy constant in the x-direction and S_i^x are the spin operators in the x-direction for the localized spins at lattice site i. We will neglect the temperature-dependence of D_x in this report as well as the second order contribution, which originates from the mutual interaction of the magnetic dipoles [39]. An energetically favourable crystallographic direction x of spontaneous magnetization is called an easy-axis, yielded

by a negative anisotropy constant D_x. Similarly, the energetically unfavourable direction is called a hard-axis, yielded by a positive anisotropy constant.

2.3 Demagnetization

Another energy contribution to the antiferromagnetic free energy originates from the magnetic dipole-dipole interaction, also called the dipole coupling. For localized spins $\vec{S}_{i,j}$ at lattice sites i, j, the potential energy is [40]

$$H_{\mathrm{D}} = -\frac{\mu_0 \gamma_i \gamma_j \hbar^2}{4\pi} \sum_{i \neq j} \frac{3(\vec{S}_i \cdot \hat{r})(\vec{S}_j \cdot \hat{r}) - \vec{S}_i \vec{S}_j)}{r_{ij}^3}, \tag{2.3}$$

where μ_0 is the vacuum permeability; $\gamma_{i,j}$ are the corresponding gyromagnetic ratios of particles with spin quanta $\vec{S}_{i,j}$; $\hat{r}$ is the unit vector pointing along the line joining the two spins, and $r_{ij} = |r_i - r_j|$ is the distance between the spins. The $\sim 1/r_{ij}^3$-dependence of the interaction between the two dipoles suggests a short ranged coupling. However, due to the number of neighbours scaling as $|r_i - r_j|$ cubed (or squared for 2-dimensional systems), the interaction is indeed long-ranged, since the effect cancels. The above sum is quite difficult to compute for larger systems. It is simpler to evaluate a total effective field at the position r_i, by replacing the sum over discretely localized spins with an integral in reference to the continuous magnetization $\vec{M}(r_i)$: $\sum_x((...) \cdot \vec{S}_i) \rightarrow \int \mathrm{d}r_i((...) \cdot \vec{M}(r_i))$. The energy contribution expressed through the self-interacting demagnetization field $\vec{N}(r_i - r_j)$ is [41]

$$H_{\mathrm{demag}}(r_i) = \int \vec{N}(r_i - r_j) M(r_j) \mathrm{d}r_j, \tag{2.4}$$

where the relevant prefactors are incorporated in the N-field.

The demagnetization field counteracts the spontaneous magnetization of a system. The field tries to enclose the magnetic field lines within the magnetic material and aligns antiparallel (to a certain extent) to the magnetization of the material. The contribution from the demagnetization in the antiferromagnetic free energy is rather limited. Since the net magnetization in antiferromagnets is close to zero, the dipole-dipole interactions are small. The magnetic moments in the antiferromagnetic arrangement are already compensated by the neighbouring moments due to the dominating exchange coupling. Therefore, we may assume the demagnetization energy to be a higher order correction to the antiferromagnetic free energy, in the same matter as quartic terms arising from the magnetocrystalline anisotropy or the Heisenberg exchange interaction [42].

2.4 Zeeman interaction

A spin-orbit coupling is the interaction between the magnetic moment of a body and an external magnetic field. Also known as a Zeeman coupling, its contribution H_Z to the spin Hamiltonian from an ensemble of electrons in an external magnetic field $\vec{h}'$ can be expressed as [43]

$$H_Z = g_e \mu_e \sum_i \vec{h}' \cdot \vec{S}_i, \tag{2.5}$$

where the g_e-factor is the dimensionless quantity that characterizes the angular momentum and magnetic moment of the electron; μ_e is the magnetic moment of the electron, and $\vec{S}_i$ is the intrinsic spin of the electron at lattice site i. By the means of parallel parametric pumping we wish to couple a magnetic field to the z-component of the electron spins

$$H_Z = \sum_i \vec{h} \cdot \vec{S}_i^z, \tag{2.6}$$

where we have merged the properties of the magnetic moment of the electron into the magnetic field $\vec{h} \equiv g_e \mu_e \vec{h}'$. The spin-orbit coupling exerts a torque on the spins of the electrons with a magnetic field and attempts to align the spins. The Zeeman interaction is a crucial requirement for the excitation of magnons.

Chapter 3

Low-energy antiferromagnetic fluctuations

As the ultimate goal of this thesis report is to build the theoretical framework of parametric pumping of magnons, we take a closer look at them. This chapter will briefly adress the history of the magnon, its characteristics, the Holstein-Primakoff representation and the ground state for a collinear antiferromagnet. We will diagonalize a hard-axis Hamiltonian for a generic antiferromagnetic system, which will be the system in discussion throughout this thesis. In the end, the dispersion relation will be derived and discussed, and we demonstrate the nature of the magnon modes with the experimental values acquired by Rezende, Rodríguez-Suárez and Azevedo [34] for the hard-axis antiferromagnet Nickel Oxide.

A magnon is a quasiparticle, an emergent phenomenon that occur when a complicated microscopic system behaves as if it held weakly interacting particles in free space. In order to explain the reduction of the magnetization in a ferromagnet, Felix Bloch [44] introduced the concept of the magnon in 1930. A Heisenberg ferromagnet at absolute zero temperature, $0\mathrm{K}$, reaches the state of minimal energy (the vaccum state), in which all of its magnetic moments align in the same direction. With incrementally increased temperature, more spins deviate at random from the alignment, reducing the net magnetization. Bloch pointed out that the state with a few misaligned spins and a non-zero temperature could be viewed as a gas of quasiparticles. In accordance with quantum mechanical laws, the reversal of a single magnetic moment is equivalent to a partial reversal of all magnetic moments in the system. This partial reversal propagates through the ferromagnet as a wave of discrete energy transferal. These quantized spin wave excitations in a magnetically ordered body were then known as magnons [44].

They carry a lattice momentum and a fixed amount of energy that correspond to an equivalent decrease in magnetic strength. Their spin-1 indicate that they obey Bose-Einstein statistics (boson behaviour) [45]

$$n_i(\epsilon_i) = \frac{g_i}{e^{\beta(\epsilon_i - \mu)} - 1}, \tag{3.1}$$

where n_i is the number of particles in energy state i; ϵ_i is the energy of state i; g_i is the degeneracy at energy level i; μ is the chemical potential and β is the so-called thermodynamic beta $\beta = 1/k_B T$, where k_B is the Boltzmann constant, and T is the absolute temperature. (A requirement for Bose-Einstein statistics is a positive argument in the exponential, $\epsilon_i > \mu$.)

3.1 Magnetic excitation and the Holstein-Primakoff representation

Spin waves are collective magnetic excitations. In this section, they will be described in the classical Heisenberg model with the localized moment approximation, as it gives a more intuitive picture of spin waves than the itinerant electron model.

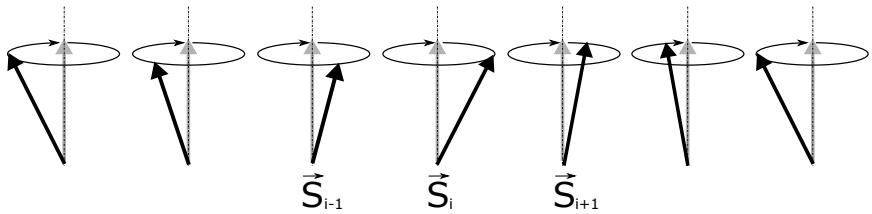

Figure 3.1: One-dimensional spin chain with a spin wave propagating from left to right. The black arrow denotes the direction of the spin vector for each electron.

In a magnetic ordered system, spin waves are regarded as the synchronic precession of the spin vectors. The waveform is the result from the constant phase difference between the nearest neighbouring spins, which is schematically shown in Fig. 3.1. As we know, the quantized magnetic excitations are magnons. A single magnon carries an angular momentum of $\hbar$ and a magnetic moment of $\gamma\hbar$ [46], where γ is the gyromagnetic ratio. Until now, the different energies of the antiferromagnetic free energy have been expressed through spin Hamiltonians. The spin operators are complicated and to be able to further examine the properties of the magnetic excitations, we need a simpler representation. The Holstein-Primakoff transformation (HP) maps the spin operators in terms of canonical bosonic creation and annihilation operators [47], and allows for simpler approximate calculatory schemes. The HP-representation for an antiferromagnetic system can be written as

$$S^+_{\mathrm{A}i} = \sqrt{2S - a_i^\dagger a_i}\, a_i, \quad S^-_{\mathrm{A}i} = a_i^\dagger \sqrt{2S - a_i^\dagger a_i}, \quad S^z_{\mathrm{A}i} = S - a_i^\dagger a_i, \tag{3.2}$$

$$S^+_{\mathrm{B}i} = b_i^\dagger \sqrt{2S - b_i^\dagger b_i}, \quad S^-_{\mathrm{B}i} = \sqrt{2S - b_i^\dagger b_i}\, b_i \quad S^z_{\mathrm{B}i} = -S + b_i^\dagger b_i, \tag{3.3}$$

where a_i and $a_i^\dagger$ (b_i and $b_i^\dagger$) are, respectively, the creation and annihilation operator for spins in sublattice A (B). On sublattice B where the spin projection is $-S$, the HP transformations are modified to reflect this, so the spin commutation relations are still

preserved. As we do not intend to include any terms larger than of quadratic nature in our Hamiltonian, we may expand the roots in the HP representation $\sqrt{2S - a_i^\dagger a_i} = \sqrt{2S}\sqrt{1 - a_i^\dagger a_i/(2S)}$ in a Taylor series in the operator $a_i^\dagger a_i/(2S)$. This simplifies Eqs. (3.2) and (3.3), and we acquire the linearly approximated HP-representation

$$S_{\mathrm{A}i}^+ = \sqrt{2S}a_i, \quad S_{\mathrm{A}i}^- = \sqrt{2S}a_i^\dagger, \quad S_{\mathrm{A}i}^z = S - a_i^\dagger a_i, \tag{3.4}$$

$$S_{\mathrm{B}i}^+ = \sqrt{2S}b_i^\dagger, \quad S_{\mathrm{B}i}^- = \sqrt{2S}b_i \quad S_{\mathrm{B}i}^z = -S + b_i^\dagger b_i. \tag{3.5}$$

3.2 Ground State for a collinear antiferromagnet

To illustrate the properties of the antiferromagnetic ground state in the simplest manner, we consider only the exchange interaction, Eq. (2.1), in the system Hamiltonian. One might mistakenly assume that the quantum ground state bears an analogy to the ground state for classical spins, as their alignment are similarly collinear (nearest neighbour spins point antiparallel to the reference spin). This state would have the form [48]

$$\prod_{i\in A} |S\rangle_i \prod_{j\in B} |-S\rangle_j \equiv |N'\rangle \tag{3.6}$$

where A and B denote the formerly established sublattices with spin projection, respectively, S and $-S$, and the eigenstates $|\pm S\rangle_{i,j}$ of S_z at the given lattice site have eigenvalues $\pm S$. When the Heisenberg Exchange Hamiltonian (2.1) acts on $|N'\rangle$, the quantum fluctuation terms containing the spin raising and lowering operators terminate the proportionality to $|N'\rangle$ [48]

$$H|N'\rangle = -\sum_{i\in A}\sum_{j\in B} J_{ij}\left(\frac{1}{2}\underbrace{S_i^+ S_j^-|N'\rangle}_{=0} + \frac{1}{2}S_i^- S_j^+|N'\rangle + S_i^z S_j^z|N'\rangle\right) \tag{3.7}$$

$$= -\sum_{i\in A}\sum_{j\in B} J_{ij}\left(\frac{1}{2}\underbrace{[S(S+1) - S(S-1)]}_{2S}\cdot ...|S-1\rangle_i ...|-S+1\rangle_j ... - S^2|N'\rangle\right), \tag{3.8}$$

where we've expressed Eq. (2.1) in terms of raising and lowering operators, shown in Appendix A (3.12). $|N'\rangle$ cannot be an eigenstate, much less the ground state. Quantum fluctuations play therefore an important role in antiferromagnetic structures (compared to the ferromagnetic case, which we will not dive further into). However, the actual ground state do still have antiferromagnetic order as displayed in Fig. 2.1. In order to find the ground state energy, the Hamiltonian for the system needs to be investigated. In the next section, we will derive a diagonalized Hamiltonian, reduced to an intuitive form, written as

$$H = \varepsilon_0 + \sum_{\boldsymbol{k}} \hbar(\omega_{\alpha\boldsymbol{k}}\alpha_{\boldsymbol{k}}^\dagger\alpha_{\boldsymbol{k}} + \omega_{\beta\boldsymbol{k}}\beta_{\boldsymbol{k}}^\dagger\beta_{\boldsymbol{k}}). \tag{3.9}$$

where ε_0 is the energy representing the zero-point fluctuations and $\alpha_{\boldsymbol{k}}^\dagger$ and $\beta_{\boldsymbol{k}}^\dagger$ with wavevector $\boldsymbol{k}$ create magnon excitations with energy $\omega_{\alpha\boldsymbol{k}}/\omega_{\beta\boldsymbol{k}}$. In the actual ground state $|N\rangle$ of

H there can be neither $\alpha_{\boldsymbol{k}}$ nor $\beta_{\boldsymbol{k}}$ operators as they supply the energy $\omega_{\alpha\boldsymbol{k}}$ and/or $\omega_{\beta\boldsymbol{k}}$ to the total energy. The ground state must therefore fullfill the relations

$$\alpha_{\boldsymbol{k}}|N\rangle = 0, \quad \beta_{\boldsymbol{k}}|N\rangle = 0, \tag{3.10}$$

for all $\boldsymbol{k}$. Thus $H|N\rangle = \varepsilon_0|N\rangle$, making the ground state energy ε_0. This system had a single ground state. Anti-ferromagnetic interactions, unlike ferromagnetism, may lead to multiple ground states. In the 2-dimensional case of an equilateral triangle with three spins, there are 8 possible states, six of which are ground states. The systems inability to find a single ground state is called geometric frustration [49], but will not be discussed further.

3.3 The antiferromagnetic Hamiltonian

The Hamiltonian examined in this thesis report is a generic hard-axis antiferromagnet. The spin Hamiltonian has exchange interaction energy (2.1), out-of-plane (x-direction) and in-plane (y-direction) magnetocrystalline anisotropy energies (2.2) and an external time-independent magnetic field. The Hamiltonian is given by

$$H = \sum_{\langle i<j\rangle} 2J\vec{S}_i \cdot \vec{S}_j + \sum_i D_x(S_i^x)^2 + \sum_i D_y(S_i^y)^2 - \gamma\hbar\Upsilon \sum_i S_i^z, \tag{3.11}$$

where the last term is the Zeeman coupling for a constant external magnetic field with field strength Υ pointing in the z-direction. In order to illustrate the nature of the eigenfrequencies, we will derive the Hamiltonian on a diagonal form. z is the direction of spin alignment. In order to apply the HP-transformation, we express the Hamiltonian (3.11) in terms of raising and lowering operators $S_i^{\pm} = S_i^x \pm iS_i^y$

$$\begin{aligned} H = {} & J\sum_{i,\delta}(S_i^+ S_{i+\delta}^- + S_i^- S_{i+\delta}^+ + 2S_i^z S_{i+\delta}^z) \\ & + \frac{1}{4}D_x \sum_i [(S_i^+)^2 + (S_i^-)^2 + S_i^+ S_i^- + S_i^- S_i^+] \\ & - \frac{1}{4}D_y \sum_i [(S_i^+)^2 + (S_i^-)^2 - S_i^+ S_i^- - S_i^- S_i^+] - \gamma\hbar\Upsilon \sum_i S_i^z. \end{aligned} \tag{3.12}$$

We now express the Hamiltonian in terms of boson creation and annihilation operators using eqs. (3.2) and (3.3)

$$H = H_{\mathrm{Heis}} + H_{\mathrm{D_x}} + H_{\mathrm{D_y}} + H_{\mathrm{Ext}}, \tag{3.13}$$

$$\begin{aligned} H_{\mathrm{Heis}} = {} & 2JS\sum_{i\in\mathrm{A}}\sum_{\delta}(a_i b_{i+\delta} + a_i^\dagger b_{i+\delta}^\dagger + a_i^\dagger a_i + b_{i+\delta}^\dagger b_{i+\delta} - S) \\ & + 2JS\sum_{j\in\mathrm{B}}\sum_{\delta}(b_j a_{j+\delta} + b_j^\dagger a_{j+\delta}^\dagger + b_j^\dagger b_j + a_{j+\delta}^\dagger a_{j+\delta} - S), \end{aligned} \tag{3.14}$$

$$H_{\mathrm{D_x}} = \frac{S}{2}D_x \sum_{i\in\mathrm{A}}(a_i a_i + a_i a_i^\dagger + \mathrm{h.c.}) + \frac{S}{2}D_x \sum_{j\in\mathrm{B}}(b_j b_j + b_j b_j^\dagger + \mathrm{h.c.}), \tag{3.15}$$

$$H_{\mathrm{D_y}} = -\frac{S}{2}D_y\sum_{i\in\mathrm{A}}(a_i a_i - a_i a_i^\dagger + \mathrm{h.c.}) - \frac{S}{2}D_y\sum_{j\in\mathrm{B}}(b_j b_j - b_j b_j^\dagger + \mathrm{h.c.}), \tag{3.16}$$

$$H_{\mathrm{Ext}} = \gamma\hbar\Upsilon\big(\sum_{i\in\mathrm{A}} a_i^\dagger a_i - \sum_{j\in\mathrm{B}} b_j^\dagger b_j\big) \tag{3.17}$$

where H_{Heis} is the interaction term; $H_{\mathrm{D_x}}$ and $H_{\mathrm{D_y}}$ are the anisotropies, and H_{Ext} is the external field contribution. Only the quadratic terms have been kept, as the quartic terms have been labeled small enough to be a higher order correction to the free energy. $a_i^\dagger$ and $b_i^\dagger$ are the creation operators, respectively, for spin deviations at sublattice A and B, and a_i and b_i are the annihilation operators, which satisfy the boson commutation rules $[a_i, a_j^\dagger] = \delta_{ij}\ [a_i, a_j] = 0\ [b_i, b_j^\dagger] = \delta_{ij}\ [b_i, b_j] = 0$. We can perform a Fourier-transform of the localized field operators with a new set of boson operators

$$a_i = \frac{1}{\sqrt{N}}\sum_{\boldsymbol{k}} e^{i\boldsymbol{k}\cdot\boldsymbol{r_i}} a_{\boldsymbol{k}}, \quad b_i = \frac{1}{\sqrt{N}}\sum_{\boldsymbol{k}} e^{i\boldsymbol{k}\cdot\boldsymbol{r_i}} b_{\boldsymbol{k}}, \quad \frac{1}{N}\sum_i e^{i(\boldsymbol{k}+\boldsymbol{k'})\boldsymbol{r_i}} = \delta_{\boldsymbol{k},-\boldsymbol{k'}}, \tag{3.18}$$

where $\boldsymbol{k}$ is a wave vector; N is the number of spins in each sublattice, and the commutation rules apply $[a_{\boldsymbol{k}}, a_{\boldsymbol{k'}}^\dagger] = \delta_{\boldsymbol{k},\boldsymbol{k'}}\ [a_{\boldsymbol{k}}, a_{\boldsymbol{k'}}] = 0\ [b_{\boldsymbol{k}}, b_{\boldsymbol{k'}}^\dagger] = \delta_{\boldsymbol{k},\boldsymbol{k'}}\ [b_{\boldsymbol{k}}, b_{\boldsymbol{k'}}] = 0$. Inserting Eqs. (3.18) in Eq. (3.13) the Hamiltonian can be written as

$$\begin{aligned} H = \hbar\sum_{\boldsymbol{k}} &(A_{\boldsymbol{k}} + \gamma\Upsilon)a_{\boldsymbol{k}}^\dagger a_{\boldsymbol{k}} + (A_{\boldsymbol{k}} - \gamma\Upsilon)b_{\boldsymbol{k}}^\dagger b_{\boldsymbol{k}} + B_{\boldsymbol{k}}(a_{\boldsymbol{k}} b_{-\boldsymbol{k}} + a_{\boldsymbol{k}}^\dagger b_{-\boldsymbol{k}}^\dagger) \\ &+ \frac{1}{2}C_{\boldsymbol{k}}(a_{\boldsymbol{k}} a_{-\boldsymbol{k}} + b_{\boldsymbol{k}} b_{-\boldsymbol{k}} + \mathrm{h.c}) + D_{\boldsymbol{k}}, \end{aligned} \tag{3.19}$$

$$A_{\boldsymbol{k}} = \gamma[H_E + (H_{Ax} + H_{Ay})/2], \tag{3.20}$$

$$B_{\boldsymbol{k}} = \gamma\gamma_{\boldsymbol{k}} H_E, \quad \gamma_{\boldsymbol{k}} = (1/z)\sum_\delta e^{i\boldsymbol{k}\cdot\boldsymbol{\delta}}, \tag{3.21}$$

$$C_{\boldsymbol{k}} = \gamma(H_{Ax} - H_{Ay})/2, \tag{3.22}$$

$$D_{\boldsymbol{k}} = SN(D_x + D_y - 2JSz), \tag{3.23}$$

where z is the number of nearest neighbours, and the effective exchange and anisotropy fields are defined as

$$H_E = 2SzJ/\gamma\hbar, \quad H_{Ax} = 2SD_x/\gamma\hbar, \quad H_{Ay} = 2SD_y/\gamma\hbar. \tag{3.24}$$

$\gamma = g_s\mu_B/\hbar$ is the gyromagnetic ratio, defined by the specific splitting factor g_s, the Bohr magneton μ_B, and the reduced Planck constant $\hbar$. The next step is a transformation of the Hamiltonian to a diagonal form of normal mode magnon creation and annihilation operators $\alpha_{\boldsymbol{k}}^\dagger\alpha_{\boldsymbol{k}}$ and $\beta_{\boldsymbol{k}}^\dagger\beta_{\boldsymbol{k}}$

$$H = \varepsilon_0 + \sum_{\boldsymbol{k}} \hbar(\omega_{\alpha\boldsymbol{k}}\alpha_{\boldsymbol{k}}^\dagger\alpha_{\boldsymbol{k}} + \omega_{\beta\boldsymbol{k}}\beta_{\boldsymbol{k}}^\dagger\beta_{\boldsymbol{k}}), \tag{3.25}$$

where the two magnon modes have the frequencies $\omega_{\alpha\boldsymbol{k}}$ and $\omega_{\beta\boldsymbol{k}}$. We write Eq. (3.19) in matrix form

$$H = \varepsilon_0 + \hbar\sum_{\boldsymbol{k}>0} H_{\boldsymbol{k}}, \quad H_{\boldsymbol{k}} = (X)^\dagger[H](X) \tag{3.26}$$

with

$$(X) = \begin{pmatrix} a_{\boldsymbol{k}} \\ b^{\dagger}_{-\boldsymbol{k}} \\ a^{\dagger}_{-\boldsymbol{k}} \\ b_{\boldsymbol{k}} \end{pmatrix}, \quad [H] = \hbar \begin{pmatrix} A_{\boldsymbol{k}} + \gamma\Upsilon & B_{\boldsymbol{k}} & C_{\boldsymbol{k}} & 0 \\ B_{\boldsymbol{k}} & A_{\boldsymbol{k}} - \gamma\Upsilon & 0 & C_{\boldsymbol{k}} \\ C_{\boldsymbol{k}} & 0 & A_{\boldsymbol{k}} + \gamma\Upsilon & B_{\boldsymbol{k}} \\ 0 & C_{\boldsymbol{k}} & B_{\boldsymbol{k}} & A_{\boldsymbol{k}} - \gamma\Upsilon \end{pmatrix}. \tag{3.27}$$

By performing a Bogoliubov transformation

$$(X) = [Q](Z), \quad (Z) = \begin{pmatrix} \alpha_{\boldsymbol{k}} \\ \beta^{\dagger}_{-\boldsymbol{k}} \\ \alpha^{\dagger}_{-\boldsymbol{k}} \\ \beta_{\boldsymbol{k}} \end{pmatrix}, \tag{3.28}$$

where $[Q]$ is the transformation matrix, the Hamiltonian can be written as

$$H = \hbar \sum_{\boldsymbol{k}} (Z)^{\dagger}[\omega](Z), \tag{3.29}$$

where $[\omega]$ is the diagonal eigenvalue matrix. In our model with no external magnetic field, the Hamiltonian in eq. (3.25) can be solved without finding $[Q]$. However, the relations necessary to find it is of interest, as we will be needing them when solving the Hamiltonian with a pumping field in Appendix B. From eq. (3.28) in eq. (3.26) in comparison with eq. (3.29), one obtains the relation

$$[Q]^{\dagger}[H][Q] = \hbar[\omega], \tag{3.30}$$

and another relation from the boson commutation rules,

$$[X, X^{\dagger}] = X(X)^{\dagger} - (X^{*}X^{T})^{T} = g, \tag{3.31}$$

$$[Z, Z^{\dagger}] = Z(Z)^{\dagger} - (Z^{*}Z^{T})^{T} = g, \tag{3.32}$$

where

$$g = \begin{pmatrix} 1 & 0 & 0 & 0 \\ 0 & -1 & 0 & 0 \\ 0 & 0 & -1 & 0 \\ 0 & 0 & 0 & 1 \end{pmatrix}. \tag{3.33}$$

Lastly, using Eq. (3.28) in Eqs. (3.31) and (3.32) to write the orthonormality relation,

$$[Q][g][Q]^{\dagger} = [g], \tag{3.34}$$

we combine Eqs. (3.29)-(3.34) to obtain the eigenvalue equation

$$[H][Q] = [g]^{-1}[Q][g]\hbar[\omega]. \tag{3.35}$$

Another method to find the frequencies without finding $[Q]$ is

$$0 = \det([g]^{-1}[H] - [\omega]) \tag{3.36}$$

which yields the following two magnon mode frequencies

$$\omega^{2}_{\alpha\boldsymbol{k}} = A^{2}_{\boldsymbol{k}} + \gamma^{2}\Upsilon^{2} - B^{2}_{\boldsymbol{k}} - C^{2}_{\boldsymbol{k}} + 2\sqrt{\gamma^{2}(A^{2}_{\boldsymbol{k}} - B^{2}_{\boldsymbol{k}})\Upsilon^{2} + B^{2}_{\boldsymbol{k}}C^{2}_{\boldsymbol{k}}}, \tag{3.37}$$

$$\omega^{2}_{\beta\boldsymbol{k}} = A^{2}_{\boldsymbol{k}} + \gamma^{2}\Upsilon^{2} - B^{2}_{\boldsymbol{k}} - C^{2}_{\boldsymbol{k}} - 2\sqrt{\gamma^{2}(A^{2}_{\boldsymbol{k}} - B^{2}_{\boldsymbol{k}})\Upsilon^{2} + B^{2}_{\boldsymbol{k}}C^{2}_{\boldsymbol{k}}}. \tag{3.38}$$

3.4 Dispersion relation

We may further study the dispersion relation in our diagonalized Hamiltonian. If the external field was absent, the magnon mode frequencies should be similar to the magnon modes in the experiment by Rezende *et al.* [34] for the hard-axis antiferromagnet Nickel Oxide. By setting the field strength $\Upsilon = 0$ in our dispersion relation, (3.37) and (3.38) take the form

$$\omega_{\alpha\boldsymbol{k}}^2 = A_{\boldsymbol{k}}^2 - (B_{\boldsymbol{k}} - C_{\boldsymbol{k}})^2, \tag{3.39}$$

$$\omega_{\beta\boldsymbol{k}}^2 = A_{\boldsymbol{k}}^2 - (B_{\boldsymbol{k}} + C_{\boldsymbol{k}})^2, \tag{3.40}$$

which are the same relations, since the field-coefficients $A_{\boldsymbol{k}}, B_{\boldsymbol{k}}, C_{\boldsymbol{k}}$ are defined identically. In terms of the effective fields defined in (3.24), the eigenfrequencies read

$$\omega_{\alpha\boldsymbol{k}}^2 = \gamma^2[H_E(H_{Ax}+H_{Ay})+H_{Ax}H_{Ay}+\gamma_{\boldsymbol{k}}H_E(H_{Ax}-H_{Ay})+H_E^2(1-\gamma_{\boldsymbol{k}}^2))], \tag{3.41}$$

$$\omega_{\beta\boldsymbol{k}}^2 = \gamma^2[H_E(H_{Ax}+H_{Ay})+H_{Ax}H_{Ay}-\gamma_{k}H_E(H_{Ax}-H_{Ay})+H_E^2(1-\gamma_{k}^2))]. \tag{3.42}$$

We demonstrate the nature of the magnon mode frequencies with the experimental values acquired by Rezende *et al.* [34]. With the g factor $g = 2.18$, the exchange field $H_E = 9684\,\mathrm{kOe}$, and the anisotropy fields $H_{Ax} = 6.35\,\mathrm{kOe}$ and $H_{Ay} = 0.11\,\mathrm{kOe}$, we display the dispersion relations (3.41) and (3.42) in Fig. 3.2 as a function of the reduced wave number $q = \boldsymbol{k}/k_m$. The values are under the assumption of a spherical Brillouin zone with a structure factor $\gamma_{\boldsymbol{k}} = \cos(\pi\boldsymbol{k}/2k_m)$, where $k_m = \pi/a_l$ and a_l is the lattice parameter for Nickel Oxide.

The plot of the dispersion relations shows a substantial difference between the α and β mode in the center of the Brillouin zone, at $\boldsymbol{k} = 0$ ($\gamma_{\boldsymbol{k}=1}$). This is supported by the math, as $H_E \gg H_{Ax}$,H_{Ay}, the frequencies of the zone center magnons are

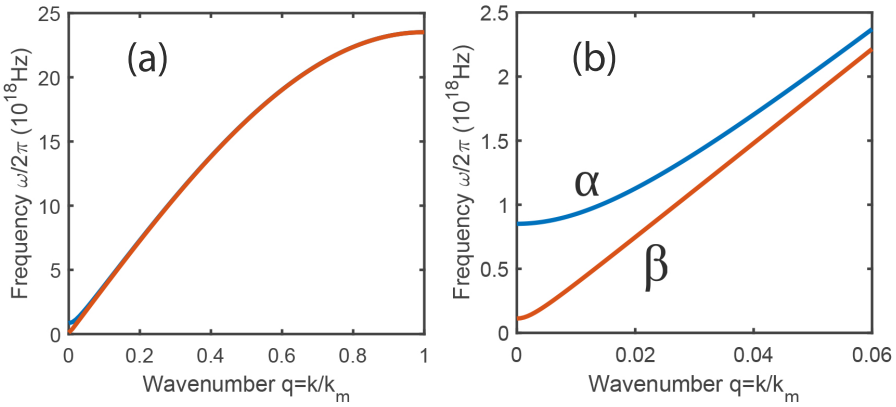

Figure 3.2: Spin-wave dispersion relations in the antiferromagnet NiO at $T = 300\,\mathrm{K}$. (a) Curves showing both magnon frequencies computed with Eqs. (3.41) and (3.42). (b) Display of the separation of the magnon modes α (upper blue curve) and β (lower red curve) in the Brillouin zone center.

$$\omega_{\alpha 0} \approx \gamma(2H_{Ax}H_E)^{1/2}, \quad \omega_{\beta 0} \approx \gamma(2H_{Ay}H_E)^{1/2}, \tag{3.43}$$

where the known magnitudes of H_{Ax} and H_{Ay} substantiate the gap between $\omega_{\alpha 0}$ and $\omega_{\beta 0}$. Notice also that the anisotropy becomes easy axis in the z direction if $D_x = D_y$. With $H_A = 2SD_x/g\mu_B$, the two dispersion relations are $\omega^2_{\alpha \boldsymbol{k}} = \omega^2_{\beta \boldsymbol{k}} = \omega^2_{\boldsymbol{k}}$, where

$$\omega_{\boldsymbol{k}} = \pm\gamma[2H_E H_A + H_A^2 + H_E^2(1-\gamma^2_{\boldsymbol{k}})]^{1/2}. \tag{3.44}$$

This is the known frequency for an antiferromagnet with easy-axis anisotropy in the absence of an external field [34]. The frequencies are however in the general model a tad more complicated expressed in terms of the effective fields

$$\begin{aligned}\left(\frac{\omega_{\alpha \boldsymbol{k}}}{\gamma}\right)^2 &= H_E(H_{Ax}+H_{Ay}) + H_{Ax}H_{Ay} + \Upsilon^2 + H_E^2(1-\gamma^2_{\boldsymbol{k}}) \\ &\quad + 2\sqrt{\left(H_E + \frac{H_{Ax}+H_{Ay}}{2}\right)^2\Upsilon^2 - \gamma^2_{\boldsymbol{k}}H_E^2\left[\Upsilon^2 - \left(\frac{H_{Ax}-H_{Ay}}{2}\right)^2\right]},\end{aligned} \tag{3.45}$$

$$\begin{aligned}\left(\frac{\omega_{\beta \boldsymbol{k}}}{\gamma}\right)^2 &= H_E(H_{Ax}+H_{Ay}) + H_{Ax}H_{Ay} + \Upsilon^2 + H_E^2(1-\gamma^2_{\boldsymbol{k}}) \\ &\quad - 2\sqrt{\left(H_E + \frac{H_{Ax}+H_{Ay}}{2}\right)^2\Upsilon^2 - \gamma^2_{\boldsymbol{k}}H_E^2\left[\Upsilon^2 - \left(\frac{H_{Ax}-H_{Ay}}{2}\right)^2\right]}.\end{aligned} \tag{3.46}$$

In the next chapter we will further examine how the dispersion relation relates to the pumping frequencies of a parallel pumping field.

Chapter 4

Parallel Parametric Pumping

In order to successfully monitor Bose-Einstein Condensation in an antiferromagnet, we wish to pump energy into a system via an external magnetic field to expedite magnon excitations. Building on the Hamiltonian from the last chapter, we will investigate the addition of parallel parametric pumping (PPP) to the system and the properties of the resulting growth rate of the magnon density.

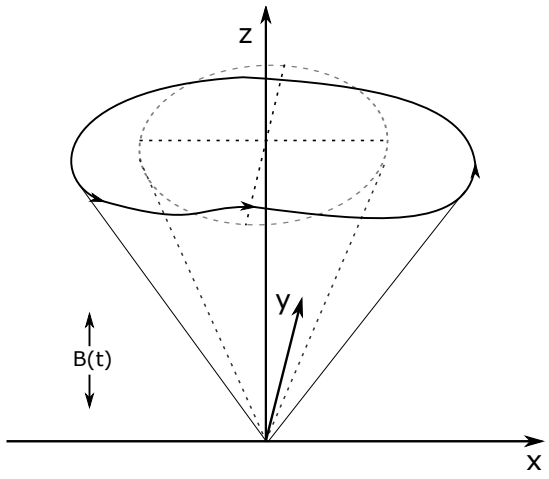

Figure 4.1: Elliptical precession of local magnetization caused from elliptically precessing spin vectors. The precession is driven by a parametric pumping field parallel to the z-axis. The dotted circle is the initial stable spin orbit.

By applying a time-dependent magnetic field $\vec{B}(t)$ parallel to the magnetization of the magnetic moments in the system and establishing a Zeeman coupling, one may influence the rate of change in the magnon density of the material. The pumping field and its oscil-

lating nature may be expressed as

$$\vec{B}(t) = he^{-i\omega_p t}, \tag{4.1}$$

where $h = |\vec{h}|$ is the scalar of the field amplitude pointing in the z-direction, and ω_p is the pumping frequency of the oscillating field. The physical nature of parallel pumping is best understood examining the orbits of individual spins. One of the conditions for magnetic excitations is a certain instability in the magnetic ordered body [50]. As illustrated in Fig. 4.1, where the magnetization and external magnetic field are parallel to the z-axis, the required instability is a result of elliptical precessions from individual spin waves directed normal to the z direction. If a spin vector precesses at a frequency $\omega_{\boldsymbol{k}}$ in the ellipse, the z-component of the orbit grows and declines periodically at a frequency $2\omega_{\boldsymbol{k}}$. The pumping energy continuously contribute to the increase of the precession angle and maintains the spins instability, which is a result of the growth rate of magnons exceeding the decay rate [50]. The various relaxation processes causing the decay rate will be discussed further in the next chapter. The condition $\omega_p = 2\omega_{\boldsymbol{k}}$ follows the conservation of energy when a single photon is converted into two magnons as displayed in Fig. 4.2. We may now examine the analytical aspect of the presence of a Zeeman coupling in an antiferromagnet.

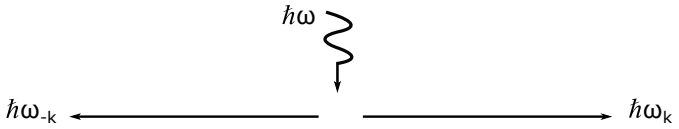

Figure 4.2: A photon from the oscillating pumping field with frequency $\omega = 2\omega_{\pm\boldsymbol{k}}$ directly excites two magnons of wave numbers $\pm\boldsymbol{k}$.

4.1 Parallel pumping in an antiferromagnet

The perturbation $H_p(t)$ from the external magnetic field is coupled to the z-components of the electron spins [51]

$$H_p(t) = he^{-i\omega_p t}\sum_{i\in A} S_i^z + \sum_{j\in B} S_j^z \tag{4.2}$$

$$= he^{-i\omega_p t}\sum_{\boldsymbol{k}} (b_{\boldsymbol{k}}^\dagger b_{\boldsymbol{k}} - a_{\boldsymbol{k}}^\dagger a_{\boldsymbol{k}}), \tag{4.3}$$

where the Holstein-Primakoff approximation in Eqs. (3.2) and (3.3) was imposed before the Fourier transform. We recall from the Bogoliubov transformation in Eq. (3.28) that

$$(X) = [Q](Z), \quad \begin{pmatrix} a_{\boldsymbol{k}} \\ b_{-\boldsymbol{k}}^\dagger \\ a_{-\boldsymbol{k}}^\dagger \\ b_{\boldsymbol{k}} \end{pmatrix} = \begin{pmatrix} Q_{11} & Q_{12} & Q_{13} & Q_{14} \\ Q_{21} & Q_{22} & Q_{23} & Q_{24} \\ Q_{31} & Q_{32} & Q_{33} & Q_{34} \\ Q_{41} & Q_{42} & Q_{43} & Q_{44} \end{pmatrix} \begin{pmatrix} \alpha_{\boldsymbol{k}} \\ \beta_{-\boldsymbol{k}}^\dagger \\ \alpha_{-\boldsymbol{k}}^\dagger \\ \beta_{\boldsymbol{k}} \end{pmatrix}, \tag{4.4}$$

which yield the following set of equations

$$a_{\boldsymbol{k}} = Q_{11}\alpha_{\boldsymbol{k}} + Q_{12}\beta^{\dagger}_{-\boldsymbol{k}} + Q_{13}\alpha^{\dagger}_{-\boldsymbol{k}} + Q_{14}\beta_{\boldsymbol{k}}, \tag{4.5}$$

$$b^{\dagger}_{-\boldsymbol{k}} = Q_{21}\alpha_{\boldsymbol{k}} + Q_{22}\beta^{\dagger}_{-\boldsymbol{k}} + Q_{23}\alpha^{\dagger}_{-\boldsymbol{k}} + Q_{24}\beta_{\boldsymbol{k}}, \tag{4.6}$$

$$a^{\dagger}_{-\boldsymbol{k}} = Q_{31}\alpha_{\boldsymbol{k}} + Q_{32}\beta^{\dagger}_{-\boldsymbol{k}} + Q_{33}\alpha^{\dagger}_{-\boldsymbol{k}} + Q_{34}\beta_{\boldsymbol{k}}, \tag{4.7}$$

$$b_{\boldsymbol{k}} = Q_{41}\alpha_{\boldsymbol{k}} + Q_{42}\beta^{\dagger}_{-\boldsymbol{k}} + Q_{43}\alpha^{\dagger}_{-\boldsymbol{k}} + Q_{44}\beta_{\boldsymbol{k}}. \tag{4.8}$$

Expressing the energy contribution from the Zeeman coupling in terms of the Bogoliubov transformed magnon mode operators is straight forward. But, as we aim to find tentative values for the expressions in the last section, we need to know the expressions for the Bogoliubov coefficients Q_{ij}-s. This process is described in detail in Appendix A and render the perturbation $H_p(t)$ and the Bogoliubov coefficients

$$\begin{aligned} H_p(t) = \sum_{\boldsymbol{k}} [&A_{1\boldsymbol{k}}(\alpha^{\dagger}_{\boldsymbol{k}}\alpha^{\dagger}_{-\boldsymbol{k}} + \alpha_{\boldsymbol{k}}\alpha_{-\boldsymbol{k}}) + A_{2\boldsymbol{k}}(\beta^{\dagger}_{\boldsymbol{k}}\beta^{\dagger}_{-\boldsymbol{k}} + \beta_{\boldsymbol{k}}\beta_{-\boldsymbol{k}}) \\ &+ B_{1\boldsymbol{k}}(\alpha^{\dagger}_{\boldsymbol{k}}\beta^{\dagger}_{-\boldsymbol{k}} + \alpha_{\boldsymbol{k}}\beta_{-\boldsymbol{k}}) + B_{2\boldsymbol{k}}(\alpha_{\boldsymbol{k}}\beta^{\dagger}_{\boldsymbol{k}} + \alpha^{\dagger}_{\boldsymbol{k}}\beta_{\boldsymbol{k}})], \end{aligned} \tag{4.9}$$

with the pumping coefficients

$$A_{1\boldsymbol{k}} = h(t)[Q_{21}(\boldsymbol{k})Q_{23}(\boldsymbol{k}) - Q_{11}(\boldsymbol{k})Q_{13}(\boldsymbol{k})], \tag{4.10}$$

$$A_{2\boldsymbol{k}} = h(t)[Q_{22}(\boldsymbol{k})Q_{24}(\boldsymbol{k}) - Q_{12}(\boldsymbol{k})Q_{14}(\boldsymbol{k})], \tag{4.11}$$

$$B_{1\boldsymbol{k}} = h(t)[Q_{23}(\boldsymbol{k})Q_{24}(\boldsymbol{k}) - Q_{11}(\boldsymbol{k})Q_{12}(\boldsymbol{k}) - Q_{13}(\boldsymbol{k})Q_{14}(\boldsymbol{k}) + Q_{21}(\boldsymbol{k})Q_{22}(\boldsymbol{k})], \tag{4.12}$$

$$B_{2\boldsymbol{k}} = h(t)[Q_{22}(\boldsymbol{k})Q_{23}(\boldsymbol{k}) - Q_{11}(\boldsymbol{k})Q_{14}(\boldsymbol{k}) - Q_{12}(\boldsymbol{k})Q_{13}(\boldsymbol{k}) + Q_{21}(\boldsymbol{k})Q_{24}(\boldsymbol{k})], \tag{4.13}$$

consisting of the pumping field $h(t) = he^{-i\omega_p t}$ and the Bogoliubov coefficients

$$\frac{Q_{21}}{Q_{11}} = \frac{B_{\boldsymbol{k}}[(A_{\boldsymbol{k}} + \gamma\Upsilon + \omega_{\alpha\boldsymbol{k}})(A_{\boldsymbol{k}} - \gamma\Upsilon - \omega_{\alpha\boldsymbol{k}}) - B^2_{\boldsymbol{k}} + C^2_{\boldsymbol{k}}]}{(A_{\boldsymbol{k}} - \gamma\Upsilon + \omega_{\alpha\boldsymbol{k}})B^2_{\boldsymbol{k}} + (A_{\boldsymbol{k}} + \gamma\Upsilon + \omega_{\alpha\boldsymbol{k}})[C^2_{\boldsymbol{k}} + \omega^2_{\alpha\boldsymbol{k}} - (A_{\boldsymbol{k}} - \gamma\Upsilon)^2]}, \tag{4.14}$$

$$\frac{Q_{23}}{Q_{11}} = \frac{-2B_{\boldsymbol{k}}C_{\boldsymbol{k}}(A_{\boldsymbol{k}} + \omega_{\alpha\boldsymbol{k}})}{(A_{\boldsymbol{k}} - \gamma\Upsilon + \omega_{\alpha\boldsymbol{k}})B^2_{\boldsymbol{k}} + (A_{\boldsymbol{k}} + \gamma\Upsilon + \omega_{\alpha\boldsymbol{k}})[C^2_{\boldsymbol{k}} + \omega^2_{\alpha\boldsymbol{k}} - (A_{\boldsymbol{k}} - \gamma\Upsilon)^2]}, \tag{4.15}$$

$$\frac{Q_{13}}{Q_{11}} = \frac{C_{\boldsymbol{k}}[(A_{\boldsymbol{k}} - \gamma\Upsilon)^2 - \omega^2_{\alpha\boldsymbol{k}} + B^2_{\boldsymbol{k}} - C^2_{\boldsymbol{k}}]}{(A_{\boldsymbol{k}} - \gamma\Upsilon + \omega_{\alpha\boldsymbol{k}})B^2_{\boldsymbol{k}} + (A_{\boldsymbol{k}} + \gamma\Upsilon + \omega_{\alpha\boldsymbol{k}})[C^2_{\boldsymbol{k}} + \omega^2_{\alpha\boldsymbol{k}} - (A_{\boldsymbol{k}} - \gamma\Upsilon)^2]}, \tag{4.16}$$

$$\frac{Q_{12}}{Q_{22}} = \frac{B_{\boldsymbol{k}}[(A_{\boldsymbol{k}} + \gamma\Upsilon - \omega_{\beta\boldsymbol{k}})(A_{\boldsymbol{k}} - \gamma\Upsilon + \omega_{\beta\boldsymbol{k}}) - B^2_{\boldsymbol{k}} + C^2_{\boldsymbol{k}}]}{(A_{\boldsymbol{k}} + \gamma\Upsilon + \omega_{\beta\boldsymbol{k}})B^2_{\boldsymbol{k}} + (A_{\boldsymbol{k}} - \gamma\Upsilon + \omega_{\beta\boldsymbol{k}})[C^2_{\boldsymbol{k}} + \omega^2_{\beta\boldsymbol{k}} - (A_{\boldsymbol{k}} + \gamma\Upsilon)^2]}, \tag{4.17}$$

$$\frac{Q_{14}}{Q_{22}} = \frac{-2B_{\boldsymbol{k}}C_{\boldsymbol{k}}(A_{\boldsymbol{k}} + \omega_{\beta\boldsymbol{k}})}{(A_{\boldsymbol{k}} + \gamma\Upsilon + \omega_{\beta\boldsymbol{k}})B^2_{\boldsymbol{k}} + (A_{\boldsymbol{k}} - \gamma\Upsilon + \omega_{\beta\boldsymbol{k}})[C^2_{\boldsymbol{k}} + \omega^2_{\beta\boldsymbol{k}} - (A_{\boldsymbol{k}} + \gamma\Upsilon)^2]}, \tag{4.18}$$

$$\frac{Q_{24}}{Q_{22}} = \frac{C_{\boldsymbol{k}}[(A_{\boldsymbol{k}} + \gamma\Upsilon)^2 - \omega^2_{\beta\boldsymbol{k}} + B^2_{\boldsymbol{k}} - C^2_{\boldsymbol{k}}]}{(A_{\boldsymbol{k}} + \gamma\Upsilon + \omega_{\beta\boldsymbol{k}})B^2_{\boldsymbol{k}} + (A_{\boldsymbol{k}} - \gamma\Upsilon + \omega_{\beta\boldsymbol{k}})[C^2_{\boldsymbol{k}} + \omega^2_{\beta\boldsymbol{k}} - (A_{\boldsymbol{k}} + \gamma\Upsilon)^2]}, \tag{4.19}$$

$$Q^2_{11} = \frac{{Q'_{12}}^2 - {Q'_{14}}^2 - {Q'_{24}}^2 + 1}{(1 - {Q'_{24}}^2)(1 - {Q'_{13}}^2) + ({Q'_{14}}^2 - {Q'_{12}}^2)({Q'_{21}}^2 - {Q'_{23}}^2)}, \tag{4.20}$$

$$Q_{22}^2 = \frac{{Q'_{21}}^2 - {Q'_{23}}^2 - {Q'_{13}}^2 + 1}{(1-{Q'_{24}}^2)(1-{Q'_{13}}^2) + ({Q'_{14}}^2 - {Q'_{12}}^2)({Q'_{21}}^2 - {Q'_{23}}^2)}, \tag{4.21}$$

where Q_{11} and Q_{22} have been expressed with reduced Q'-coefficients

$$\frac{Q_{21}}{Q_{11}} \equiv Q'_{21}, \quad \frac{Q_{23}}{Q_{11}} \equiv Q'_{23}, \quad \frac{Q_{13}}{Q_{11}} \equiv Q'_{13}, \tag{4.22}$$

$$\frac{Q_{12}}{Q_{22}} \equiv Q'_{12}, \quad \frac{Q_{14}}{Q_{22}} \equiv Q'_{14}, \quad \frac{Q_{24}}{Q_{22}} \equiv Q'_{24}. \tag{4.23}$$

This convention is introduced in addition to not expressing Q_{11} and Q_{22} by the effective fields, due to the complexity of the expressions.

4.2 Magnon growth due to PPP

Now the system Hamiltonian is given by

$$H = \varepsilon_0 + \sum_{\boldsymbol{k}} \hbar(\omega_{\alpha\boldsymbol{k}}\alpha^\dagger_{\boldsymbol{k}}\alpha_{\boldsymbol{k}} + \omega_{\beta\boldsymbol{k}}\beta^\dagger_{\boldsymbol{k}}\beta_{\boldsymbol{k}}) + H_p(t). \tag{4.24}$$

Now, we wish to learn how the parallel parametric pumping influences the growth of magnons in the general hard-axis antiferromagnet. We therefore aim to determine the rate of change of the magnon density. We start with analyzing the simplest case in which there are only excitations of α-magnons. By determining the equation of motion from the Heisenberg equation for $\alpha_{\boldsymbol{k}}$ and $\alpha^\dagger_{\boldsymbol{k}}$ we can find the characteristic growing of magnons due to parallel parametric pumping. We use the Heisenberg equation with our expanded Hamiltonian

$$i\hbar\dot{O} = [O, H], \tag{4.25}$$

and acquire the following equations

$$i\hbar\frac{\partial\alpha_{\boldsymbol{k}}}{\partial t} = \hbar\omega_{\alpha\boldsymbol{k}}\alpha_{\boldsymbol{k}} + A_{1\boldsymbol{k}}\alpha^\dagger_{-\boldsymbol{k}} + B_{1\boldsymbol{k}}\beta^\dagger_{-\boldsymbol{k}} + B_{2\boldsymbol{k}}\beta_{\boldsymbol{k}}, \tag{4.26}$$

$$-i\hbar\frac{\partial\alpha^\dagger_{\boldsymbol{k}}}{\partial t} = \hbar\omega_{\alpha\boldsymbol{k}}\alpha_{\boldsymbol{k}^\dagger} + A^*_{1\boldsymbol{k}}\alpha_{-\boldsymbol{k}} + B^*_{1\boldsymbol{k}}\beta_{-\boldsymbol{k}} + B^*_{2\boldsymbol{k}}\beta_{\boldsymbol{k}^\dagger}, \tag{4.27}$$

where hence forth the summation over all $\boldsymbol{k}$ on the right-hand-side is implicit. Before advancing, we familiarize ourselves with the density of magnons $n_{\alpha\boldsymbol{k}} = \alpha^\dagger_{\boldsymbol{k}}\alpha_{\boldsymbol{k}}$, and also the convenient pumping operator $P_{\boldsymbol{k}}(t) = \alpha_{\boldsymbol{k}}\alpha_{-\boldsymbol{k}}$ [51] as it will make the upcoming calculatory efforts easier. The rate of change of the magnon density is given by

$$\begin{aligned} i\hbar\frac{\partial n_{\alpha\boldsymbol{k}}}{\partial t} &= i\hbar\frac{\partial\alpha^\dagger_{\boldsymbol{k}}}{\partial t}\alpha_{\boldsymbol{k}} + i\hbar\alpha^\dagger_{\boldsymbol{k}}\frac{\partial\alpha_{\boldsymbol{k}}}{\partial t} \\ &= -2i\hbar\eta n_{\alpha\boldsymbol{k}} + A_{1\boldsymbol{k}}P^\dagger_{\boldsymbol{k}}(t) - A^*_{1\boldsymbol{k}}P_{\boldsymbol{k}}(t), \end{aligned} \tag{4.28}$$

where we've set $\omega_{\alpha\boldsymbol{k}} \to \omega_{\alpha\boldsymbol{k}} - i\eta$ and neglected every term containing a $\beta_{\boldsymbol{k}}$-operator, as we only analyze pairs of excited α-magnons. The first step to eliminate the pumping operators in eq. (4.28) is finding

$$i\hbar\frac{\partial P_{\boldsymbol{k}}(t)}{\partial t} = 2\hbar(\omega_{\alpha\boldsymbol{k}} - i\eta)P_{\boldsymbol{k}}(t) + A_{1\boldsymbol{k}}(2n_{\alpha\boldsymbol{k}} + 1) \tag{4.29}$$

and rewriting the pumping term as $P_{\boldsymbol{k}}(t) = P_{\boldsymbol{k}} e^{-i\omega_p t}$. Eq. (4.29) is now given by

$$\hbar\omega_p P_{\boldsymbol{k}} e^{-i\omega_p t} = 2\hbar(\omega_{\alpha\boldsymbol{k}} - i\eta) P_{\boldsymbol{k}} e^{-i\omega_p t} + A_{1\boldsymbol{k}}(2n_{\alpha\boldsymbol{k}} + 1), \tag{4.30}$$

and we solve for $P_{\boldsymbol{k}}(t)$ and $P^{\dagger}_{\boldsymbol{k}}(t)$

$$P_{\boldsymbol{k}} e^{-i\omega_p t} = \frac{A_{1\boldsymbol{k}}(2n_{\alpha\boldsymbol{k}} + 1)}{\hbar[(\omega_p - 2\omega_{\alpha\boldsymbol{k}}) + 2i\eta]}, \tag{4.31}$$

$$\Rightarrow P^{\dagger}_{\boldsymbol{k}} e^{i\omega_p t} = \frac{A^{*}_{1\boldsymbol{k}}(2n_{\alpha\boldsymbol{k}} + 1)}{\hbar[(\omega_p - 2\omega_{\alpha\boldsymbol{k}})^2 + 4\eta^2]} \bigg((\omega_p - 2\omega_{\alpha\boldsymbol{k}}) + 2i\eta \bigg). \tag{4.32}$$

The rate of change of the magnon density then takes the form

$$\frac{\partial n_{\alpha\boldsymbol{k}}}{\partial t} = -2\eta n_{\alpha\boldsymbol{k}} + \frac{|A_{1\boldsymbol{k}}|^2}{\hbar^2}(2n_{\alpha\boldsymbol{k}} + 1)\frac{4\eta}{(\omega_p - 2\omega_{\alpha\boldsymbol{k}})^2 + 4\eta^2}, \tag{4.33}$$

which in turn with the pumping coefficient found in eq. (4.10) can be written

$$\begin{aligned} \frac{\partial n_{\alpha\boldsymbol{k}}}{\partial t} &= -2\eta n_{\alpha\boldsymbol{k}} + \frac{|h(t)p(\boldsymbol{k})|^2}{\hbar^2}(2n_{\alpha\boldsymbol{k}} + 1)\frac{4\eta}{(\omega_p - 2\omega_{\alpha\boldsymbol{k}})^2 + 4\eta^2}, \\ &= -2\eta n_{\alpha\boldsymbol{k}} + \frac{h^2|p(\boldsymbol{k})|^2}{\hbar^2}(2n_{\alpha\boldsymbol{k}} + 1)\frac{4\eta}{(\omega_p - 2\omega_{\alpha\boldsymbol{k}})^2 + 4\eta^2}, \end{aligned} \tag{4.34}$$

where $p(\boldsymbol{k}) \equiv Q_{21}(\boldsymbol{k})Q_{23}(\boldsymbol{k}) - Q_{11}(\boldsymbol{k})Q_{13}(\boldsymbol{k})$ for convenience and the pumping field amplitude h is assumed to be non-imaginary.

Chapter 5

The magnon condensate and the thermal cloud

After the successful creation of Bose-Einstein condensation (BEC) in a trapped atomic gas in 1995, the amount of research on ultracold quantum gases has been enormous. Many of the theoretical studies however, have ignored the dynamical implications of thermally excited atoms. Most of both the experimental and the theoretical research has concentrated on gases at temperatures well below the BEC transition temperature T_{BEC}, where the effective end result is a pure Bose condensate. In these experiments, the fraction of noncondensate atoms of the total number of atoms can be as small as 10% [52]. As the thermal cloud is spread over a considerably larger spatial region compared with the condensate localized at the centre of the trapping potential, as illustrated in Fig. 5.1, the thermally excited magnons amount to a negligable low-density cloud. Thus the studies tend to concentrate entirely on the condensate degree of freedom, as this region is very rich in physics. However, as demonstrated by Griffin, Nikuni and Zaremba [52], one may evaluate the new physics which arises from the correlated motions of the condensate and noncondensate degrees of freedom by limiting the starting point to a relatively simple microscopic model. In this chapter, we introduce a system of coupled equations for the condensate and the thermal cloud coupled with the parametric parallel pumping. The equations will be evaluated in thermal equilibrium and at the steady state limit.

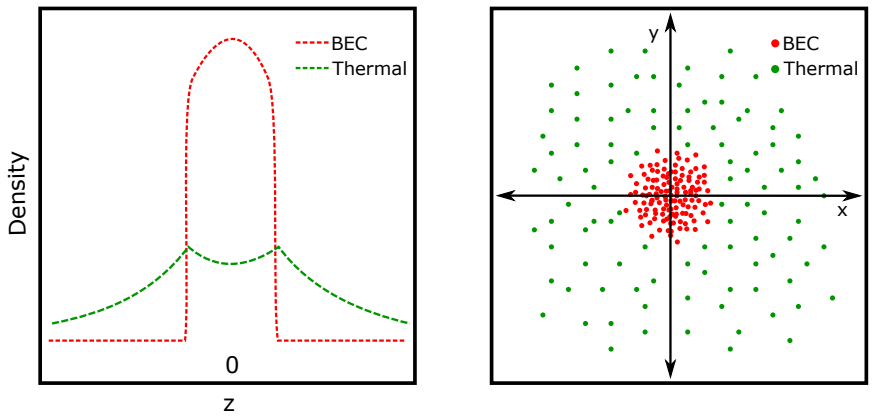

Figure 5.1: Illustrative renditions of the fractions of condensate magnons (red particles) compared to thermal magnons (green particles). The left plot illustrates the high concentration of condensate magnons in the center of the Brilluoin zone compared to the thermal cloud. The right plot illustrates the spatial regions the thermal and condensate magnons occupy with notably different densities.

5.1 Bose-Einstein Condensation

The statistics of a dilute gas follow quantum mechanical rules if the individual particle's wave packets are large enough to overlap [13]. The indistinguishability of identical particles is the cause to the resulting quantum mechanical properties. Whether the particles are bosons or fermions determines a drastically different behaviour. As the behaviour of fermions is irrelevant in the scope of this thesis, we will not delve deeper into this behaviour. As shown in the illustration in Fig. 5.2, each particle in a classical gas has its own energy and the ability to move freely. Bosons are allowed to have the same energy simultaneously. If the gas cools down, the particle energies naturally decrease. Now their quantum nature causes the particles to behave as waves. As the temperature decreases, the waves increase in size. At sufficiently low temperatures, the extent of the waves grows larger than the mean distance between two particles. When the gas reaches a very low temperature, a large fraction of the bosons occupy the same quantum state at the same energy level. They condense into a single collective quantum wave known as a Bose-Einstein condensate. This joint wave formed from microscopic bosons is apparent macroscopically. This transition occurs below a critical temperature, which can be determined from finding the gas degeneracy using Bose-Einstein statistics in a Bose gas [13], as introduced in (3.1). A three-dimensional uniform gas of non-interacting bosons with no evident internal degrees of freedom obides by the critical temperature

$$T_{\mathrm{BEC}} = \frac{2\pi\hbar^2}{mk_B}\left(\frac{n_p}{\zeta(3/2)}\right) \approx 3.3125\frac{\hbar^2 n^{2/3}}{mk_B}, \tag{5.1}$$

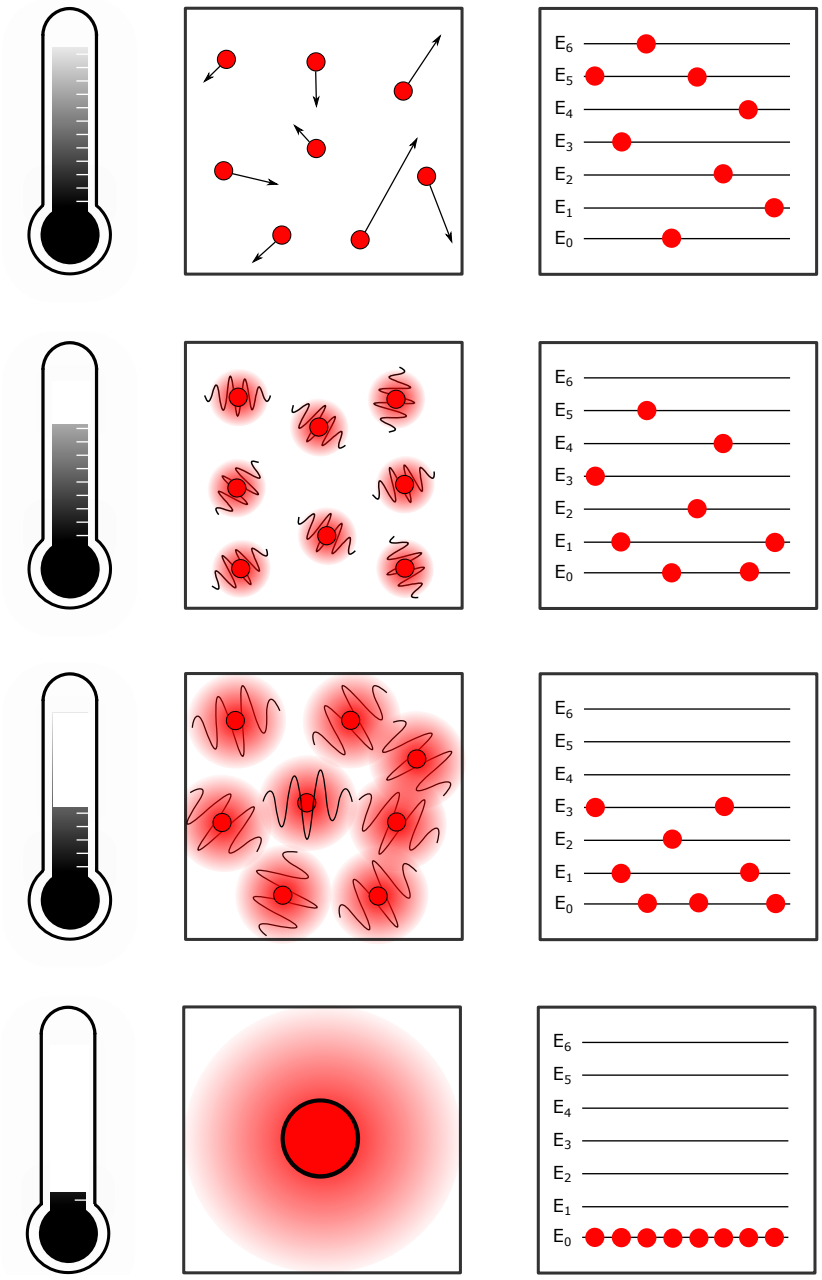

Figure 5.2: A four-stage illustration of Bose-Einstein condensation. At a high temperature, particles move freely. As the temperature sinks, so does the energy of the particles and they develop wave-like behaviour. As the temperature continues to sink, the waves continue to expand, and at a sufficient temperature, T_{BEC}, the particles condense into a collective wave known as a Bose-Einstein condensate.

where T_{BEC} is the critical temperature; n_p is the particle density characterized with the subscript p to differentiate it from the thermal density n; m is the singular boson mass, and $\zeta(s)$ is the Riemann zeta function

$$\zeta(s) = \sum_{n=1}^{\infty} \frac{1}{n^s}. \tag{5.2}$$

5.1.1 The Bose macroscopic wavefunction and the single-particle distribution function

The theoretical framework of our model of interacting Bose-condensed fluids will be expressed using quantum field operators, $\hat{\psi}$. The initial approach by Nikolay Bogoliubov [53], formalized and systematized by Spartak Beliav [54, 55] and many others [56–58], was to isolate the condensate component in the quantum field operators. With

$$\hat{\psi}(\boldsymbol{r}) = \langle \hat{\psi}(\boldsymbol{r}) \rangle + \tilde{\psi}(\boldsymbol{r}), \tag{5.3}$$

where

$$\langle \hat{\psi}(\boldsymbol{r}) \rangle \equiv \Phi(\boldsymbol{r}), \tag{5.4}$$

represents the Bose macroscopic wavefunction and $\tilde{\psi}(\boldsymbol{r})$ describes the fluctuations around Φ. The Bose macroscopic wavefunction is the two-component "order parameter" for the Bose superfluid phase transition:

$$\Phi(\boldsymbol{r}) \begin{cases} 0, & \text{if } T > T_{\mathrm{BEC}}, \\ \neq 0, & \text{if } T < T_{\mathrm{BEC}}, \end{cases} \tag{5.5}$$

where $\Phi(\boldsymbol{r}) = \sqrt{\rho} e^{i\theta}$ has an amplitude dependent on the condensate density ρ and a phase [58]. Rather than identifying as a Fock state of fixed N without a well-defined phase, this condensate wavefunction is a coherent state, with a "clamped" phase-value. The definition of the thermal average $\langle \hat{\psi}(\boldsymbol{r}) \rangle$ involves the introduction of some small symmetry-breaking perturbation H_{SB} that allows the Bose wavefunction to be finite,

$$H_{\mathrm{SB}} = \lim_{\eta \to 0} \int \mathrm{d}\boldsymbol{r} \left[\eta(\boldsymbol{r}) \hat{\psi}^{\dagger}(\boldsymbol{r}) + \eta^*(\boldsymbol{r}) \hat{\psi}(\boldsymbol{r}) \right]. \tag{5.6}$$

Since quantum fluctuations are insignificant with a large number of condensate atoms N_c in the single-particle condensate wavefunction, the order parameter $\Phi(\boldsymbol{r})$ acts like a classical field. Generic two-fluid hydrodynamics was developed by Lev Davidovitsj Landau by generalizing the standard theory of classical hydrodynamics to incorporate the equations of motion for the new "superfluid" degree of freedom, see [59]. Subsequent to the work of Ludwig Boltzmann and James Clerk Maxwell in the 1880s [60], a fluid may be described hydrodynamically by just the local density $n(\boldsymbol{r}, t)$ and the local velocity $\boldsymbol{v}(\boldsymbol{r}, t)$ if the collisions between the particles are of a large enough magnitude to produce "local equilibrium". By introducing a kinetic equation in this microscopic basis, Boltzmann managed to describe the behaviour of atoms in a dilute classical gas in nonequilibrium. He proposed the idea that the process towards thermal equilibrium for such a gas would

involve several distinct stages. Even though the initial dynamics is rather complex, the gas eventually reaches the manageable "kinetic" stage. The system may then be characterised by a single-particle distribution function $f(\boldsymbol{p}, \boldsymbol{r}, t)$, which is given by solving the kinetic equation Boltzmann introduced. The general structure of said equation is given by

$$\mathscr{L} f(\boldsymbol{p}, \boldsymbol{r}, t) = C[f(\boldsymbol{p}, \boldsymbol{r}, t)], \tag{5.7}$$

where $\mathscr{L}$ is a differential operator, and C is a collision integral functional of $f(\boldsymbol{p}, \boldsymbol{r}, t)$. $\mathscr{L}$ outlines the dynamical changes caused by external (and internal if it is self-induced) fields in $f(\boldsymbol{p}, \boldsymbol{r}, t)$ over time. If the collision integral is negligible in a first approximation,

$$\mathscr{L} f = 0, \tag{5.8}$$

then f is the solution to the so-called *collisionless* limit. If f takes on a special form $f = \tilde{f}$, the system reaches the opposite limit,

$$C[\tilde{f}] = 0, \tag{5.9}$$

where $\tilde{f}$ is determined by the collisions. Note that these limits are in no sense based on the same conditions. Whereas the collision term in (5.7) is entirely neglected, the integral is in general finite. It vanishes in (5.9) as $\tilde{f}$ is the unique solution in local equilibrium enforced by rapid collisions. This special distribution function is indistinguishable from the Bose distribution. $\tilde{f}$ describes thermal equilibrium, with the thermodynamic variables such as chemical potential, temperature and pressure now being dependent on position and time. These local parameters characterize the domain the system reaches before complete thermal equilibrium, the so-called "local hydrodynamic equilibrium" (hydrodynamic stage).

In this thesis, we study a dilute trapped Bose gas at finite temperatures composed of a Bose-Einstein condensate and a thermal cloud (the noncondensate) under influence of a parametric parallel pumping field. The main goal is to investigate the chemical potential, μ, and map its dependency of the pumping field amplitude h. It is of paramount interest in BEC experiments to know which values of the pumping field parameters invoke the proper chemical potential. To realize this dependency, an equation of motion for the entire coupled system is needed. The condensate and the thermal cloud alone satisfy quite different equations of motions. The condensate is best described by the Gross-Pitaevskii equation and the thermal magnons by the Boltzmann equation [52]. We will show that these equations can be strongly coupled, and that this coupling brings in a whole new class of phenomena.

5.2 The equations of motion for the condensate density

As previously stated, the BEC order parameter $\Phi(\boldsymbol{r}, t)$ plays a central role in the theories of collective oscillations of atomic condensates. In 1961, Eugene P. Gross and Lev P. Pitaevskii, independently of each other [61, 62], demonstrated the first extension of Beliaevs general quantum field theoretic formalism [54] for the BEC order parameter. This extension led to the famous Gross-Pitaevskii (GP) equation of motion for $\Phi(\boldsymbol{r}, t)$, which

could be used with nonuniform Bose condensates. In order to catalog the generalizations made in the following subsections, we establish the Hartree GP equation at T = 0, ergo in a gas with a negligible thermal cloud

$$i\hbar\frac{\partial\Phi(\boldsymbol{r},t)}{\partial t} = \Big[-\frac{\hbar^2\nabla^2}{2m} + V_{\mathrm{trap}}(\boldsymbol{r}) + V_{\mathrm{H}}(\boldsymbol{r},t)\Big]\Phi(\boldsymbol{r},t), \tag{5.10}$$

where m is the mass of a condensate atom. The trapping potential describes an anisotropic harmonic potential of the form

$$V_{\mathrm{trap}}(\boldsymbol{r}) = \frac{1}{2}m(\omega_x^2x^2 + \omega_y^2y^2 + \omega_z^2z^2), \tag{5.11}$$

in terms of the three trap frequencies ω_i. We will however assume the potential to be a constant position invariant magnon gap $V_{\mathrm{trap}}(\boldsymbol{r}) = \varepsilon_0$ for the rest of the thesis. The last term is the self-consistent condensate Hartree potential

$$V_{\mathrm{H}}(\boldsymbol{r},t) = \int \mathrm{d}\boldsymbol{r}^{'}v\big(\boldsymbol{r}-\boldsymbol{r}^{'}\big)\rho(\boldsymbol{r},t), \tag{5.12}$$

where $v\big(\boldsymbol{r}-\boldsymbol{r}^{'}\big)$ is the interatomic potential and $\rho(\boldsymbol{r},t)$ is the condensate density expressed by the macroscopic wavefunction as $\rho(\boldsymbol{r},t) = |\Phi(\boldsymbol{r},t)|^2$. When dealing with extremely low energy atoms at the ultracold temperatures relevant to BEC experiments, we can use s-wave approximation to rewrite the interatomic potential [63]. For low energy scattering an established doctrine is the assumption that only the waves of the s-orbitals take part in the scattering process [64]. As a result, the interatomic potential can be described by a pseudopotential

$$\begin{aligned} v\big(\boldsymbol{r}-\boldsymbol{r}^{'}\big) &= \frac{4\pi a\hbar^2}{m}\delta\big(\boldsymbol{r}-\boldsymbol{r}^{'}\big), \\ &\equiv g\delta\big(\boldsymbol{r}-\boldsymbol{r}^{'}\big), \end{aligned} \tag{5.13}$$

where a is the s-wave scattering length and g is defined as the coupling constant. Since $m = \hbar^2/2a$ [51], g can be expressed solely by a as $g = 8\pi a^2$. The s-wave scattering length for magnon-magnon interaction is however not well understood [48, 63, 65], so to determine a tentative magnitude of g in chapter 6, the coupling constant may be estimated by the assumption [51]

$$g \sim \frac{D}{2N}, \tag{5.14}$$

where D is the estimated magnitude of the anisotropy constants in the antiferromagnetic Hamiltonian introduced in Eq. (3.11) and $2N$ is the total number of spins in the system, as we previously have defined N as the number of spins in each sublattice. The initial GP-equation (5.10) produced with the condensate density expressed by the Bose order parameter takes the form of a nonlinear Schrödinger equation for $\Phi(\boldsymbol{r},t)$ given by

$$i\hbar\frac{\partial\Phi(\boldsymbol{r},t)}{\partial t} = \Big[-\frac{\hbar^2\nabla^2}{2m} + \varepsilon_0 + g|\Phi(\boldsymbol{r},t)|^2\Big]\Phi(\boldsymbol{r},t). \tag{5.15}$$

The next step is to incorporate the thermal cloud of magnons. Achieving a set of coupled equations that describe the system realistically is not a cakewalk. Therefore, the thermal cloud will in this thesis be described by one of the simpler microscopic model approximations that captures the prominent physics. By considering only temperatures high enough ($T \geq 0.4T_{BEC}$), it is possible using a particle-like Hartree-Fock (HF) spectrum to describe the noncondensate atoms [66]. Under these finite temperatures, the thermal cloud can be described by the Boltzmann equation for the single-particle distribution function $f(\boldsymbol{p}, \boldsymbol{r}, t)$. Firstly, in order to derive a generalized GP equation, we use the Heisenberg equation of motion for the quantum field operator $\hat{\psi}(\boldsymbol{r}, t)$

$$i\hbar \frac{\partial \hat{\psi}(\boldsymbol{r}, t)}{\partial t} = \left[-\frac{\hbar^2 \nabla^2}{2m} + \varepsilon_0 \right] \hat{\psi}(\boldsymbol{r}, t) + g\hat{\psi}^\dagger(\boldsymbol{r}, t)\hat{\psi}(\boldsymbol{r}, t)\hat{\psi}(\boldsymbol{r}, t), \tag{5.16}$$

where ε_0 is the confining potential, and the assumption that the interaction potential can be described by the zero-range pseudopotential strength $g = 4\pi a\hbar^2/m$ still holds. As the condensate wavefunction is the expectation value of the quantum field operator, $\Phi(\boldsymbol{r}, t) = \langle \hat{\psi}(\boldsymbol{r}) \rangle$, the exact equation for the condensate wavefunction is hence obtained by taking an average of Eq. (5.16)

$$i\hbar \frac{\partial \Phi(\boldsymbol{r}, t)}{\partial t} = \left[-\frac{\hbar^2 \nabla^2}{2m} + \varepsilon_0 \right] \Phi(\boldsymbol{r}, t) + g\langle \hat{\psi}^\dagger(\boldsymbol{r}, t)\hat{\psi}(\boldsymbol{r}, t)\hat{\psi}(\boldsymbol{r}, t) \rangle, \tag{5.17}$$

where the average was taken corresponding to a broken-symmetry ensemble in nonequilibrium. The assumption that the expectation value of the quantum field operator is nonzero is implicit. The last term on the r.h.s. of Eq. (5.17) is easier to analyze by introducing the two component field operator in Eq. (5.3)

$$\hat{\psi}(\boldsymbol{r}, t) = \langle \hat{\psi}(\boldsymbol{r}, t) \rangle + \tilde{\psi}(\boldsymbol{r}, t), \tag{5.18}$$

which yields

$$\hat{\psi}^\dagger \hat{\psi} \hat{\psi} = |\Phi|^2 \Phi + 2|\Phi|^2 \tilde{\psi} + \Phi^2 \tilde{\psi}^\dagger + \Phi^* \tilde{\psi}\tilde{\psi} + 2\Phi \tilde{\psi}^\dagger \tilde{\psi} + \tilde{\psi}^\dagger \tilde{\psi}\tilde{\psi}, \tag{5.19}$$

where the position- and time dependency temporarily is conveniently left out to save space. With $\langle \tilde{\psi}(\boldsymbol{r}, t) \rangle = 0$, the symmetry-breaking average of $\hat{\psi}^\dagger \hat{\psi}\hat{\psi}$ reduces to

$$\langle \hat{\psi}^\dagger \hat{\psi} \hat{\psi} \rangle = \rho\Phi + \tilde{m}\Phi^* + 2n\Phi + \langle \tilde{\psi}^\dagger \tilde{\psi}\tilde{\psi} \rangle, \tag{5.20}$$

where the following quantity definitions apply:

$$\begin{aligned}
&\rho(\boldsymbol{r}, t) \equiv |\Phi(\boldsymbol{r}, t)|^2, \quad \text{the local condensate density;} \\
&n(\boldsymbol{r}, t) \equiv \langle \tilde{\psi}^\dagger(\boldsymbol{r}, t)\tilde{\psi}(\boldsymbol{r}, t) \rangle, \quad \text{the thermal cloud density;} \\
&\tilde{m}(\boldsymbol{r}, t) \equiv \langle \tilde{\psi}(\boldsymbol{r}, t)\tilde{\psi}(\boldsymbol{r}, t) \rangle, \quad \text{the off-diagonal (anomalous) noncondensate density [67].}
\end{aligned} \tag{5.21}$$

Replacing the expectation value in Eq. (5.17) with Eq. (5.20), the generalized GP equation of motion for $\Phi(\boldsymbol{r}, t)$ reads

$$\begin{aligned}
i\hbar \frac{\partial \Phi(\boldsymbol{r}, t)}{\partial t} = &\left[-\frac{\hbar^2 \nabla^2}{2m} + \varepsilon_0 + g\rho(\boldsymbol{r}, t) + 2gn(\boldsymbol{r}, t) \right] \Phi(\boldsymbol{r}, t) \\
&+ g\tilde{m}(\boldsymbol{r}, t)\Phi^* + g\langle \tilde{\psi}^\dagger(\boldsymbol{r}, t)\tilde{\psi}(\boldsymbol{r}, t)\tilde{\psi}(\boldsymbol{r}, t) \rangle,
\end{aligned} \tag{5.22}$$

where $\langle\tilde{\psi}^\dagger\tilde{\psi}\tilde{\psi}\rangle$ is the three-field correlation function [67]. Within the pseudopotential approximation, Eq. (5.22) is a formally exact equation of motion for $\Phi(\boldsymbol{r},t)$. It will however be tedious to work with, unless the effect of the mean field characterised by the off-diagonal density $\tilde{m}$ and $\langle\tilde{\psi}^\dagger\tilde{\psi}\tilde{\psi}\rangle$ is explicitly given for our model. As the current literature regarding BEC in gases under parametric parallel pumping does not provide any exact analytical expressions for $\tilde{m}$ and $\langle\tilde{\psi}^\dagger\tilde{\psi}\tilde{\psi}\rangle$, it is sufficient to limit the scope of these calculations to dominant thermal excitations at finite temperatures. These excitations will be regarded as high-energy noncondensate atoms acting in a self-consistent dynamic HF mean field $U(\boldsymbol{r},t)$ with local energy

$$\begin{aligned}\tilde{\varepsilon}_p(\boldsymbol{r},t) &= \frac{p^2}{2m} + \varepsilon_0 + 2g[\rho(\boldsymbol{r},t) + n(\boldsymbol{r},t)] \\ &\equiv \frac{p^2}{2m} + U(\boldsymbol{r},t) \\ &\equiv \varepsilon_p + U(\boldsymbol{r},t),\end{aligned} \tag{5.23}$$

where $p = |\boldsymbol{p}|$ is the local momentum. The tilde operator will continue to label parameters associated with the noncondensate in this thesis. Under this approximation of the thermal excitations, we neglect the terms in (5.22) of order g^2 or higher. Even though current literature is scarce on intelligible expressions for $\tilde{m}$ and $\langle\tilde{\psi}^\dagger\tilde{\psi}\tilde{\psi}\rangle$, there is high consensus of these quantities to be of order g and thus vanishing in noninteracting Bose gases [52]. Yet, we want to keep the imaginary parts of the three-field correlation function $\langle\tilde{\psi}^\dagger\tilde{\psi}\tilde{\psi}\rangle$ as they describe the collisional damping of the condensate motion. The GGP equation now reads

$$i\hbar\frac{\partial\Phi(\boldsymbol{r},t)}{\partial t} = \left[-\frac{\hbar^2\nabla^2}{2m} + \varepsilon_0 + g\rho(\boldsymbol{r},t) + 2gn(\boldsymbol{r},t)\right]\Phi(\boldsymbol{r},t) + g\mathrm{Im}[\langle\tilde{\psi}^\dagger\tilde{\psi}\tilde{\psi}\rangle], \tag{5.24}$$

however, it does not account for the loss of magnons due to various relaxation processes in the two-fluid gas under influence of a parametric parallel pumping field. Relaxation mechanisms such as scattering of magnons with impurities, magnon-magnon (Umklapp) scattering and magnon-phonon scattering contribute varyingly to magnon conservation and magnon loss. These processes are not well understood, so at small energies one of the more sensible approaches to describe the magnon loss, is by assuming Gilbert damping as the only relaxiation mechanism [68]. In "clean" systems at low temperatures the Landau-Lifshitz-Gilbert phenomenology describes the relaxation accurately [68], leading to the following damping term G_α in the generalized GP equation

$$i\hbar G_\alpha = -i\alpha\hbar\omega_E\Phi(\boldsymbol{r},t), \tag{5.25}$$

where α is the dimensionless Gilbert damping constant and ω_E is the AF resonance frequency. The generalized GP equation (GGP) with the damping term now reads

$$\begin{aligned}i\hbar\frac{\partial\Phi(\boldsymbol{r},t)}{\partial t} = &\left[-\frac{\hbar^2\nabla^2}{2m} + \varepsilon_0 + g\rho(\boldsymbol{r},t) + 2gn(\boldsymbol{r},t) - i\alpha\hbar\omega_E\right]\Phi(\boldsymbol{r},t) \\ &+ g\mathrm{Im}[\langle\tilde{\psi}^\dagger\tilde{\psi}\tilde{\psi}\rangle].\end{aligned} \tag{5.26}$$

Introducing the phase and amplitude variables of $\Phi(\boldsymbol{r},t)=\sqrt{\rho(\boldsymbol{r},t)}e^{i\theta(\boldsymbol{r},t)}$ in Eq. (5.22) one eventually finds the following equations of motion for the condensate density and the condensate velocity on a hydrodynamic form, see Appendix B for full derivation,

$$\hbar\dot{\rho}+\hbar\nabla(\rho\boldsymbol{v}_c)=-\Gamma_{12}[f,\Phi]-2\alpha\hbar\omega_E\rho, \tag{5.27}$$

$$m\nabla\boldsymbol{v}_c=-\nabla\Big(\mu_c+\frac{1}{2}m\boldsymbol{v}_c^2\Big)=-\nabla\varepsilon_c. \tag{5.28}$$

The condensate velocity field is defined as

$$\boldsymbol{v}_c\equiv\frac{\hbar}{m}\frac{\partial\theta}{\partial t}, \tag{5.29}$$

the chemical potential for the condensate μ_c is given by

$$\mu_c(\boldsymbol{r},t)\equiv-\frac{\hbar^2}{2m}\frac{\nabla^2\sqrt{\rho(\boldsymbol{r},t)}}{\sqrt{\rho(\boldsymbol{r},t)}}+\varepsilon_0+g\rho(\boldsymbol{r},t)+2gn(\boldsymbol{r},t), \tag{5.30}$$

and the local energy ε_c of a condensate atom with potential energy μ_c and kinetic energy $\frac{1}{2}m\boldsymbol{v}_c^2$ follows the intuitive definition

$$\varepsilon_c\equiv\mu_c+\frac{1}{2}m\boldsymbol{v}_c^2. \tag{5.31}$$

On the r.h.s. of the condensate density continuity equation in (5.27) a new function has been introduced, namely

$$\Gamma_{12}[f,\Phi]\equiv-2g\mathrm{Im}[\Phi^*\langle\tilde{\psi}^\dagger\tilde{\psi}\tilde{\psi}\rangle]. \tag{5.32}$$

Γ_{12} plays a crucial role, not only as a local "source term" in (5.32), but especially in the behaviour of the condensate in its interaction with the thermal cloud [69–71]. It is clearly a function of both the single-particle distribution function $f(\boldsymbol{p},\boldsymbol{r},t)$ and $\Phi(\boldsymbol{r},t)$, and it can both be positive (condensate damping) or negative (condensate growth). A proper equation for Γ_{12} will be defined in the next chapter. The definition of the superfluid condensate velocity field (5.29) applies at all temperatures for all Bose superfluids. Compared with Bose condensation, the fact that the motion exhibited by the condensate can be identified with the phase gradient is the cornerstone of all of the aspects associated with the "superfluidity" of a Bose superfluid [69]. This means that the motion of the condensate is irrotational, since the curl of a gradient equals zero $\nabla\boldsymbol{v}_c=0$. Instances of velocities with localized singularities corresponding to vortices render the fluid not irrotational, but this case will not be discussed further.

5.3 Equation of motion for the thermal magnon density

Let us derive a kinetic equation for the noncondensate magnons. The dynamics of the thermal fluctuations $\tilde{\psi}(\boldsymbol{r})$ given by the field operator definition in Eq. (5.3) yield the

following equation of motion from the GP-equation in Eq. (5.16)

$$
\begin{aligned}
i\hbar\frac{\partial\tilde{\psi}}{\partial t} = \Big(-\frac{\hbar^2\nabla^2}{2m} + \varepsilon_0 + 2g(\rho+n)\Big)\tilde{\psi} - 2gn\tilde{\psi} + g\Phi^2\tilde{\psi}^\dagger \\
+ g\Phi^*(\tilde{\psi}\tilde{\psi} - \tilde{m}) + 2g\Phi(\tilde{\psi}^\dagger\tilde{\psi} - n) + g\Big(\tilde{\psi}^\dagger\tilde{\psi}\tilde{\psi} - \langle\tilde{\psi}^\dagger\tilde{\psi}\tilde{\psi}\rangle\Big),
\end{aligned}
\tag{5.33}
$$

where the position and time dependencies has temporarily been left out for convenience, and the condition $\langle\tilde{\psi}\rangle = 0$ is preserved as a function of time. We define the time evolution with the unitary operator $\hat{S}(t,t_0)$ following the work of Kirkpatrick and Dorfman [72] on uniform gases by

$$
\tilde{\psi}(\boldsymbol{r},t) = \hat{S}^\dagger(t,t_0)\tilde{\psi}(\boldsymbol{r},t_0)\hat{S}(t,t_0), \tag{5.34}
$$

where $\hat{S}(t,t_0)$ evolves in accordance with to the equation of motion

$$
i\hbar\frac{\mathrm{d}\hat{S}(t,t_0)}{\mathrm{d}t} = \hat{H}_{\mathrm{eff}}(t)\hat{S}(t,t_0) \tag{5.35}
$$

with $\hat{S}(t_0,t_0) = 1$; t_0 is a specified time for the initial nonequilibrium density matrix $\hat{\rho}(t_0)$ and $\hat{H}_{\mathrm{eff}(t)}$ is the effective Hamiltonian given by

$$
\hat{H}_{\mathrm{eff}}(t) = \hat{H}_0(t) + \hat{H}^{'}(t), \tag{5.36}
$$

$$
\hat{H}^{'}(t) = \hat{H}_1(t) + \hat{H}_2(t) + \hat{H}_3(t) + \hat{H}_4(t). \tag{5.37}
$$

$\hat{H}_0(t)$ is the leading Hartree-Fock term, and the remaining four terms are perturbation contributions. Together, these contributions reproduce Eq. (5.33) and read

$$
\hat{H}_0(t) = \int \mathrm{d}\boldsymbol{r}\tilde{\psi}^\dagger\left[-\frac{\hbar^2\nabla^2}{2m} + U(\boldsymbol{r},t)\right]\tilde{\psi}, \tag{5.38}
$$

$$
\hat{H}_1(t) = \int \mathrm{d}\boldsymbol{r}\Big[L_1(\boldsymbol{r},t)\tilde{\psi}^\dagger + L_1^*(\boldsymbol{r},t)\tilde{\psi}\Big], \tag{5.39}
$$

$$
\hat{H}_2(t) = \frac{g}{2}\int \mathrm{d}\boldsymbol{r}\Big[\Phi^2(\boldsymbol{r},t)\tilde{\psi}^\dagger\tilde{\psi}^\dagger + \Phi^{*2}(\boldsymbol{r},t)\tilde{\psi}\tilde{\psi}\Big], \tag{5.40}
$$

$$
\hat{H}_3(t) = g\int \mathrm{d}\boldsymbol{r}\Big[\Phi^*(\boldsymbol{r},t)\tilde{\psi}^\dagger\tilde{\psi}\tilde{\psi} + \Phi^*(\boldsymbol{r},t)\tilde{\psi}^\dagger\tilde{\psi}^\dagger\tilde{\psi}\Big], \tag{5.41}
$$

$$
\hat{H}_4(t) = \frac{g}{2}\int \mathrm{d}\boldsymbol{r}\tilde{\psi}^\dagger\tilde{\psi}^\dagger\tilde{\psi}\tilde{\psi} - 2g\int \mathrm{d}\boldsymbol{r}n(\boldsymbol{r},t)\tilde{\psi}^\dagger\tilde{\psi}, \tag{5.42}
$$

where $U(\boldsymbol{r},t)$ defined in (5.23) serves as the total self-consistent Hartree-Fock (HF) mean field, and $L_1(\boldsymbol{r},t)$ is given by

$$
L_1(\boldsymbol{r},t) \equiv -g\big[2n(\boldsymbol{r},t)\Phi(\boldsymbol{r},t) + \tilde{m}(\boldsymbol{r},t)\Phi^*(\boldsymbol{r},t) + \langle\tilde{\psi}^\dagger\tilde{\psi}\tilde{\psi}\rangle\big]. \tag{5.43}
$$

The arguments of the field operators are $\boldsymbol{r}$ and t_0. The approach in which Eq. (5.36) is constructed manifests $\hat{H}^{'(t)}$ as a perturbation to the zeroth-order contribution $\hat{H}_0(t)$. Note

that the zeroth-order Hamiltonian can be chosen differently. One could define a dynamic Bogoliubov Hamiltonian by combining $\hat{H}_0(t)$ and $\hat{H}_2(t)$, which would be appropriate when working with very low temperatures [52].

The next step is to consider an arbitrary operator $\hat{\mathcal{O}}(t)$ containing any combination of the thermal fluctuation field operators $\tilde{\psi}(\boldsymbol{r},t)$ and $\tilde{\psi}^\dagger(\boldsymbol{r},t)$. A convenient operator would be the local noncondensate density $n(\boldsymbol{r},t) \equiv \tilde{\psi}^\dagger(\boldsymbol{r},t)\tilde{\psi}(\boldsymbol{r},t)$. We can make use of the definition of the time evolution of $\tilde{\psi}$ in Eq. (5.34) and with respect to the initial density matrix $\hat{\rho}(t_0)$, the expectation value of the arbitrary operator can be defined as

$$\begin{aligned}\langle\hat{\mathcal{O}}(t)\rangle \equiv \langle\hat{\mathcal{O}}\rangle_t &= \mathrm{Tr}\hat{\rho}(t_0)\hat{\mathcal{O}}(t) \\ &= \mathrm{Tr}\tilde{\rho}(t,t_0)\hat{\mathcal{O}}(t_0),\end{aligned} \tag{5.44}$$

with $\tilde{\rho}(t,t_0) \equiv \hat{S}(t,t_0)\hat{\rho}(t_0)\hat{S}^\dagger(t,t_0)$ satisfying the following relation [67]

$$i\hbar\frac{\mathrm{d}\tilde{\rho}(t,t_0)}{\mathrm{d}t} = [\hat{H}_{\mathrm{eff}}(t),\tilde{\rho}(t,t_0)]. \tag{5.45}$$

Further, in order to reach a quantum kinetic equation describing the noncondensate, we define the Wigner operator [73]

$$\hat{f}(\boldsymbol{p},\boldsymbol{r},t_0) \equiv \int \mathrm{d}\boldsymbol{r}' e^{i\boldsymbol{p}\boldsymbol{r}'/\hbar}\tilde{\psi}^\dagger(\boldsymbol{r}+\frac{1}{2}\boldsymbol{r}',t_0)\tilde{\psi}(\boldsymbol{r}-\frac{1}{2}\boldsymbol{r}',t_0). \tag{5.46}$$

The Wigner operator expectation value then returns the Wigner distribution function

$$f(\boldsymbol{p},\boldsymbol{r},t) = \mathrm{Tr}\tilde{\rho}(t,t_0)\hat{f}(\boldsymbol{p},\boldsymbol{r},t_0). \tag{5.47}$$

Various nonequilibrium expectation values can be calculated with proper knowledge of this distribution, including the density for the thermal fluctuations

$$n(\boldsymbol{r},t) = \int \frac{\mathrm{d}\boldsymbol{p}}{(2\pi\hbar)^3} f(\boldsymbol{p},\boldsymbol{r},t). \tag{5.48}$$

Introducing this distribution function in Eq. (5.45), the equation of motion for f is

$$\begin{aligned}\frac{\partial f(\boldsymbol{p},\boldsymbol{r},t)}{\partial t} &= \frac{1}{i\hbar}\mathrm{Tr}\tilde{\rho}(t,t_0)[\hat{f}(\boldsymbol{p},\boldsymbol{r},t_0),\hat{H}_{\mathrm{eff}}(t)] \\ &= \frac{1}{i\hbar}\mathrm{Tr}\tilde{\rho}(t,t_0)[\hat{f}(\boldsymbol{p},\boldsymbol{r},t_0),\hat{H}_0(t)] \\ &+ \frac{1}{i\hbar}\mathrm{Tr}\tilde{\rho}(t,t_0)[\hat{f}(\boldsymbol{p},\boldsymbol{r},t_0),\hat{H}'(t)].\end{aligned} \tag{5.49}$$

In the kinetic equation, the term with the zeroth order Hamiltonian $\hat{H}_0(t)$ on the right hand side of Eq. (5.49) is the free-streaming operator. If we assume only slow spatial variation of the self-consistent mean-field $U(\boldsymbol{r},t)$ in Eq. (5.38) for $\hat{H}_0(t)$, then the equation of motion reads

$$\begin{aligned}\frac{\partial f(\boldsymbol{p},\boldsymbol{r},t)}{\partial t} &+ \frac{\boldsymbol{p}}{m}\cdot\nabla_{\boldsymbol{r}} f(\boldsymbol{p},\boldsymbol{r},t) - \nabla U\cdot\nabla_{\boldsymbol{p}} f(\boldsymbol{p},\boldsymbol{r},t) \\ &= \frac{1}{i\hbar}\mathrm{Tr}\tilde{\rho}(t,t_0)[\hat{f}(\boldsymbol{p},\boldsymbol{r},t_0),\hat{H}'(t)],\end{aligned} \tag{5.50}$$

with the right hand side representing the physical picture of the inter-particle collisions on the single-particle distribution function $f(\boldsymbol{p}, \boldsymbol{r}, t)$. This right hand side may after a lengthy exercise be reduced to a binary collision integral [67]

$$\left(\frac{\partial f}{\partial t}\right)\bigg|_{\text{coll}} = C_{12}[f, \Phi] + C_{22}[f], \tag{5.51}$$

where the contributions are given by

$$\begin{aligned} C_{12}[f, \Phi] = \frac{2g^2\rho}{(2\pi)^2\hbar^4} \int \mathrm{d}\boldsymbol{p}_1 \int \mathrm{d}\boldsymbol{p}_2 \int \mathrm{d}\boldsymbol{p}_3 \delta(m\boldsymbol{v}_c + \boldsymbol{p}_1 - \boldsymbol{p}_2 - \boldsymbol{p}_3) \\ \times \delta(\varepsilon_{\boldsymbol{p}_c} + \tilde{\varepsilon}_{\boldsymbol{p}_1} - \tilde{\varepsilon}_{\boldsymbol{p}_2} - \tilde{\varepsilon}_{\boldsymbol{p}_3})[\delta(\boldsymbol{p}_c - \boldsymbol{p}_1) - \delta(\boldsymbol{p}_c - \boldsymbol{p}_2) - \delta(\boldsymbol{p}_c - \boldsymbol{p}_3)] \\ \times [(1 + f_1)f_2 f_3 - f_1(1 + f_2)(1 + f_3)], \end{aligned} \tag{5.52}$$

$$\begin{aligned} C_{22}[f] = \frac{2g^2}{(2\pi)^5\hbar^7} \int \mathrm{d}\boldsymbol{p}_2 \int \mathrm{d}\boldsymbol{p}_3 \int \mathrm{d}\boldsymbol{p}_4 \delta(\boldsymbol{p} + \boldsymbol{p}_2 - \boldsymbol{p}_3 - \boldsymbol{p}_4) \times \\ \delta(\tilde{\varepsilon}_{\boldsymbol{p}} + \tilde{\varepsilon}_{\boldsymbol{p}_2} - \tilde{\varepsilon}_{\boldsymbol{p}_3} - \tilde{\varepsilon}_{\boldsymbol{p}_4})[(1 + f)(1 + f_2)f_3 f_4 - f f_2(1 + f_3)(1 + f_4)], \end{aligned} \tag{5.53}$$

with $\varepsilon_{\boldsymbol{p}_c}$ representing the local condensate energy defined in Eq. (5.31); $\tilde{\varepsilon}_{\boldsymbol{p}_i}$ representing the local nonondensate energy given in Eq. (5.23) and the distribution function following the definition $f_i \equiv f_i[\boldsymbol{p}_i, \boldsymbol{r}, t]$. Again, ρ, $\boldsymbol{v}_c$, $\varepsilon_{\boldsymbol{p}_c}$ and $\tilde{\varepsilon}_{\boldsymbol{p}i}$ are functions of $\boldsymbol{r}$ and t. As these expressions will be used in the context of magnons (which obey Bose statistics), the creation of a magnon indexed i is represented by the statistical factor $1 + f_i$. The destruction of a magnon indexed i is represented by the statistical factor f_i. The collision integrals are generally indexed in the context of the combination of interacting atoms. As one can read from Eq. (5.53), the term describes collisions between two excited atoms with initial momenta $\boldsymbol{p}$ and $\boldsymbol{p}_2$ and final momenta $\boldsymbol{p}_3$ and $\boldsymbol{p}_4$, see Fig. 5.3. These integrals describe the collision of two incoming thermal magnons, exiting as two thermal magnons. Both C_{12} and C_{22} maintain energy and momentum conservation in the collisions. However, in contrast to C_{22}, C_{12} does not conserve the number of condensate atoms. This term expresses the scattering of atoms in and out of the condensate. C_{12} describes the collisions between two thermal magnons resulting in one thermal magnon and one condensate magnon (or the opposite reaction depending on whether the source term is positive or negative). This notation and these subscripts introduced by Kirkpatrick and Dorfman [72] are self-explanatory, when remembering that the momentum $m\boldsymbol{v}_c$ and energy $\varepsilon_{\boldsymbol{p}_c}$ of the one condensate magnon in Fig. 5.3 is characterized from the thermal magnons in Eq. (5.52) with the subscript c.

The kinetic equation (5.50) with the collision integrals now reads

$$\frac{\partial f(\boldsymbol{p}, \boldsymbol{r}, t)}{\partial t} + \frac{\boldsymbol{p}}{m} \cdot \nabla_{\boldsymbol{r}} f(\boldsymbol{p}, \boldsymbol{r}, t) - \nabla U \cdot \nabla_{\boldsymbol{p}} f(\boldsymbol{p}, \boldsymbol{r}, t) = \left(\frac{\partial f(\boldsymbol{p}, \boldsymbol{r}, t)}{\partial t}\right)\bigg|_{\text{coll}}. \tag{5.54}$$

Let us implement the effect of the parametric parallel pumping. In section 4.2, the resulting magnon growth of PPP is given by

$$\frac{\partial n_{\alpha\boldsymbol{k}}}{\partial t} = -2\eta n_{\alpha\boldsymbol{k}} + \frac{h^2|p(\boldsymbol{k})|^2}{\hbar^2}(2n_{\alpha\boldsymbol{k}} + 1)\frac{4\eta}{(\omega_p - 2\omega_{\alpha\boldsymbol{k}})^2 + 4\eta^2}. \tag{5.55}$$

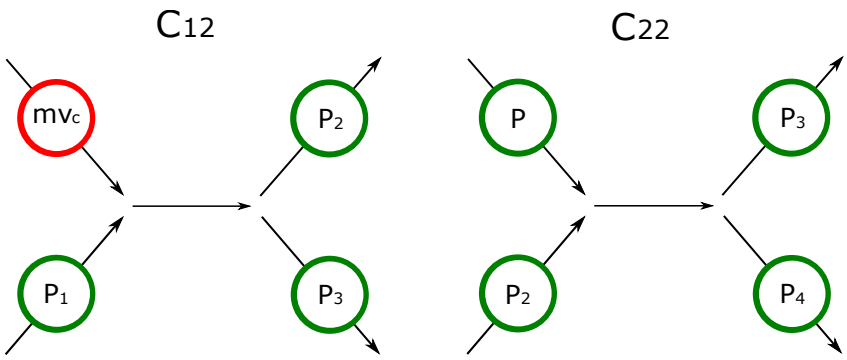

Figure 5.3: Illustration of C_{12}-collisions (left) between one condensate- and one thermal magnon resulting in two thermal magnons, and C_{22}-collisions (right) between two thermal magnons resulting in two thermal magnons.

As the relaxation rate η in this model is rather small, it is beneficial to work in the limit of $\eta \to 0$,

$$\lim_{\eta\to 0} \frac{\partial n_{\alpha \boldsymbol{k}}}{\partial t} = \frac{h^2|p(\boldsymbol{k})|^2}{\hbar^2}(2n_{\alpha\boldsymbol{k}}+1)\delta(\omega_p - 2\omega_{\alpha\boldsymbol{k}}). \tag{5.56}$$

Since Eq. (5.48) expressed in k-space gives $n_{\alpha\boldsymbol{k}} = \int \mathrm{d}\boldsymbol{k} f[\boldsymbol{k},t]$ for the pumping processes of pairs of α-magnons, the pumping term of the Boltzmann equation reads

$$\left(\frac{\partial f[\boldsymbol{k}_0,t]}{\partial t}\right)\bigg|_{\text{pump}} = \frac{\partial}{\partial \boldsymbol{k}}\Big(h^2|p(\boldsymbol{k})|^2(2f[\boldsymbol{k},t]+1)\delta(\omega_p - 2\omega_{\alpha\boldsymbol{k}})/\hbar^2\Big), \tag{5.57}$$

where the $f[\boldsymbol{k}_0,t]$ indicates the dependence of $\boldsymbol{k}$ in the limit of $\eta \to 0$. The coupling between the phonon bath and the thermal cloud also contributes to the damping of the thermal magnons [68]

$$\left(\frac{\partial f[\boldsymbol{k},t]}{\partial t}\right)\bigg|_{\text{phonons}} = -2\alpha\omega_E f[\boldsymbol{k},t] \tag{5.58}$$

where Gilbert damping is assumed. The quantum kinetic equation for the thermal bath in $\boldsymbol{k}$-space now reads

$$\frac{\partial f[\boldsymbol{k},t]}{\partial t} = \left(\frac{\partial f[\boldsymbol{k},t]}{\partial t}\right)\bigg|_{\text{phonons}} + \left(\frac{\partial f[\boldsymbol{k}_0,t]}{\partial t}\right)\bigg|_{\text{pump}} + \left(\frac{\partial f[\boldsymbol{k},t]}{\partial t}\right)\bigg|_{\text{coll}}, \tag{5.59}$$

where we have assumed no driving dc force. We have arrived at the fully descriptive equation of the thermal cloud of magnons influenced by PPP, also known as the Boltzmann equation. If the collision rate is high among the excited magnons, the distribution function is driven efficiently from the collision integral C_{22} towards the local equilibrium Bose distribution

$$\tilde{f}[\boldsymbol{p}_i - m\boldsymbol{v}_n, t] \equiv \tilde{f}[\tilde{\boldsymbol{p}}_i, t] = \frac{1}{e^{\beta[\tilde{\varepsilon}_{\tilde{\boldsymbol{p}}_i} - \tilde{\mu}]} - 1} = \frac{1}{e^{\beta[\varepsilon_{\boldsymbol{p}_i - m\boldsymbol{v}_n} + U - \tilde{\mu}]} - 1}, \tag{5.60}$$

where the local temperature, β, the mean field, $U = \varepsilon_0 + 2g(\rho + n)$, and the chemical potential, $\tilde{\mu}$, for the thermal cloud are all functions of position and time. This solution to the local equilibrium is guaranteed by the condition $C_{22}[\tilde{f}] = 0$, which is proven in Appendix C. Additionally, in Appendix C, we illustrate that the collision integral $C_{12}[\tilde{f}]$ equals

$$\begin{aligned} C_{12}[\tilde{f}] = \frac{2g^2\rho}{(2\pi)^2\hbar^4 k_B T}(\tilde{\mu} - m(\boldsymbol{v}_c - \boldsymbol{v}_n)^2/2 - \mu_c) \int \mathrm{d}\tilde{\boldsymbol{p}}_1 \int \mathrm{d}\tilde{\boldsymbol{p}}_2 \int \mathrm{d}\tilde{\boldsymbol{p}}_3 \\ \times \delta(m\boldsymbol{v}_c + \tilde{\boldsymbol{p}}_1 - \tilde{\boldsymbol{p}}_2 - \tilde{\boldsymbol{p}}_3)\delta(\varepsilon_{\tilde{\boldsymbol{p}}_c} + \tilde{\varepsilon}_{\tilde{\boldsymbol{p}}_1} - \tilde{\varepsilon}_{\tilde{\boldsymbol{p}}_2} - \tilde{\varepsilon}_{\tilde{\boldsymbol{p}}_3}) \\ \times [\delta(\tilde{\boldsymbol{p}}_c - \tilde{\boldsymbol{p}}_1) - \delta(\tilde{\boldsymbol{p}}_c - \tilde{\boldsymbol{p}}_2) - \delta(\tilde{\boldsymbol{p}}_c - \tilde{\boldsymbol{p}}_3)](1 + \tilde{f}_1)\tilde{f}_2\tilde{f}_3. \end{aligned} \tag{5.61}$$

The collisions expressed by this integral tie to the source term Γ_{12} introduced in Eq. (5.32) by integrating them over all momentum space

$$\Gamma_{12}[\tilde{f}, \Phi] = \int \frac{\mathrm{d}\tilde{\boldsymbol{p}}}{(2\pi\hbar)^3} C_{12}[f(\tilde{\boldsymbol{p}}, \boldsymbol{r}, t), \Phi(\boldsymbol{r}, t)]. \tag{5.62}$$

Now, we are ready to integrate the Boltzmann equation over all momentum space by using the distribution function from Eq. (5.60) in Eq. (5.48)

$$n = \int \frac{\mathrm{d}\boldsymbol{p}}{(2\pi\hbar)^3} f(\tilde{\boldsymbol{p}}, t). \tag{5.63}$$

We derive the equation of motion for the thermal density

$$\hbar\dot{n} + 2\alpha\hbar\omega_E n = h^2|p(\boldsymbol{k}_0^p)|^2(2f[\boldsymbol{k}_0^p, t] + 1)/\hbar + \eta(\mu_c + m(\boldsymbol{v}_n - \boldsymbol{v}_c)^2/2 - \tilde{\mu})\rho \tag{5.64}$$

where the notation $\boldsymbol{k}_0^p$ indicates the use of $\boldsymbol{k}_0$ at $\omega_{\alpha\boldsymbol{k}} = \omega_p/2$, and η has been defined as

$$\begin{aligned} \eta = \frac{2g^2}{(2\pi)^5\hbar^7 k_B T} \int \mathrm{d}\tilde{\boldsymbol{p}}_1 \int \mathrm{d}\tilde{\boldsymbol{p}}_2 \int \mathrm{d}\tilde{\boldsymbol{p}}_3 \delta(m\boldsymbol{v}_c + \tilde{\boldsymbol{p}}_1 - \tilde{\boldsymbol{p}}_2 - \tilde{\boldsymbol{p}}_3) \\ \times \delta(\varepsilon_{\tilde{\boldsymbol{p}}_c} + \tilde{\varepsilon}_{\tilde{\boldsymbol{p}}_1} - \tilde{\varepsilon}_{\tilde{\boldsymbol{p}}_2} - \tilde{\varepsilon}_{\tilde{\boldsymbol{p}}_3})(1 + \tilde{f}_1)\tilde{f}_2\tilde{f}_3. \end{aligned} \tag{5.65}$$

Now we shall study the time evolution of the condensate density and the density of thermal magnons. We assume

- $\boldsymbol{v}_n = \boldsymbol{v}_c = 0$,
- high temperature, constant and homogeneous.

By parametric parallel pumping a large amount of magnons are injected into the system. Let us assume the magnon-magnon coupling to be stronger than the phonon bath coupling. This condition allows efficient magnon thermalization to a local equilibrium Bose distribution. A convenient representation of the dynamics of this thermal density is a time-dependent chemical potential $\tilde{\mu} = \mu(t)$ in the Bose distribution

$$f[\boldsymbol{p}, t] = \frac{1}{e^{\beta[\varepsilon_{\boldsymbol{p}} + \varepsilon_0 + 2g(\rho+n) - \mu(t)]} - 1}. \tag{5.66}$$

At high temperatures we make the assumption $\beta\varepsilon(\boldsymbol{p}) \to \beta\bar{\omega}_E|\boldsymbol{p}|$, resulting in the convenient substitution variable $p \equiv |\boldsymbol{p}| = y/(\beta\omega_E)$. We may now express the thermal density

$$\begin{aligned} n(t) &= \int \mathrm{d}\boldsymbol{p} f[\boldsymbol{p},t] \approx \int_0^{2\pi} \mathrm{d}\phi \int_0^{\pi} \mathrm{d}\theta \int_0^{\infty} \mathrm{d}p p^2 \frac{1}{e^y z^{-1}(t) - 1} \\ &= \frac{4\pi}{(\beta\bar{\omega}_E)^3} \int_0^{\infty} \mathrm{d}y \frac{y^2}{e^y z^{-1}(t) - 1} = \frac{4\pi}{(\beta\bar{\omega}_E)^3} \mathrm{Li}_3(z), \end{aligned} \tag{5.67}$$

with the local fugacity $z(t) = e^{-\beta(\varepsilon_0 + 2g(\rho+n) - \mu(t))}$. Note that $n(t)$ on this form is a complicated transcendental function and that a definite value for the noncondensate density is not easily calculated. However, by evaluating the polylogarithm

$$n(t) = \frac{4\pi}{(\beta\bar{\omega}_E)^3} \int_0^{\infty} \mathrm{d}y \frac{y^2}{e^y e^{2\beta g n} e^{\beta(\varepsilon_0 + 2g\rho - \mu(t))} - 1}, \tag{5.68}$$

it is clear that the n-dependence of $z(t)$ only contributes to the polylogarithm if $|2\beta g n| \gg 0$. The magnitudes of β and g roughly cancels and the preliminaries for BEC dictate a small n. This is confirmed by the prefactor $\frac{4\pi}{(\beta\bar{\omega}_E)^3}$ and it is reasonable to assume

$$e^{2\beta g n} \simeq 1, \quad \Rightarrow \quad z(t) = e^{-\beta(\varepsilon_0 + 2g\rho - \mu(t))}. \tag{5.69}$$

Luckily, this approximation will render unnecessary in this thesis, as we will show that the transcendence of n is eliminated in the steady state limit. The equations of motion for the condensate and non-condensate are

$$\dot{\rho} + 2\alpha\hbar\omega_E \rho = -\eta(\mu_c - \mu)\rho, \tag{5.70}$$

$$\hbar\dot{n} + 2\alpha\hbar\omega_E n = \frac{\hbar^2 |p(\boldsymbol{k}_0^p)|^2}{\hbar} \left(\frac{e^{\beta[\varepsilon_{\boldsymbol{p}_0} + \varepsilon_0 + 2g(\rho+n) - \mu(t)]} + 1}{e^{\beta[\varepsilon_{\boldsymbol{p}_0} + \varepsilon_0 + 2g(\rho+n) - \mu(t)]} - 1} \right) + \eta(\mu_c - \mu)\rho, \tag{5.71}$$

with the chemical potential given by Eq. (5.30) and $\varepsilon_{\boldsymbol{p}_0}$ is the local energy at $\boldsymbol{p}_0 = \hbar\boldsymbol{k}_0^p$.

Chapter 6

The chemical potential in the steady state limit

In this chapter, we examine the chemical potential for the coupled clouds in the steady state limit. First, the expressions for the pumping field strength and the chemical potential will be derived, and a set of default magnitudes for the parameters of these expressions will be chosen. The relative influence of some of the parameters on μ and h will be illustrated, and we determine whether their expressions may be simplified without losing any generality in the steady state limit.

6.1 The steady state limit

In the steady state limit, where both the superfluid and the non-condensate have constant densities, i.e., $\dot{\rho} = 0$ and $\dot{n} = 0$, the condensate chemical potential from Eq. (5.30) reduces to

$$\mu_c = \varepsilon_0 + g(\rho + 2n). \tag{6.1}$$

Further, the equation of motion for ρ in Eq. (5.70) solved for the chemical potential μ reads

$$\mu = \varepsilon_0 + g(\rho + 2n) + \frac{2\alpha\hbar\omega_E}{\eta}. \tag{6.2}$$

As foreshadowed in the last chapter, this μ cancels the transcendence of n in Eq. (5.67), which now is given by

$$n = \frac{4\pi}{(\beta\bar{\omega}_E)^3}\mathrm{Li}_3\left[e^{-\beta\left(g\rho - \frac{2\alpha\hbar\omega_E}{\eta}\right)}\right], \tag{6.3}$$

and in turn renders μ as

$$\mu = \varepsilon_0 + g\left(\frac{8\pi}{(\beta\bar{\omega}_E)^3}\mathrm{Li}_3\left[e^{-\beta\left(g\rho - \frac{2\alpha\hbar\omega_E}{\eta}\right)}\right] + \rho\right) + \frac{2\alpha\hbar\omega_E}{\eta}. \tag{6.4}$$

Last, the equation of motion (5.71) for n returns an expression for h, which reads

$$h = \sqrt{\frac{2\alpha\hbar^2\omega_E}{|p(\boldsymbol{k}_0^p)|^2}\left(\frac{4\pi}{(\beta\bar{\omega}_E)^3}\mathrm{Li}_3\left[e^{-\beta\left(g\rho-\frac{2\alpha\hbar\omega_E}{\eta}\right)}\right]+\rho\right)\left(1-\frac{2}{e^{\beta\left[\frac{\boldsymbol{P}_0^2}{2m}+g\rho-\frac{2\alpha\hbar\omega_E}{\eta}\right]}+1}\right)}. \tag{6.5}$$

Let us investigate the following equations of motions to determine how the chemical potential of the thermal magnons μ is influenced by the pumping field amplitude h. In order to calculate the pumping coefficient $|p(\boldsymbol{k}_0^p)|^2$, we first determine $\boldsymbol{k}_0^p$. As established in Eq. (5.64) the p-label of $\boldsymbol{k}_0^p$ defines it as the $\pm\boldsymbol{k}$-value at parallel pumping of alpha magnons only and given at

$$\omega_{\alpha\boldsymbol{k}} = \omega_p/2. \tag{6.6}$$

$\boldsymbol{k}_0^p$ is then found by using Eq. (6.6) in the dispersion relation (3.37),

$$\left(\frac{\omega_p}{2}\right)^2 = A_{\boldsymbol{k}_0^p}^2 + \gamma^2\Upsilon^2 - B_{\boldsymbol{k}_0^p}^2 - C_{\boldsymbol{k}_0^p}^2 + 2\sqrt{\gamma^2(A_{\boldsymbol{k}_0^p}^2 - B_{\boldsymbol{k}_0^p}^2)\Upsilon^2 + B_{\boldsymbol{k}_0^p}^2 C_{\boldsymbol{k}_0^p}^2}. \tag{6.7}$$

Only $B_{\boldsymbol{k}_0^p}$ is dependent of $\boldsymbol{k}_0^p$, so we display $A_{\boldsymbol{k}_0^p}/\gamma \equiv A$ and $C_{\boldsymbol{k}_0^p}/\gamma \equiv C$ as constants and write $B_{\boldsymbol{k}_0^p}$ out to acquire the following relation

$$\left(\frac{\omega_p}{2\gamma}\right)^2 = A^2 + \Upsilon^2 - \gamma_{\boldsymbol{k}_0^p}^2 H_E^2 - C^2 + 2\sqrt{\Upsilon^2 A^2 + \gamma_{\boldsymbol{k}_0^p}^2 H_E^2 (C^2 - \Upsilon^2)}, \tag{6.8}$$

in order to isolate the $\boldsymbol{k}$-dependence. After some algebra $\gamma_{\boldsymbol{k}_0^p}^2$ takes the form

$$\gamma_{\boldsymbol{k}_0^p}^2 = \frac{A^2 + C^2 - \Upsilon^2 - \left(\frac{\omega_p}{2\gamma}\right)^2 \pm 2\sqrt{\left(\frac{\omega_p}{2\gamma}\right)^2(\Upsilon^2 - C^2) + A^2C^2}}{H_E^2}. \tag{6.9}$$

Without pertaining to a specific material Table 6.1 lists the chosen default magnitudes of the parameters used in the upcoming calculations. Most values reflect the experimental findings of Rezende *et al.* [34] and Barak *et al.* [74] and are tentative magnitudes mostly approximated to the nearest power of 10. The exception of the parallel pumping field strength will be investigated in the interval $h \in [90, 95]$kOe, as it is a familiar domain relative to the magnitudes in Table 6.1 [74,75]. By using the default magnitudes from Table 6.1 in Eq. (6.9), and knowing from Eq. (3.24) that A is the only coefficient dependent on H_E it becomes clear that

$$\frac{A^2}{H_E^2} \gg \frac{C^2 - \Upsilon^2 - \left(\frac{\omega_p}{2\gamma}\right)^2 \pm 2\sqrt{\left(\frac{\omega_p}{2\gamma}\right)^2(\Upsilon^2 - C^2) + A^2C^2}}{H_E^2}, \tag{6.10}$$

due to the relative strengths of the effective fields $H_E \gg H_{Ax}, H_{Ay}$. As established in chapter 2.1, the Heisenberg exchange is ordinarily the dominating energy source, so this is not surprising. The resulting $\gamma_{\boldsymbol{k}_0^p}^2$ within these magnitudes reduces to

$$\gamma_{\boldsymbol{k}_0^p}^2 \simeq \frac{A^2}{H_E^2} = \frac{(H_E + (H_{Ax} + H_{Ay})/2)^2}{H_E^2} \simeq 1. \tag{6.11}$$

Parameter	Symbol	Magnitude	Unit
Heisenberg exchange constant	J	10^{-16} [34, 75–77]	J
x-anisotropy constant	D_x	10^{-18} [34, 75–77]	J
y-anisotropy constant	D_y	10^{-19} [34, 75–77]	J
Effective exchange field	H_E	10^4 [34, 74, 78]	kOe
Effective x-anisotropy field	H_{Ax}	10 [34, 74, 78]	kOe
Effective y-anisotropy field	H_{Ay}	10^{-1} [34, 74, 78]	kOe
External field strength	Υ	1 [79, 80]	kOe
Specific splitting factor	g_s	1 [34, 81]	-
Lattice parameter	c_l	5 [82]	Å
Gilbert damping constant	α	10^{-3} [83, 84]	-
System temperature	T	1 [74]	K
AF resonance frequency	ω_E	1 [85, 86]	THz
Relaxation rate	η	10^5 [74]	1/s
Pumping frequency	ω_p	0.01 [74, 79]	THz
Pumping field strength	h	$90 - 95$ [74, 75]	kOe
Total number of spins	$2N$	$10^4 - 10^8$ [87, 88]	-

Table 6.1: A list of parameters and their magnitudes necessary in the computation of the chemical potential of an antiferromagnet influenced by parallel pumping, given by Eq. (6.4). The magnitudes are chosen based on experimental studies with similar theoretical frameworks with the intention of being analytically consistent. The magnitudes were chosen with the aim to not pertain to any specific material.

We continue to assume a spherical Brillouin zone with a structure factor $\gamma_{\boldsymbol{k}} = \cos(\pi \boldsymbol{k}/2k_m)$, where $k_m = \pi/c_l$. This renders $\boldsymbol{k}_0^p$ to be zero, which indicates excitations of α-magnons purely in the center of the Brillouin zone. With these magnitudes, the dispersion relation loses its $\boldsymbol{k}$-dependence in addition to $\varepsilon_{\boldsymbol{p}_0} = \frac{\hbar^2 \boldsymbol{k}^2}{2m}$ also becoming zero. In order to have $\boldsymbol{k}_0^p \neq 0$, one possibility would be to increase the pumping frequency to a magnitude of $\omega_p/\mathrm{kOe} \sim 100\,\mathrm{THz}$. In recent experimental work, the pumping frequency is rarely increased above a magnitude of $\omega_p \sim 30\,\mathrm{GHz}$ [65, 74, 79]. Unless we infringe on the relations between the effective fields, the only other scenario is an increase of the external field strength to $\Upsilon \sim 10^4\,\mathrm{kOe}$, which would be a field strength a hundred times as large as the pumping field. The measured magnitudes of H_E, H_{Ax} and H_{Ay} vary [34, 74], but the relation between them is rigid, $\frac{H_A}{H_E} \sim 10^{-3}$. Alternations of this relation might easily result in a non-realistic model, which will be impossible to replicate. Small variations of the external field would be possible to replicate without breaking the physics of the coupled clouds, but it would have a negligible impact on the structure factor. Therefore, H_E, H_{Ax}, H_{Ay} and Υ will be treated as fixed parameters for the rest of the thesis. For now, we use the default value of ω_p and $\gamma_{\boldsymbol{k}} = 1$, until chapter 6.2, where we will investigate how different pumping frequencies affects the chemical potential. We will continue to assume

a spherical Brillouin zone, at which $\boldsymbol{k}_0^p$ will be calculated by the expression

$$\boldsymbol{k}_0^p = \frac{2\arccos\left(\gamma_{\boldsymbol{k}_0^p}\right)}{c_l}. \tag{6.12}$$

By using the default parameters of Table 6.1 in Eq. (6.5), the interval of the pumping field strength results in a condensate density of $\rho \sim 10^{33}\,\mathrm{m}^{-3}$ and a thermal magnon density of $n \sim 0\,\mathrm{m}^{-3}$. Since $\beta \sim 10^{23}\,\mathrm{J}^{-1}$, the inverse local fugacity will be enormous, which leads to

$$n = \frac{4\pi}{(\beta\bar{\omega}_E)^3}\int_0^\infty \mathrm{d}y \frac{y^2}{e^y e^{\beta\left(g\rho - \frac{2\alpha\hbar\omega_E}{\eta}\right)} - 1} \simeq \frac{4\pi}{(\beta\bar{\omega}_E)^3}\int_0^\infty \mathrm{d}y \frac{y^2}{\infty} = 0. \tag{6.13}$$

We define a simplified expression for the pumping field strength

$$h_s \equiv \sqrt{\frac{2\alpha\hbar^2\omega_E}{|p(\boldsymbol{k}_0^p)|^2}\rho\left(1 - \frac{2}{e^{\beta\left[\frac{\boldsymbol{p}_0^2}{2m} + g\rho - \frac{2\alpha\hbar\omega_E}{\eta}\right]} + 1}\right)}, \tag{6.14}$$

and a simplified expression for the chemical potential

$$\mu_s \equiv \varepsilon_0 + g\rho + \frac{2\alpha\hbar\omega_E}{\eta}. \tag{6.15}$$

h_s may be simplified further, as the expression $e^{\beta\left[\frac{\boldsymbol{p}_0^2}{2m} + g\rho - \frac{2\alpha\hbar\omega_E}{\eta}\right]} \to \infty$, which leads to

$$h_s \simeq \sqrt{\frac{2\alpha\hbar^2\omega_E}{|p(\boldsymbol{k}_0^p)|^2}\rho\left(1 - \frac{2}{\infty}\right)} = \sqrt{\frac{2\alpha\hbar^2\omega_E}{|p(\boldsymbol{k}_0^p)|^2}\rho}. \tag{6.16}$$

Eq. (6.16) is easily rewritten as

$$\rho = \frac{h_s^2|p(\boldsymbol{k}_0^p)|^2}{2\alpha\hbar^2\omega_E}, \tag{6.17}$$

which when added to Eq. (6.15) acquires a simplified expression for the chemical potential without the ρ-dependence, which reads

$$\mu_s = \varepsilon_0 + g\frac{h_s^2|p(\boldsymbol{k}_0^p)|^2}{2\alpha\hbar^2\omega_E} + \frac{2\alpha\hbar\omega_E}{\eta}. \tag{6.18}$$

We finalize the simplified chemical potential by writing

$$\mu_s \simeq g\frac{h_s^2|p(\boldsymbol{k}_0^p)|^2}{2\alpha\hbar^2\omega_E}, \tag{6.19}$$

as

$$\varepsilon_0 + \frac{2\alpha\hbar\omega_E}{\eta} \ll g\frac{h_s^2|p(\boldsymbol{k}_0^p)|^2}{2\alpha\hbar^2\omega_E}. \tag{6.20}$$

In the following chapter, we will examine the unsimplified chemical potential in Eq. (6.4) and the pumping field strength in Eq. (6.5) and compare them to their simplified analogues in Eqs. (6.16) and (6.19).

6.2 Computations of the chemical potential

In this section, unless explicitly specified, the default magnitudes listed in Table 6.1 are used in the following calculations. One of the approximations made in chapters 2-5, was to overlook the temperature-dependence of most of the parameters in Table 6.1. Even though the Heisenberg exchange constant and the anisotropy constants traditionally are treated as constants in analytical work, other parameters such as the relaxation rate and the cloud densities are highly dependent on the temperature. A parallel pumping study of magnon damping in $\mathrm{MnF_2}$ by Barak *et al.* [74] found the temperature of the magnon relaxation rates to become a T^4 dependence at $T < 5\,\mathrm{K}$. The left plot in Fig. 6.1 displays this behaviour as a function of the critical field h_c (which is obtained through the balance of individual modes from the PPP magnon growth in Eq. (4.34) as $(\mathrm{d}n_{\boldsymbol{k}}/\mathrm{d}t)_{\boldsymbol{p}} = -(\mathrm{d}n_{\boldsymbol{k}}/\mathrm{d}t)_{\boldsymbol{r}}$ [51]), which has a linear relation to the relaxation rate $h_c \sim \eta$ [74]. The right plot in Fig. 6.1 also illustrates a substantial depence of T at small temperatures near the Brillouin zone. In the vicinity of $T = 1 - 4\,\mathrm{K}$, the relaxation rates were measured in the range $\eta \sim 10^4 - 10^5\,\mathrm{s}^{-1}$.

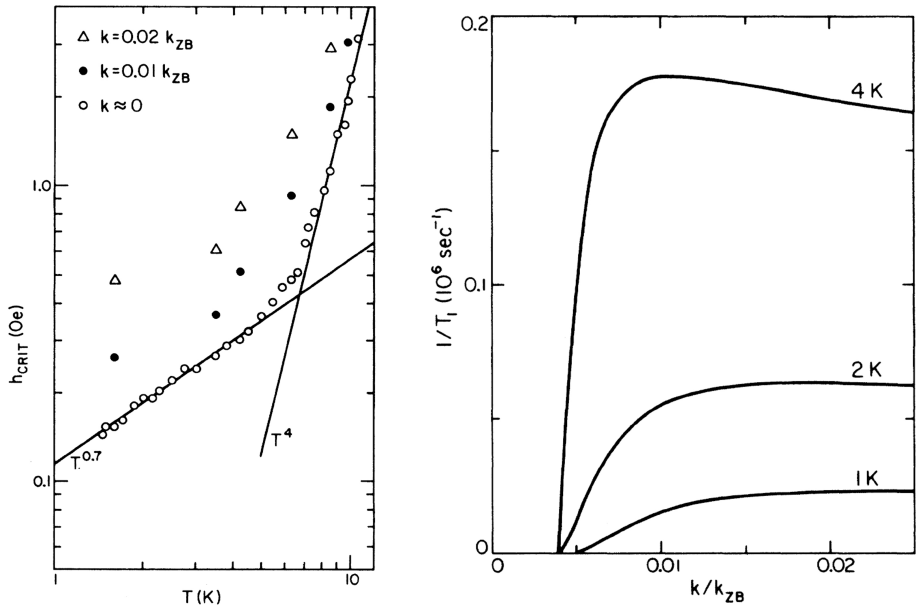

Figure 6.1: Left plot: Measured relaxation rates displayed as the critical field $h_c \sim \eta$ in comparison with theoretical rates as a function of temperature for $\mathrm{MnF_2}$ magnons. Right plot: Variation of relaxation rates vs wave-vector amplitude at several temperatures. Both plots are from Barak *et al.* [74].

The temperature dependence of μ was also neglected in chapter 5, so we should anticipate a relatively constant $\mu(T)$, despite it being unrealistic for real atoms. Therefore, our equation for the chemical potential should not hold for higher temperatures. Eq. (6.4) was

derived on the condition of ultracold atoms, and as shown in Fig. 6.2, our equation does not differentiate between a system at $T = 1\,\mathrm{K}$ and room temperature. As the T dependence was eliminated in the expression for the simplified chemical potential in Eq. (6.19), we could expect the similar outcome. Eq. (6.4) therefore holds only for small temperatures. For the rest of the thesis, the calculations will be done at $T = 1\,\mathrm{K}$ and $\eta = 10^5\,\mathrm{s}^{-1}$.

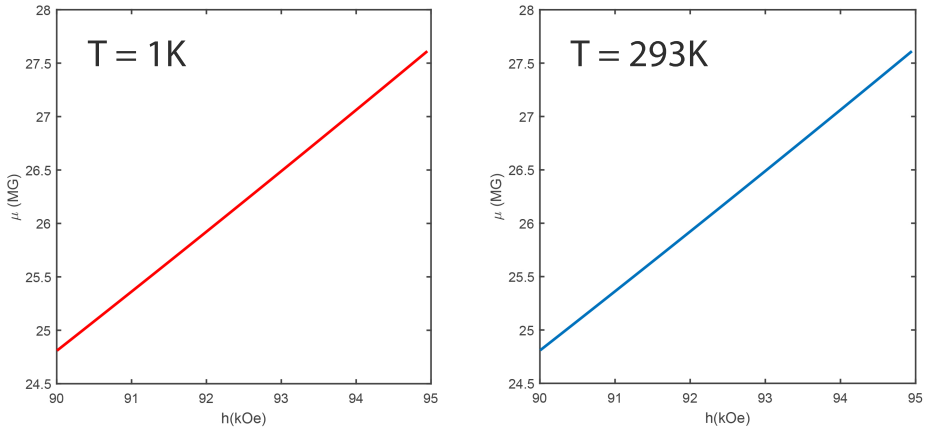

Figure 6.2: The chemical potential, μ given in Eq. (6.4), as a function of the pumping field strength, h given in Eq. (6.5), at $T = 1\,\mathrm{K}$ and room temperature. The lines are presented separately to avoid complete overlap.

If the sample size is changed, a predictable pattern forms. Since no other default parameter has been altered, the observations made during the simplifications of μ_s and h_s still holds, making the pumping field essentially invariant to the total spin number (unless N reaches very large quantities, as shown in Fig. (6.4)). The only parameters dependent of N are the coupling constant, g, and the energy representing the zero-point fluctuations, ε_0. If we expand Eq. (6.4) with the Eqs. (5.14) and (3.23), μ reads

$$\begin{aligned}\mu \sim\, & SN(D_x + D_y - 2JSz) + \frac{2\alpha\hbar\omega_E}{\eta} \\ & + \frac{D_x}{2N}\left(\frac{8\pi}{(\beta\bar{\omega}_E)^3}\mathrm{Li}_3\left[e^{-\beta\left(\frac{D_x}{2N}\rho - \frac{2\alpha\hbar\omega_E}{\eta}\right)}\right] + \rho\right),\end{aligned} \tag{6.21}$$

and supports the inverse proportionality illustrated in Fig. 6.3 and 6.4 since the last term on the right hand side is the clear-cut dominant contribution to μ. We specify that 6.21 is not a proper expression for μ, as the magnitude of $g \sim D_x/2N$ is only tentatively estimated from its proportionality to D_x and N. Considering the small magnitude of the magnon gap, a larger sample size naturally results in a proportionally smaller chemical potential.

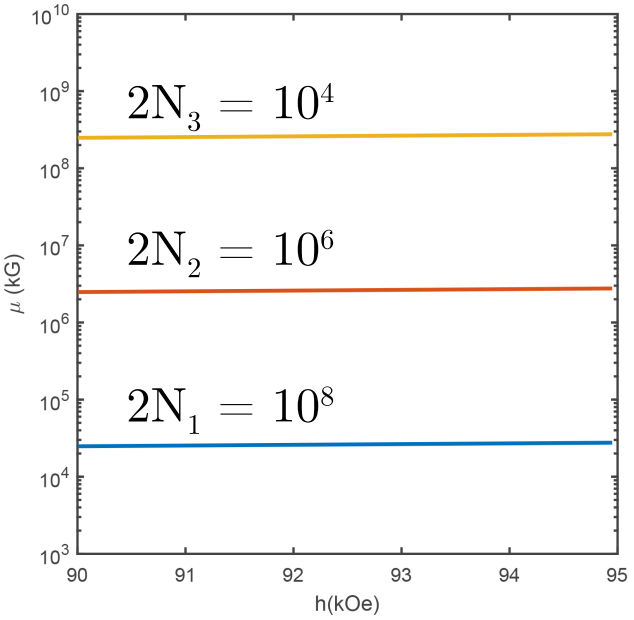

Figure 6.3: The chemical potential, μ given in Eq. (6.4), plotted logarithmically as a function of the pumping field strength, h given in Eq. (6.5), at different spin numbers, $2N_1 = 10^8$, $2N_2 = 10^6$ and $2N_3 = 10^4$.

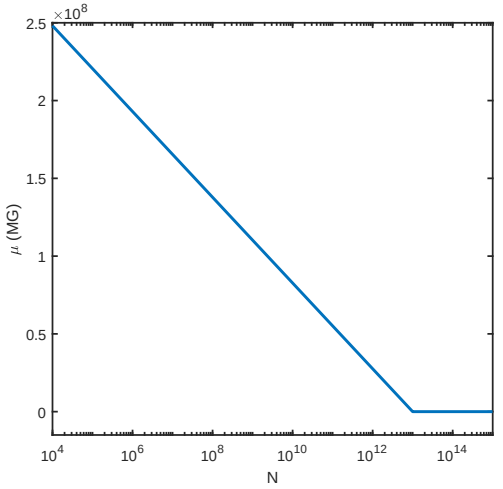

Figure 6.4: The chemical potential, μ given in Eq. (6.4), plotted as a function of the total spin number N, plotted logarithmically.

Fig. 6.4 also illustrates that the spin number needs to surpass $N_0 \sim 10^{13}$ in order to have a zero-value μ, as this is the point where

$$SN_0(D_x + D_y - 2JSz) + \frac{2\alpha\hbar\omega_E}{\eta} \approx \frac{D_x}{2N_0}\left(\frac{8\pi}{(\beta\bar{\omega}_E)^3}\mathrm{Li}_3\left[e^{-\beta\left(\frac{D_x}{2N_0}\rho - \frac{2\alpha\hbar\omega_E}{\eta}\right)}\right] + \rho\right). \tag{6.22}$$

The default values in Table 6.1 represent however studies with far smaller sample sizes, so we will not delve deeper into any larger values of N.

Until now, the choice of parameters has resulted in excitations of α-magnons exclusively in the Brillouin zone. We will now investigate the behaviour of the chemical potential outside the Brillouin zone. In order to have a nonzero $\boldsymbol{k}_0^p$, the structure factor needs to be smaller than 1, as of Eq. (6.12). One analytically feasible possibility to achieve magnon growth outside the Brillouin center is by increasing the pumping frequency. The analysis of the structure factor in Eqs. (6.10) and (6.11) determined that pumping frequency must be large enough to fulfill the condition

$$A^2 - \left(\frac{\omega_p}{2\gamma}\right)^2 \ll H_E^2, \tag{6.23}$$

if the other terms are neglected, which the conditions in Eqs. (6.10) and (6.11) prove is reasonable. Since $A^2 \sim 10^8\,\mathrm{kOe}^2$ and the gyromagnetic ratio is tentatively $\gamma \sim 10^{10}$, the pumping frequency needs to have a magnitude of $\omega_p/\mathrm{kOe} \sim 100\,\mathrm{THz}$ in order to have an impact on the structure factor. Therefore, we will compute the chemical potential and the pumping field strength at $\omega_p/\mathrm{kOe} = 100\,\mathrm{THz}$, $\omega_p/\mathrm{kOe} = 150\,\mathrm{THz}$ and $\omega_p/\mathrm{kOe} = 200\,\mathrm{THz}$ in the following subsections. As excitations of magnons outside the Brillouin zone is a more general case than the center [79], μ and h will be compared to the simplified formulae μ_s and h_s derived in Eqs. (6.16) and (6.19). These comparisons will hopefully determine the prominence of the thermal density in the steady state limit by our expression of μ.

6.2.1 Pumping frequency $\omega_p/\mathrm{kOe} = 100\,\mathrm{THz}$

For every frequency, the simplified and the unaltered chemical potential will be computed as a function of the pumping field amplitude, and the simplified and the unaltered pumping field strength will be computed as a function of the condensate density. Since the chemical potentials and the field strengths separately were too similar to display in the same graphics (due to complete overlap of curves), the differences were also plotted. Fig. 6.5 displays the computations. If we compare Fig. 6.2 with the chemical potentials in Fig. 6.5, we observe a substantial decrease of the chemical potential outside the Brillouin zone. The decrease of the structure factor only impacts the pumping coefficient of α-magnons $p(\boldsymbol{k}_0^p) = Q_{21}(\boldsymbol{k})Q_{23}(\boldsymbol{k}) - Q_{11}(\boldsymbol{k})Q_{13}(\boldsymbol{k})$, as the Bogoliubov coefficients are the only components of Eq. (6.4) containing the structure factor. The Bogoliubov coefficients, listed in Eqs. (4.14), (4.15), (6.26) and (6.28), give the pumping coefficient the tentative dependence $p(\gamma_{\boldsymbol{k}_0^p}) \sim \gamma_{\boldsymbol{k}_0^p}^2$, which advocates the decrease in the chemical potential. Plot (e) in Fig. 6.5 illustrates the difference between μ and μ_s as a function of h.

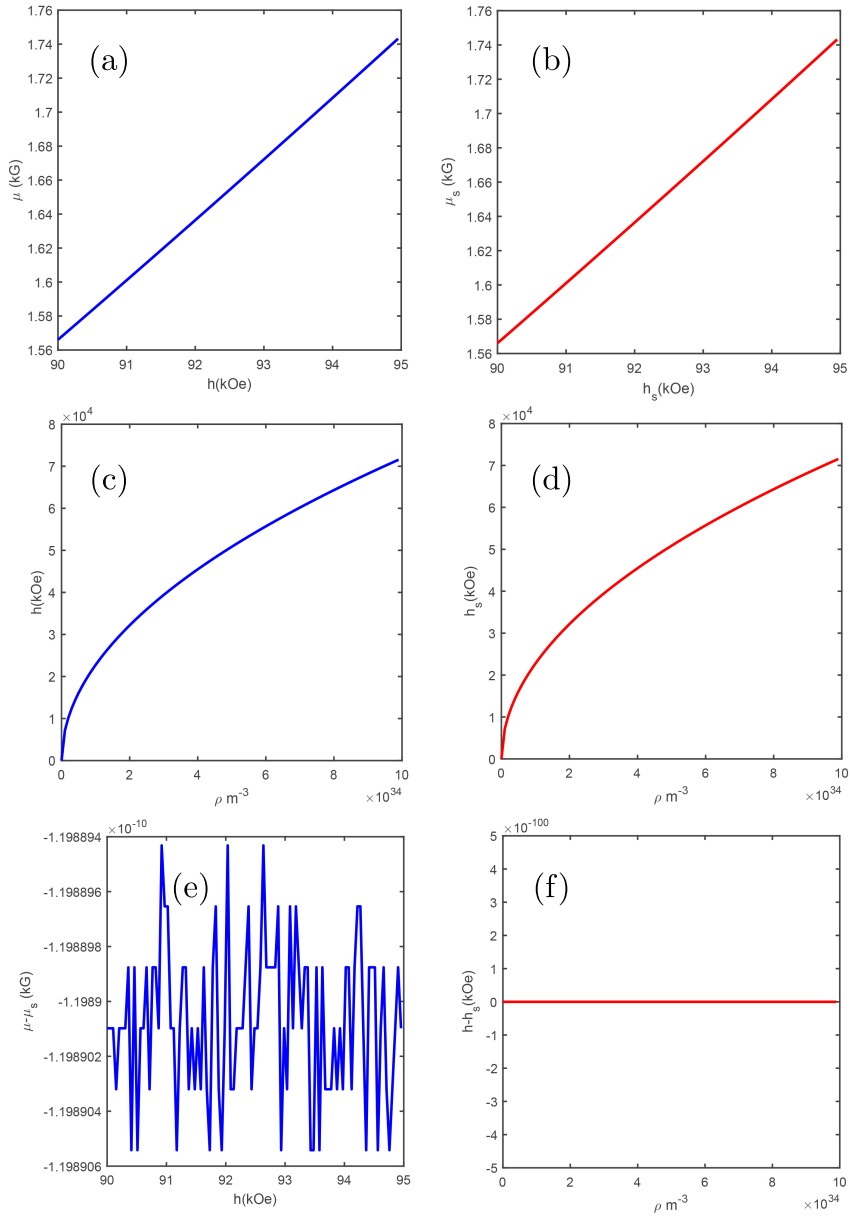

Figure 6.5: Computations at $\omega_p/\mathrm{kOe} = 100\,\mathrm{THz}$. (a) The chemical potential, Eq. (6.4), as a function of the pumping field amplitude, Eq. (6.5). (b) The simplified chemical potential, Eq. (6.19), as a function of the simplified pumping field amplitude, Eq. (6.16) (c) The pumping field amplitude, Eq. (6.5), as a function of the condensate density. (d) The simplified pumping field amplitude, Eq. (6.5), as a function of the condensate density. (e) The difference between the unaltered chemical potential in (a) and the simplified chemical potential in (b) as a function of the pumping field amplitude. (f) The difference between the unaltered pumping field amplitude in (c) and the simplified pumping field amplitude in (d) as a function of the condensate density.

The reason $\mu - \mu_s$ was not plotted as a function of h_s was an arbitrary choice, due to the information provided by plot (f). Down to the notion of $h - h_s \sim 10^{-100}$, the magnitudes of h and h_s are equal at all values of $\rho \in [0\,, 10^{35}\,]\mathrm{m}^{-3}$. The implications of this result will be discussed thoroughly in section 6.3. At first glance, the distribution of $\mu - \mu_s$ in plot (e) over the default interval of h has the form of a set of random values scattered around $\mu - \mu_s \approx -1.989 \times 10^{-10}$. On closer inspection, the measure points hit 6 discrete values of $\mu - \mu_s$, as depicted in Fig. 6.6. The measure points indicate no particular relation to the evolution of h. By evaluating Eq. (6.4) for μ, knowing $h = h_s$ and the last step in the derivation of μ_s in Eq. (6.19) involved neglecting ε_0, it is fair to assume a constant difference between μ and μ_s. The magnon gap, ε_0, is invariant of the pumping frequency and has the value $\varepsilon_0 = -1.989 \times 10^{-10}$, which coincides perfectly with the mean value in plot (e). The deviations from ε_0 are presumably automatic rounding errors originated during the computations.

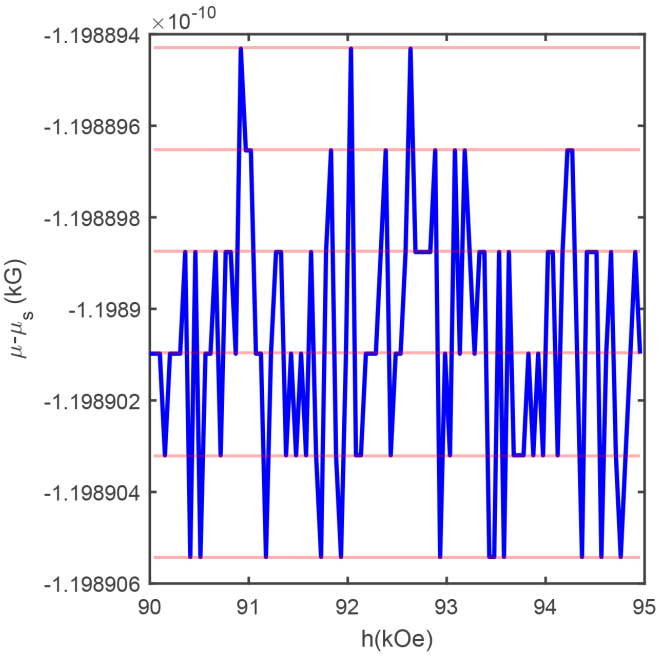

Figure 6.6: A closer inspection of plot (e) from Fig. 6.5. The six discrete values of $\mu - \mu_s$ are outlined by horizontal translucent orange lines.

6.2.2 Pumping frequency $\omega_p/\mathrm{kOe} = 150\,\mathrm{THz}$

Fig. 6.7 illustrates the same computations as in Fig. 6.5 for a pumping frequency of $\omega_p/\mathrm{kOe} = 150\,\mathrm{THz}$. We observe similar behaviour of the chemical potentials and the pumping field amplitudes. The increase in the pumping amplitude has resulted in another decrease in the chemical potentials, along with increased pumping field amplitudes. As $h, h_s \sim |p(\boldsymbol{k}_0^p)|^{-1}$ and the pumping coefficient takes on values of $|p(\boldsymbol{k}_0^p)| \ll 1$, the increased pumping frequency justifies the increased field strength. Table 6.2 contains the structural factors corresponding to the different pumping frequencies. Equally in Fig. 6.7, plot (f) shows that there is no difference between h and h_c. The difference between μ and μ_s in plot (e) illustrates the same discrete distribution of values as Fig. 6.6. The measure points do seemingly not display any dependence of h and are distributed randomly around the mean value $\mu - \mu_s \approx -1.989 \times 10^{-10}$. This coincides with the assumption of a constant difference between the chemical potentials invariant of h, with $\mu - \mu_s = \varepsilon_0$. In the last approximation made during the derivation of μ_s, the precise reduction of μ consisted of $\varepsilon_0 + 2\alpha\hbar\omega_E/\eta \gg g\rho$. However, we treat ε_0 as the notable difference between μ and μ_s, since $|\varepsilon_0| \sim 10^{-10}$ and $|2\alpha\hbar\omega_E/\eta| \sim 10^{-33}$.

ω_p/kOe	$\gamma_{\boldsymbol{k}}$
100 THz	0.8661
150 THz	0.6617
200 THz	0.0284

Table 6.2: The structure factors, given by Eq. (6.12), corresponding to pumping frequencies in Figs. 6.5, 6.7 and 6.8.

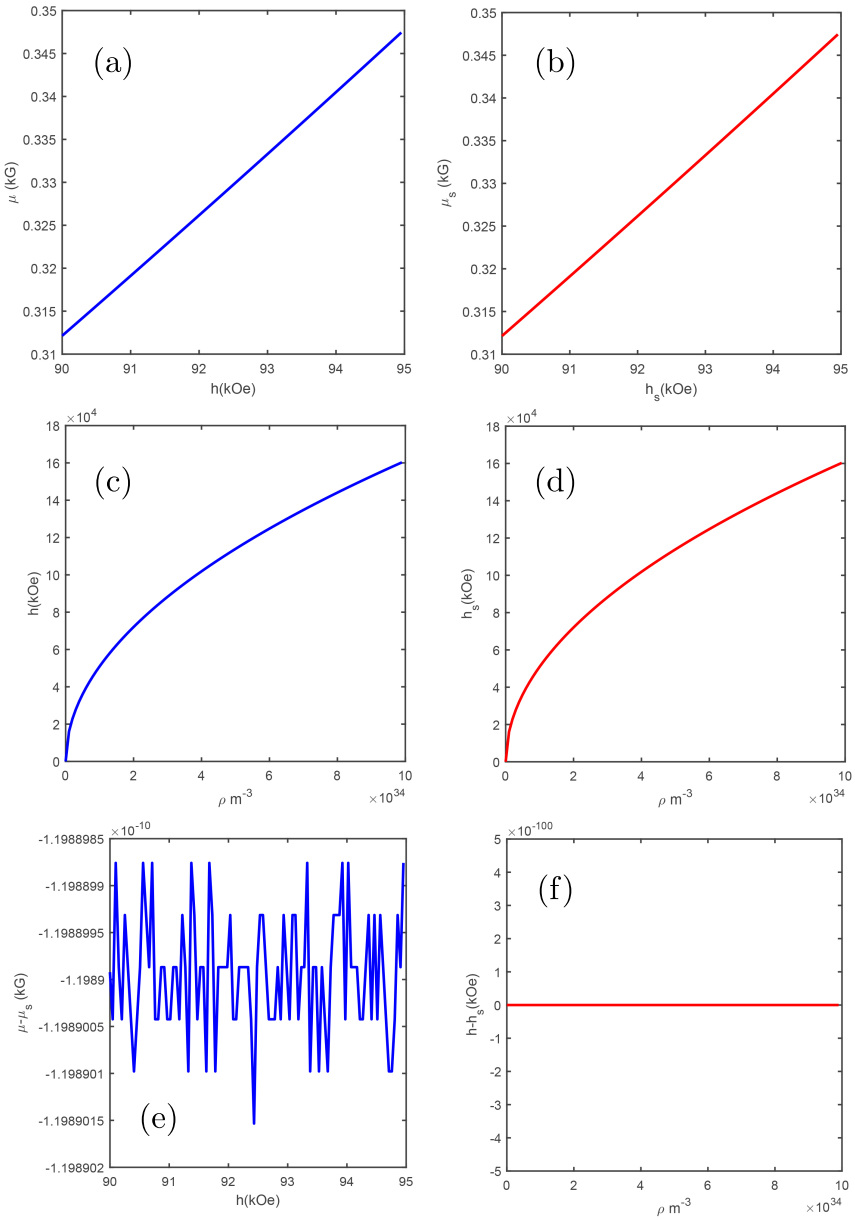

Figure 6.7: Computations at $\omega_p/\mathrm{kOe} = 150\,\mathrm{THz}$. (a) The chemical potential, Eq. (6.4), as a function of the pumping field amplitude, Eq. (6.5). (b) The simplified chemical potential, Eq. (6.19), as a function of the simplified pumping field amplitude, Eq. (6.16) (c) The pumping field amplitude, Eq. (6.5), as a function of the condensate density. (d) The simplified pumping field amplitude, Eq. (6.5), as a function of the condensate density. (e) The difference between the unaltered chemical potential in (a) and the simplified chemical potential in (b) as a function of the pumping field amplitude. (f) The difference between the unaltered pumping field amplitude in (c) and the simplified pumping field amplitude in (d) as a function of the condensate density.

6.2.3 Pumping frequency $\omega_p/\mathrm{kOe} = 200\,\mathrm{THz}$

At this particular pumping frequency, we can see from Table 6.2 that the structure factor is very close to zero. In the limit $\gamma_{\boldsymbol{k}_0^p} \to 0$, the algebraic complexity of the dispersion relation and the Bogoliubov coefficients representing the pumping coefficient would be reduced to

$$\frac{Q_{21}}{Q_{11}} \equiv Q'_{21} = 0, \quad \frac{Q_{23}}{Q_{11}} \equiv Q'_{23} = 0, \tag{6.24}$$

$$\frac{Q_{12}}{Q_{22}} \equiv Q'_{12} = 0, \quad \frac{Q_{14}}{Q_{22}} \equiv Q'_{14} = 0, \tag{6.25}$$

$$\frac{Q_{13}}{Q_{11}} \equiv Q'_{13} = -\frac{C_{\boldsymbol{k}}}{(A_{\boldsymbol{k}} + \gamma\Upsilon + \omega_{\alpha\boldsymbol{k}})}, \tag{6.26}$$

$$\frac{Q_{24}}{Q_{22}} \equiv Q'_{24} = -\frac{C_{\boldsymbol{k}}}{(A_{\boldsymbol{k}} - \gamma\Upsilon + \omega_{\beta\boldsymbol{k}})}, \tag{6.27}$$

$$Q_{11}^2 = \frac{1}{(1 - {Q'_{13}}^2)} = \frac{(A_{\boldsymbol{k}} - \gamma\Upsilon + \omega_{\beta\boldsymbol{k}})}{(A_{\boldsymbol{k}} - \gamma\Upsilon + \omega_{\beta\boldsymbol{k}}) + C_{\boldsymbol{k}}}, \tag{6.28}$$

$$\left(\frac{\omega_{\beta\boldsymbol{k}}}{\gamma}\right)^2 = H_E(H_{Ax}+H_{Ay})+H_{Ax}H_{Ay}+\Upsilon^2+H_E^2+2\left(H_E+\frac{H_{Ax}+H_{Ay}}{2}\right)\Upsilon, \tag{6.29}$$

$$\left(\frac{\omega_{\beta\boldsymbol{k}}}{\gamma}\right)^2 = H_E(H_{Ax}+H_{Ay})+H_{Ax}H_{Ay}+\Upsilon^2+H_E^2-2\left(H_E+\frac{H_{Ax}+H_{Ay}}{2}\right)\Upsilon. \tag{6.30}$$

However, we will not delve deeper into this limit in this thesis. Fig. 6.8 illustrates the same computations as in Fig. 6.5 and 6.7 for a pumping frequency of $\omega_p/\mathrm{kOe} = 200\,\mathrm{THz}$. Again, we observe similar behaviour of the chemical potentials and the pumping field amplitudes.

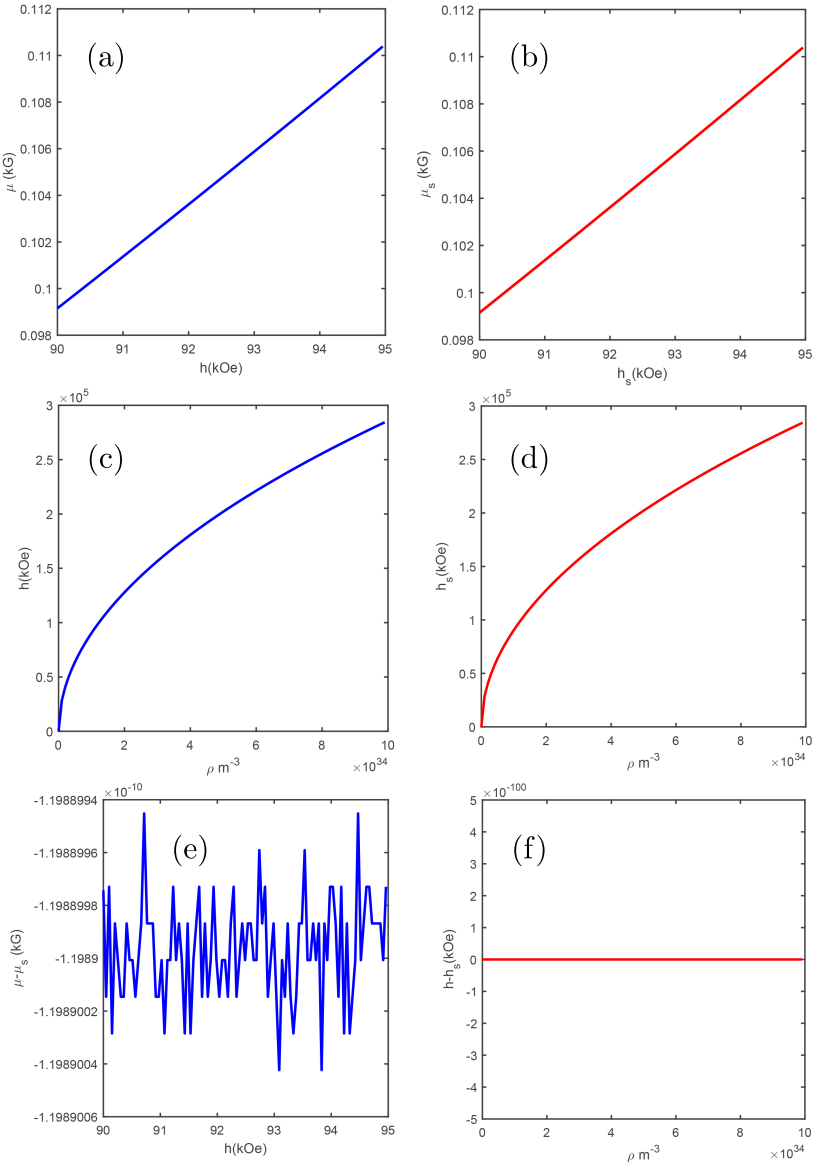

Figure 6.8: Computations at $\omega_p/\mathrm{kOe} = 200\,\mathrm{THz}$. (a) The chemical potential, Eq. (6.4), as a function of the pumping field amplitude, Eq. (6.5). (b) The simplified chemical potential, Eq. (6.19), as a function of the simplified pumping field amplitude, Eq. (6.16) (c) The pumping field amplitude, Eq. (6.5), as a function of the condensate density. (d) The simplified pumping field amplitude, Eq. (6.5), as a function of the condensate density. (e) The difference between the unaltered chemical potential in (a) and the simplified chemical potential in (b) as a function of the pumping field amplitude. (f) The difference between the unaltered pumping field amplitude in (c) and the simplified pumping field amplitude in (d) as a function of the condensate density.

6.3 Discussion

The unaltered and the simplified pumping field amplitudes have for every pumping frequency been equal. We may then label the nature of the chemical potentials in the (a) and (b) computations in Figs. 6.5, 6.7 and 6.8. μ as a function of h illustrates seemingly linear behaviour, but since $h = h_s$, μ must follow a parabolic nature, as $\mu_s \sim kh_s^2$ is established in Eq. (6.19). By analyzing the amplitudes

$$h = h_s \tag{6.31}$$

$$\Rightarrow \sqrt{\frac{2\alpha\hbar^2\omega_E}{|p(\boldsymbol{k}_0^p)|^2}\left(n+\rho\right)\left(1-\frac{2}{e^{\beta\left[\frac{\boldsymbol{p}_0^2}{2m}+g\rho-\frac{2\alpha\hbar\omega_E}{\eta}\right]}+1}\right)} = \sqrt{\frac{2\alpha\hbar^2\omega_E}{|p(\boldsymbol{k}_0^p)|^2}\rho}, \tag{6.32}$$

the assumptions made in the process of simplifying h, namely

$$\left(1-\frac{2}{e^{\beta\left[\frac{\boldsymbol{p}_0^2}{2m}+g\rho-\frac{2\alpha\hbar\omega_E}{\eta}\right]}+1}\right) = 1, \tag{6.33}$$

and

$$n = 0, \tag{6.34}$$

are validated. As the argument of the exponential in Eq. (6.33) develops a tentative magnitude of $\sim 10^{23} - 10^{29}$, this assumption was never implausible. The fact that this model realizes a thermal density so small that it becomes zero is however problematic. The goal of this thesis was to couple the condensate and the thermal cloud and derive equations of motion that would represent the density of the thermal cloud. Chapter 5 was introduced with the statement that the number of thermal magnons realistically claims a minimum of 10% of the total magnon number [52]. 10% of the magnon number in the computations illustrated in Figs. 6.5, 6.7 and 6.8 should have produced $n \sim 10^{28}\,\mathrm{m}^{-3}$, however this is far from the case. By writing out n using Eq. (5.67) in Eq. (6.3), n reads

$$n = \frac{4\pi}{(\beta\bar{\omega}_E)^3}\int_0^\infty \mathrm{d}y \frac{y^2}{e^y e^{2\beta g n} e^{\beta\left(g\rho-\frac{2\alpha\hbar\omega_E}{\eta}\right)}-1}, \tag{6.35}$$

in the steady-state limit. With the default magnitudes from Table 6.1, a realistic relation between ρ and n would be seemingly impossible. However, the steady-state limit might be an unfortunate case which represents the model inaccurately. The equations of motion for ρ and n in Eqs. (5.70) and (5.71) might describe a realistic system when accounting for the nonzero change rates of the densities. Yet, the expression of n in Eq. (5.67) was derived under the assumption of high temperatures, leading to the approximation $\beta\varepsilon(\boldsymbol{p}) \to \beta\bar{\omega}_E|\boldsymbol{p}|$, in order to acquire a convenient substitution variable $p \equiv |\boldsymbol{p}| = y/(\beta\omega_E)$ in Eq. (5.67). The model has consistently been derived under the condition of ultracold atoms, with this exception. From Eq. (6.35), the prefactor alone following Table 6.1 is remarkably small $4\pi/(\beta\bar{\omega}_E)^3 \sim 10^{-104}$. If we were to investigate $\beta\varepsilon(\boldsymbol{p}) \to \beta\bar{\omega}_E|\boldsymbol{p}|$, we see that it holds in the Brillouin center at $\boldsymbol{k} = 0 \to \boldsymbol{p} = \varepsilon(\boldsymbol{p}) = 0$. Anywhere else in the Brillouin zone, say for the values of $\boldsymbol{k}$ derived at $\omega_p/\mathrm{kOe} = 200\,\mathrm{THz}$ the approximation does not hold $\beta\varepsilon(\boldsymbol{p}) \sim 10^{29} \neq \beta\bar{\omega}_E|\boldsymbol{p}| \sim 10^{21}$. The current expression of n should be

reconsidered and expressed in another matter to uphold the consistency of the condition of ultracold atoms.

Another issue with the computations stems from the choice of some of the magnitudes in 6.1, and might partially explain the unrealistic massive values of the condensate density and the chemical potential. The magnitudes of the effective fields, H_E, H_{Ax} and H_{Ay} were chosen based off experimental values for similar experiments on antiferromagnets [34, 74, 78]. Simultaneously, the exchange- and anisotropy constants were chosen in order to have an analytical consistency with the effective fields. J, D_x and D_y were estimated based on the experimental values of H_E, H_{Ax} and H_{Ay} and the relations expressed in Eq. (3.24). This resulted in J, D_x and D_y being considerably larger than typical experimental values [34, 75–77]. For instance, a study by Achleitner on the AFM EuTe and other studies on other AFMs, see [75–77, 89], measured exchange- and anisotropy constants with magnitudes $J, D_A \sim [10^{-22}, 10^{-25}]$J. In hindsight, it could have been beneficial to use the experimental values for J, D_x and D_y, and then have chosen the effective fields in order to maintain an analytical consistency. Yet, H_E, H_{Ax} and H_{Ay} would become very small. Based on the computations of this thesis, it is unclear whether maintaining analytical consistency for the effective field magnitudes is beneficial to computing a tentatively realistic chemical potential. Smaller values of H_E, H_{Ax} and H_{Ay} might also solve the structure factor being almost invariant of the pumping frequency. As illustrated in subchapter 6.2, the default magnitudes for the effective fields were so large that the pumping frequency would not influence the structure factor unless it was raised to a monumental number. The fact that experimental measurements of H_E, H_{Ax} and H_{Ay} do not match the measurements of J, D_x and D_y analytically in our model, could suggest an initial lacking Hamiltonian chosen in chapter 3. It would explain why representative magnitudes consistent of each other is troublesome. One possibility could be to extend the Hamiltonian in order to take account for the demagnetization.

Chapter 7

Conclusion

In this thesis, an examination of the chemical potential was attempted, in a hard-axis antiferromagnet influenced by parametric parallel pumping to induce Bose-Einstein condensation. The influence of PPP on the growth of magnons was determined by deriving the Hamiltonian for a collinear antiferromagnet subjected to exchange interaction, out-of-plane and in-plane magnetocrystalline anisotropies, a time-independent Zeeman coupling and an external oscillating time-dependent magnetic field parallel to the antiferromagnetic spins in the z-direction. Treating PPP as a perturbation, the Hamiltonian underwent diagonalization through a Fourier- and a Bogoliubov-transformation, where only the quadratic terms were kept. Only nearest-neighbour interactions between the spins were accounted for as the remaining interactions were assumed negligible in comparison. The final Hamiltonian consisted of normal mode magnon creation and annihilation operators and their corresponding frequencies. The dispersion relation was plotted, examined in the center of the Brillouin zone and compared to the known frequencies of the hard-axis antiferromagnet Nickel Oxide. We then elaborated on the physical nature of the effect of PPP before introducing the pumping field to the Hamiltonian. After using the Heisenberg equation, we finalized an equation of motion for the magnon density of α-magnons, which described the growth of thermal magnons due to PPP.

The goal was to describe the chemical potential of a system undergoing BEC without ignoring the noncondensate magnons in the antiferromagnet. Using the two-fluid model and the work of Bogoliubov and the generalization by Beliaev of the Bose macroscopic wavefunction, a generalized Gross-Pitaevskii (GGP) equation was used to describe the condensate magnons. The GGP accounted for collisions with thermal magnons and assumed Gilbert damping as the only relaxation mechanism. The GGP was then written on a hydrodynamic form, rendering the equations of motion for the condensate density and velocity. To describe the thermal cloud, we started with the GP-equation for the thermal fluctuations. Following the work of Kirkpatrick and Dorfman a quantum kinetic equation for the thermal magnons was derived. The end result was the Boltzmann equation for a single-particle local equilibrium Bose distribution function describing the coupling with the phonon bath, the PPP and the contribution from magnon collisions, assuming no driv-

ing dc force. By assuming zero condensate velocity, high temperature in a constant and homogeneous system, an equation of motion for the thermal density was reached.

The equations of motion were examined in the steady state limit and combined to find the pumping field amplitude and the chemical potential as functions of the condensate density. Without pertaining to a specific material, a set of general magnitudes for the variables were chosen based on prior experimental measurements. The behaviour of the chemical potential and the pumping field strength was explored by varying the parameters. The default magnitudes resulted in a distinguishable thermal density and only pumping of magnons in the center of the Brillouin zone. Additionally, the computed values of the condensate density and the chemical potential were unrealistically high. An evaluation of the chosen parameter magnitudes revealed a lack of analytical consistency with experimental measurements for the effective fields. Additionally, a rundown of the derivation of the thermal density revealed a problematic approximation for the magnon growth outside the Brillouin center. Hopefully, the tentative behaviour of the chemical potential in the steady state limit could be useful in future studies of parametric pumping. If the thermal density was revisited along with the parameter magnitudes, the computations of the chemical potential might have been more successful.

7.1 Outlook

In further studies of this particular model, the system should be evaluated outside the steady state limit. This thesis examined the case of a system influenced by a high magnetic field, with just one polarization and one prominent condensate. Instead of handling just the α-magnon condensate, the next step should be to evaluate a more generic case with a low magnetic field. This would result in two polarizations with both α- and β-magnon condensates, which would render more valuable information about the chemical potential for future experiments. The collision integrals describing the coupling between the condensates and the thermal bath would then account for collisions between thermal magnons of both α- and β-magnons represented by different distribution functions. It would also be beneficial to study the ZNG framework [52] by Zaremba, Nikuni and Griffin, and incorporate the effect of parametric parallel pumping in this framework. The model only accounts for Gilbert damping. If analytical expressions for other relaxation mechanisms could be integrated in the model, the improved insight in the magnon damping would be valuable. We have also ignored the temperature dependence of several of the parameters in our model. If representative analytical time dependencies of the chemical potential and the condensate- and noncondensate densities could be incorporated, one could provide better estimates for the magnitudes used in the calculations in this thesis. However, these dependencies are most certainly not analytically trivial, and not much researched [90] for systems influenced by parametric parallel pumping.

Appendices

Appendix A

Bogoliubov coefficients

The system Hamiltonian before introducing the Zeeman coupling for the parametric parallel pumping is

$$H = \hbar \sum_{\boldsymbol{k}} (A_{\boldsymbol{k}} + \gamma\Upsilon) a^{\dagger}_{\boldsymbol{k}} a_{\boldsymbol{k}} + (A_{\boldsymbol{k}} - \gamma\Upsilon) b^{\dagger}_{\boldsymbol{k}} b_{\boldsymbol{k}} + B_{\boldsymbol{k}} (a_{\boldsymbol{k}} b_{-\boldsymbol{k}} + a^{\dagger}_{\boldsymbol{k}} b^{\dagger}_{-\boldsymbol{k}}) + \frac{1}{2} C_{\boldsymbol{k}} (a_{\boldsymbol{k}} a_{-\boldsymbol{k}} + b_{\boldsymbol{k}} b_{-\boldsymbol{k}} + \text{h.c}) + D_{\boldsymbol{k}}, \tag{A1}$$

with the definitions of $A_{\boldsymbol{k}}$, $B_{\boldsymbol{k}}$, $C_{\boldsymbol{k}}$ and $D_{\boldsymbol{k}}$ given in (3.20)-(3.24). A transformation of the Hamiltonian to a diagonal form of normal mode magnon creation and annihilation operators $\alpha^{\dagger}_{\boldsymbol{k}} \alpha_{\boldsymbol{k}}$ and $\beta^{\dagger}_{\boldsymbol{k}} \beta_{\boldsymbol{k}}$ will take the form

$$H = \varepsilon_0 + \sum_{\boldsymbol{k}} \hbar (\omega_{\alpha \boldsymbol{k}} \alpha^{\dagger}_{\boldsymbol{k}} \alpha_{\boldsymbol{k}} + \omega_{\beta \boldsymbol{k}} \beta^{\dagger}_{\boldsymbol{k}} \beta_{\boldsymbol{k}}), \tag{A2}$$

where the two magnon modes have the frequencies $\omega_{\alpha \boldsymbol{k}}$ and $\omega_{\beta \boldsymbol{k}}$. We write Eq. (A1) in matrix form

$$H = \hbar \sum_{\boldsymbol{k}>0} H_{\boldsymbol{k}}, \quad H_{\boldsymbol{k}} = (X)^{\dagger} [H] (X) \tag{A3}$$

with

$$(X) = \begin{pmatrix} a_{\boldsymbol{k}} \\ b^{\dagger}_{-\boldsymbol{k}} \\ a^{\dagger}_{-\boldsymbol{k}} \\ b_{\boldsymbol{k}} \end{pmatrix}, \quad [H] = \hbar \begin{pmatrix} A_{\boldsymbol{k}} + \gamma\Upsilon & B_{\boldsymbol{k}} & C_{\boldsymbol{k}} & 0 \\ B_{\boldsymbol{k}} & A_{\boldsymbol{k}} - \gamma\Upsilon & 0 & C_{\boldsymbol{k}} \\ C_{\boldsymbol{k}} & 0 & A_{\boldsymbol{k}} + \gamma\Upsilon & B_{\boldsymbol{k}} \\ 0 & C_{\boldsymbol{k}} & B_{\boldsymbol{k}} & A_{\boldsymbol{k}} - \gamma\Upsilon \end{pmatrix}. \tag{A4}$$

and perform a Bogoliubov transformation

$$(X) = [Q](Z), \quad \begin{pmatrix} a_{\boldsymbol{k}} \\ b^{\dagger}_{-\boldsymbol{k}} \\ a^{\dagger}_{-\boldsymbol{k}} \\ b_{\boldsymbol{k}} \end{pmatrix} = \begin{pmatrix} Q_{11} & Q_{12} & Q_{13} & Q_{14} \\ Q_{21} & Q_{22} & Q_{23} & Q_{24} \\ Q_{31} & Q_{32} & Q_{33} & Q_{34} \\ Q_{41} & Q_{42} & Q_{43} & Q_{44} \end{pmatrix} \begin{pmatrix} \alpha_{\boldsymbol{k}} \\ \beta^{\dagger}_{-\boldsymbol{k}} \\ \alpha^{\dagger}_{-\boldsymbol{k}} \\ \beta_{\boldsymbol{k}} \end{pmatrix}, \tag{A5}$$

where $[Q]$ is the transformation matrix. The transformation yield the following set of equations

$$a_{\boldsymbol{k}} = Q_{11}\alpha_{\boldsymbol{k}} + Q_{12}\beta^{\dagger}_{-\boldsymbol{k}} + Q_{13}\alpha^{\dagger}_{-\boldsymbol{k}} + Q_{14}\beta_{\boldsymbol{k}}, \tag{A6}$$

$$b^{\dagger}_{-\boldsymbol{k}} = Q_{21}\alpha_{\boldsymbol{k}} + Q_{22}\beta^{\dagger}_{-\boldsymbol{k}} + Q_{23}\alpha^{\dagger}_{-\boldsymbol{k}} + Q_{24}\beta_{\boldsymbol{k}}, \tag{A7}$$

$$a^{\dagger}_{-\boldsymbol{k}} = Q_{31}\alpha_{\boldsymbol{k}} + Q_{32}\beta^{\dagger}_{-\boldsymbol{k}} + Q_{33}\alpha^{\dagger}_{-\boldsymbol{k}} + Q_{34}\beta_{\boldsymbol{k}}, \tag{A8}$$

$$b_{\boldsymbol{k}} = Q_{41}\alpha_{\boldsymbol{k}} + Q_{42}\beta^{\dagger}_{-\boldsymbol{k}} + Q_{43}\alpha^{\dagger}_{-\boldsymbol{k}} + Q_{44}\beta_{\boldsymbol{k}}. \tag{A9}$$

By writing the Hermitian conjugates of Eqs. (A8) and (A9),

$$a_{\boldsymbol{k}} = Q^{*}_{31}(-\boldsymbol{k})\alpha^{\dagger}_{-\boldsymbol{k}} + Q^{*}_{32}(-\boldsymbol{k})\beta_{\boldsymbol{k}} + Q^{*}_{33}(-\boldsymbol{k})\alpha_{\boldsymbol{k}} + Q^{*}_{34}(-\boldsymbol{k})\beta^{\dagger}_{-\boldsymbol{k}}, \tag{A10}$$

$$b^{\dagger}_{-\boldsymbol{k}} = Q^{*}_{41}(-\boldsymbol{k})\alpha^{\dagger}_{-\boldsymbol{k}} + Q^{*}_{42}(-\boldsymbol{k})\beta_{\boldsymbol{k}} + Q^{*}_{43}(-\boldsymbol{k})\alpha_{\boldsymbol{k}} + Q^{*}_{44}(-\boldsymbol{k})\beta^{\dagger}_{-\boldsymbol{k}}. \tag{A11}$$

we deduct the following symmetry requirements for $[Q]$

$$\begin{aligned} &Q_{11}(\boldsymbol{k}) = Q^{*}_{33}(-\boldsymbol{k}), \quad Q_{12}(\boldsymbol{k}) = Q^{*}_{34}(-\boldsymbol{k}), \quad Q_{13}(\boldsymbol{k}) = Q^{*}_{31}(-\boldsymbol{k}), \\ &Q_{14}(\boldsymbol{k}) = Q^{*}_{32}(-\boldsymbol{k}), \quad Q_{21}(\boldsymbol{k}) = Q^{*}_{43}(-\boldsymbol{k}), \quad Q_{22}(\boldsymbol{k}) = Q^{*}_{44}(-\boldsymbol{k}), \\ &Q_{23}(\boldsymbol{k}) = Q^{*}_{41}(-\boldsymbol{k}), \quad Q_{24}(\boldsymbol{k}) = Q^{*}_{42}(-\boldsymbol{k}). \end{aligned} \tag{A12}$$

We further assume $Q_{ij}(\boldsymbol{k}) = Q^{*}_{ij}(-\boldsymbol{k})$, then rewrite the transformation matrix

$$[Q] = \begin{pmatrix} Q_{11} & Q_{12} & Q_{13} & Q_{14} \\ Q_{21} & Q_{22} & Q_{23} & Q_{24} \\ Q_{13} & Q_{14} & Q_{11} & Q_{12} \\ Q_{23} & Q_{24} & Q_{21} & Q_{22} \end{pmatrix}, \tag{A13}$$

and write the system of equations from the eigenvalue equation (3.35)

$$(A_{\boldsymbol{k}}-\omega_{\alpha\boldsymbol{k}})Q_{11}+B_{\boldsymbol{k}}Q_{21}+C_{\boldsymbol{k}}Q_{13} = 0, \quad (A_{\boldsymbol{k}}+\omega_{\beta\boldsymbol{k}})Q_{12}+B_{\boldsymbol{k}}Q_{22}+C_{\boldsymbol{k}}Q_{14} = 0, \tag{A14}$$

$$(A_{\boldsymbol{k}}+\omega_{\alpha\boldsymbol{k}})Q_{21}+B_{\boldsymbol{k}}Q_{11}+C_{\boldsymbol{k}}Q_{23} = 0, \quad (A_{\boldsymbol{k}}-\omega_{\beta\boldsymbol{k}})Q_{22}+B_{\boldsymbol{k}}Q_{12}+C_{\boldsymbol{k}}Q_{24} = 0, \tag{A15}$$

$$(A_{\boldsymbol{k}}+\omega_{\alpha\boldsymbol{k}})Q_{13}+B_{\boldsymbol{k}}Q_{23}+C_{\boldsymbol{k}}Q_{11} = 0, \quad (A_{\boldsymbol{k}}-\omega_{\beta\boldsymbol{k}})Q_{14}+B_{\boldsymbol{k}}Q_{24}+C_{\boldsymbol{k}}Q_{12} = 0, \tag{A16}$$

$$(A_{\boldsymbol{k}}-\omega_{\alpha\boldsymbol{k}})Q_{23}+B_{\boldsymbol{k}}Q_{13}+C_{\boldsymbol{k}}Q_{21} = 0, \quad (A_{\boldsymbol{k}}+\omega_{\beta\boldsymbol{k}})Q_{24}+B_{\boldsymbol{k}}Q_{14}+C_{\boldsymbol{k}}Q_{22} = 0. \tag{A17}$$

We solve for the Bogoliubov-coefficients, who take the form

$$\frac{Q_{21}}{Q_{11}} = \frac{B_{\boldsymbol{k}}[(A_{\boldsymbol{k}}+\gamma\Upsilon+\omega_{\alpha\boldsymbol{k}})(A_{\boldsymbol{k}}-\gamma\Upsilon-\omega_{\alpha\boldsymbol{k}}) - B^2_{\boldsymbol{k}} + C^2_{\boldsymbol{k}}]}{(A_{\boldsymbol{k}}-\gamma\Upsilon+\omega_{\alpha\boldsymbol{k}})B^2_{\boldsymbol{k}} + (A_{\boldsymbol{k}}+\gamma\Upsilon+\omega_{\alpha\boldsymbol{k}})[C^2_{\boldsymbol{k}} + \omega^2_{\alpha\boldsymbol{k}} - (A_{\boldsymbol{k}}-\gamma\Upsilon)^2]}, \tag{A18}$$

$$\frac{Q_{23}}{Q_{11}} = \frac{-2B_{\boldsymbol{k}}C_{\boldsymbol{k}}(A_{\boldsymbol{k}}+\omega_{\alpha\boldsymbol{k}})}{(A_{\boldsymbol{k}}-\gamma\Upsilon+\omega_{\alpha\boldsymbol{k}})B^2_{\boldsymbol{k}} + (A_{\boldsymbol{k}}+\gamma\Upsilon+\omega_{\alpha\boldsymbol{k}})[C^2_{\boldsymbol{k}} + \omega^2_{\alpha\boldsymbol{k}} - (A_{\boldsymbol{k}}-\gamma\Upsilon)^2]}, \tag{A19}$$

$$\frac{Q_{13}}{Q_{11}} = \frac{C_{\boldsymbol{k}}[(A_{\boldsymbol{k}}-\gamma\Upsilon)^2 - \omega^2_{\alpha\boldsymbol{k}} + B^2_{\boldsymbol{k}} - C^2_{\boldsymbol{k}}]}{(A_{\boldsymbol{k}}-\gamma\Upsilon+\omega_{\alpha\boldsymbol{k}})B^2_{\boldsymbol{k}} + (A_{\boldsymbol{k}}+\gamma\Upsilon+\omega_{\alpha\boldsymbol{k}})[C^2_{\boldsymbol{k}} + \omega^2_{\alpha\boldsymbol{k}} - (A_{\boldsymbol{k}}-\gamma\Upsilon)^2]}, \tag{A20}$$

$$\frac{Q_{12}}{Q_{22}} = \frac{B_{\boldsymbol{k}}[(A_{\boldsymbol{k}}+\gamma\Upsilon-\omega_{\beta\boldsymbol{k}})(A_{\boldsymbol{k}}-\gamma\Upsilon+\omega_{\beta\boldsymbol{k}}) - B^2_{\boldsymbol{k}} + C^2_{\boldsymbol{k}}]}{(A_{\boldsymbol{k}}+\gamma\Upsilon+\omega_{\beta\boldsymbol{k}})B^2_{\boldsymbol{k}} + (A_{\boldsymbol{k}}-\gamma\Upsilon+\omega_{\beta\boldsymbol{k}})[C^2_{\boldsymbol{k}} + \omega^2_{\beta\boldsymbol{k}} - (A_{\boldsymbol{k}}+\gamma\Upsilon)^2]}, \tag{A21}$$

$$\frac{Q_{14}}{Q_{22}} = \frac{-2B_{\boldsymbol{k}}C_{\boldsymbol{k}}(A_{\boldsymbol{k}}+\omega_{\beta\boldsymbol{k}})}{(A_{\boldsymbol{k}}+\gamma\Upsilon+\omega_{\beta\boldsymbol{k}})B_{\boldsymbol{k}}^2+(A_{\boldsymbol{k}}-\gamma\Upsilon+\omega_{\beta\boldsymbol{k}})[C_{\boldsymbol{k}}^2+\omega_{\beta\boldsymbol{k}}^2-(A_{\boldsymbol{k}}+\gamma\Upsilon)^2]}, \quad \text{(A22)}$$

$$\frac{Q_{24}}{Q_{22}} = \frac{C_{\boldsymbol{k}}[(A_{\boldsymbol{k}}+\gamma\Upsilon)^2-\omega_{\beta\boldsymbol{k}}^2+B_{\boldsymbol{k}}^2-C_{\boldsymbol{k}}^2]}{(A_{\boldsymbol{k}}+\gamma\Upsilon+\omega_{\beta\boldsymbol{k}})B_{\boldsymbol{k}}^2+(A_{\boldsymbol{k}}-\gamma\Upsilon+\omega_{\beta\boldsymbol{k}})[C_{\boldsymbol{k}}^2+\omega_{\beta\boldsymbol{k}}^2-(A_{\boldsymbol{k}}+\gamma\Upsilon)^2]}, \quad \text{(A23)}$$

As we will show it is substantially more practical to express Q_{11} and Q_{22} by reduced Q'-coefficients (than effective fields) given by

$$\frac{Q_{21}}{Q_{11}} \equiv Q'_{21}, \quad \frac{Q_{23}}{Q_{11}} \equiv Q'_{23}, \quad \frac{Q_{13}}{Q_{11}} \equiv Q'_{13}, \quad \text{(A24)}$$

$$\frac{Q_{12}}{Q_{22}} \equiv Q'_{12}, \quad \frac{Q_{14}}{Q_{22}} \equiv Q'_{14}, \quad \frac{Q_{24}}{Q_{22}} \equiv Q'_{24}. \quad \text{(A25)}$$

The relation between Q_{11} and Q_{22} is obtainable through the orthonormality relation (3.34)

$$Q_{11}^2 - Q_{12}^2 - Q_{13}^2 + Q_{14}^2 = 1, \quad \text{(A26)}$$

$$Q_{21}^2 - Q_{22}^2 - Q_{23}^2 + Q_{24}^2 = -1, \quad \text{(A27)}$$

and after a little algebra, we end up with

$$\Rightarrow Q_{11}^2 = \frac{{Q'_{12}}^2 - {Q'_{14}}^2 - {Q'_{24}}^2 + 1}{(1-{Q'_{24}}^2)(1-{Q'_{13}}^2)+({Q'_{14}}^2-{Q'_{12}}^2)({Q'_{21}}^2-{Q'_{23}}^2)}, \quad \text{(A28)}$$

$$\Rightarrow Q_{22}^2 = \frac{{Q'_{21}}^2 - {Q'_{23}}^2 - {Q'_{13}}^2 + 1}{(1-{Q'_{24}}^2)(1-{Q'_{13}}^2)+({Q'_{14}}^2-{Q'_{12}}^2)({Q'_{21}}^2-{Q'_{23}}^2)}. \quad \text{(A29)}$$

Appendix B

Hydrodynamic form of the generalized Gross-Pitaevskii equation

The starting point is the generalized Gross-Pitaevskii equation from (5.26)

$$i\hbar\frac{\partial\Phi(\boldsymbol{r},t)}{\partial t} = \Big[-\frac{\hbar^2\nabla^2}{2m} + \varepsilon_0 + g\rho(\boldsymbol{r},t) + 2gn(\boldsymbol{r},t) - i\alpha\hbar\omega_E\Big]\Phi(\boldsymbol{r},t) + g\mathrm{Im}[\langle\tilde{\psi}^\dagger\tilde{\psi}\tilde{\psi}\rangle], \tag{B1}$$

where $\Phi(\boldsymbol{r},t)$ is the position- and time dependent macroscopic Bose wavefunction; m is the boson mass; ε_0 is an anisotropic harmonic potential; g is the zero-range pseudopotential strength for the interatomic potential; $\rho(\boldsymbol{r},t)$ is the condensate density; $n(\boldsymbol{r},t)$ is the noncondensate (thermal cloud) density; $\mathrm{Im}[\langle\tilde{\psi}^\dagger\tilde{\psi}\tilde{\psi}\rangle]$ is the imaginary parts of the three-field correlation function expressed through the quantum field operator $\tilde{\psi}$ describing the thermal fluctuations around $\Phi(\boldsymbol{r},t)$; α is the dimensionless Gilbert damping constant and ω_E is the AF resonance frequency. In order to reduce the GGP to a convenient hydrodynamic form for the condensate density and the condensate velocity, we solve the equation of motion with the ρ- and phase dependent, θ, macroscopic Bose wavefunction $\Phi(\boldsymbol{r},t) = \sqrt{\rho(\boldsymbol{r},t)}e^{i\theta(\boldsymbol{r},t)}$. The position- and time depence will be left out of the following calculations. The l.h.s. of eq. (B1) reads

$$i\hbar\frac{\partial\Phi}{\partial t} = \Big(\frac{i\hbar}{2\rho}\nabla\rho - \hbar\nabla\theta\Big)\Phi, \tag{B2}$$

and the kinetic term reads

$$\begin{aligned} -\frac{\hbar^2}{2m}\nabla^2\Phi &= -\frac{\hbar^2}{2m}\Big(-\frac{1}{4\rho^2}(\nabla\rho)^2 + \frac{1}{2\rho}\nabla^2 + \rho + \frac{i}{\rho}\nabla\rho\theta + i\nabla^2\theta - (\nabla\theta)^2\Big)\Phi \\ &= \Big(-\frac{\hbar^2}{2m}\frac{\nabla^2\sqrt{\rho}}{\sqrt{\rho}} + \frac{\hbar^2}{2m}|\nabla\theta|^2 - \frac{i\hbar^2}{2m\rho}(\nabla\rho\nabla\theta + \rho\nabla^2\theta)\Big)\Phi. \end{aligned} \tag{B3}$$

Rewriting the GGP

$$i\hbar\frac{\partial\Phi}{\partial t} = \Big[-\frac{\hbar^2\nabla^2}{2m} + \varepsilon_0 + g\rho + 2gn - i\Big(\alpha\hbar\omega_E - \frac{g}{\rho}\mathrm{Im}[\Phi^*\langle\tilde{\psi}^\dagger\tilde{\psi}\tilde{\psi}\rangle]\Big)\Big]\Phi, \tag{B4}$$

allows for the elimination of Φ when using (B2) and (B3) in the GGP. The resulting expression takes the form

$$\begin{aligned}\Big(\frac{i\hbar}{2\rho}\nabla\rho - \hbar\nabla\theta\Big) = &-\frac{\hbar^2}{2m}\frac{\nabla^2\sqrt{\rho}}{\sqrt{\rho}} + \frac{\hbar^2}{2m}|\nabla\theta|^2 - \frac{i\hbar^2}{2m\rho}(\nabla\rho\nabla\theta + \rho\nabla^2\theta) \\ &+ \varepsilon_0 + g\rho + 2gn - i\Big(\alpha\hbar\omega_E - \frac{g}{\rho}\mathrm{Im}[\Phi^*\langle\tilde{\psi}^\dagger\tilde{\psi}\tilde{\psi}\rangle]\Big).\end{aligned} \tag{B5}$$

Separating the real and imaginary terms render the two equations of motion for the condensate density ρ and the condensate velocity $\boldsymbol{v}_c$. The real terms give

$$\hbar\nabla\theta = -(\mu_c + \frac{1}{2}m\boldsymbol{v}_c^2), \tag{B6}$$

where the condensate chemical potential μ_c is given by

$$\mu_c(\boldsymbol{r},t) \equiv -\frac{\hbar^2}{2m}\frac{\nabla^2\sqrt{\rho(\boldsymbol{r},t)}}{\sqrt{\rho(\boldsymbol{r},t)}} + \varepsilon_0 + g\rho(\boldsymbol{r},t) + 2gn(\boldsymbol{r},t) \tag{B7}$$

and the condensate velocity field

$$\boldsymbol{v}_c \equiv \frac{\hbar}{m}\nabla\theta. \tag{B8}$$

Substituting the phase gradient $\nabla\theta$ in (B6) with the definition of $\boldsymbol{v}_c$ in (B8) finalize the equation of motion for the condensate velocity

$$m\nabla\boldsymbol{v}_c = -\nabla\Big(\mu_c + \frac{1}{2}m\boldsymbol{v}_c^2\Big) = -\nabla\varepsilon_c, \tag{B9}$$

where $\varepsilon_c \equiv \mu_c + \frac{1}{2}m\boldsymbol{v}_c^2$ is the local energy of a condensate atom with potential energy μ_c and kinetic energy $\frac{1}{2}m\boldsymbol{v}_c^2$. From the imaginary terms of (B5), the equation of motion for the condensate density takes the form

$$\hbar\dot{\rho} + \hbar\nabla(\rho\boldsymbol{v}_c) = -\Gamma_{12}[f,\Phi] - 2\alpha\hbar\omega_E\rho, \tag{B10}$$

where we have introduced the new function

$$\Gamma_{12}[f,\Phi] \equiv -2g\mathrm{Im}[\Phi^*\langle\tilde{\psi}^\dagger\tilde{\psi}\tilde{\psi}\rangle]. \tag{B11}$$

Appendix C

Collision integral contributions in a strong magnetic field

The Boltzmann equation describe the thermal magnons and reads

$$\frac{\partial f[\boldsymbol{k},t]}{\partial t} = \left(\frac{\partial f[\boldsymbol{k},t]}{\partial t}\right)\Big|_{\text{phonons}} + \left(\frac{\partial f[\boldsymbol{k}_0,t]}{\partial t}\right)\Big|_{pump} + \left(\frac{\partial f[\boldsymbol{k},t]}{\partial t}\right)\Big|_{coll}, \tag{C1}$$

where the collision term has two contributions

$$\left(\frac{\partial f[\boldsymbol{k},t]}{\partial t}\right)\Big|_{coll} = C_{12}[f,\Phi] + C_{22}[f]. \tag{C2}$$

The contributions are given by

$$\begin{aligned} C_{12}[f,\Phi] = \frac{2g^2\rho}{(2\pi)^2\hbar^4}\int \mathrm{d}\boldsymbol{p}_1 \int \mathrm{d}\boldsymbol{p}_2 \int \mathrm{d}\boldsymbol{p}_3 \delta(m\boldsymbol{v}_c + \boldsymbol{p}_1 - \boldsymbol{p}_2 - \boldsymbol{p}_3) \\ \times \delta(\varepsilon_{\boldsymbol{p}_c} + \tilde{\varepsilon}_{\boldsymbol{p}_1} - \tilde{\varepsilon}_{\boldsymbol{p}_2} - \tilde{\varepsilon}_{\boldsymbol{p}_3})[\delta(\boldsymbol{p}_c - \boldsymbol{p}_1) - \delta(\boldsymbol{p}_c - \boldsymbol{p}_2) - \delta(\boldsymbol{p}_c - \boldsymbol{p}_3)] \\ \times [(1+f_1)f_2f_3 - f_1(1+f_2)(1+f_3)], \end{aligned} \tag{C3}$$

$$\begin{aligned} C_{22}[f] = \frac{2g^2}{(2\pi)^5\hbar^7}\int \mathrm{d}\boldsymbol{p}_2 \int \mathrm{d}\boldsymbol{p}_3 \int \mathrm{d}\boldsymbol{p}_4 \delta(\boldsymbol{p} + \boldsymbol{p}_2 - \boldsymbol{p}_3 - \boldsymbol{p}_4)\times \\ \delta(\tilde{\varepsilon}_p + \tilde{\varepsilon}_{p_2} - \tilde{\varepsilon}_{p_3} - \tilde{\varepsilon}_{p_4})[(1+f)(1+f_2)f_3f_4 - ff_2(1+f_3)(1+f_4)], \end{aligned} \tag{C4}$$

where $\varepsilon_{\boldsymbol{p}_c} = \mu_c + \frac{1}{2}m\boldsymbol{v}_c^2$; $\tilde{\varepsilon}_p = \varepsilon_p + U(\boldsymbol{r},t)$; $U(\boldsymbol{r},t) = \varepsilon_0 + 2g(\rho(\boldsymbol{r},t) + n(\boldsymbol{r},t))$ and the distribution function $f_i \equiv f_i[\boldsymbol{p}_i,\boldsymbol{r},t]$. If the collision rate is high among the excited magnons, the distribution function is driven efficiently from the collision integral C_{22} towards the local equilibrium Bose distribution

$$\tilde{f}[\boldsymbol{p}_i - m\boldsymbol{v}_n,t] \equiv \tilde{f}[\tilde{\boldsymbol{p}}_i,t] = \frac{1}{e^{\beta[\varepsilon_{\boldsymbol{p}_i - m\boldsymbol{v}_n} + U - \tilde{\mu}]} - 1}, \tag{C5}$$

where the local temperature β, mean field U and chemical potential $\tilde{\mu}$ are all functions of position and time. This solution to the local equilibrium is guaranteed by the condition $C_{22}[\tilde{f}] = 0$. Let's show this. We first establish a helpful identity.

$$f_x + 1 = \frac{1}{e^x - 1} + 1 = \frac{1 + e^x - 1}{e^x - 1} = e^x f_x \tag{C6}$$

C_{22} in equilibrium takes the form

$$\begin{aligned} C_{22}[\tilde{f}] = \frac{2g^2}{(2\pi)^5\hbar^7} \int \mathrm{d}\tilde{\boldsymbol{p}}_2 \int \mathrm{d}\tilde{\boldsymbol{p}}_3 \int \mathrm{d}\tilde{\boldsymbol{p}}_4 \delta(\tilde{\boldsymbol{p}} + \tilde{\boldsymbol{p}}_2 - \tilde{\boldsymbol{p}}_3 - \tilde{\boldsymbol{p}}_4) \\ \times \delta(\tilde{\varepsilon}_{\tilde{\boldsymbol{p}}} + \tilde{\varepsilon}_{\tilde{\boldsymbol{p}}_2} - \tilde{\varepsilon}_{\tilde{\boldsymbol{p}}_3} - \tilde{\varepsilon}_{\tilde{\boldsymbol{p}}_4})[(1 + \tilde{f})(1 + \tilde{f}_2)\tilde{f}_3\tilde{f}_4 - \tilde{f}\tilde{f}_2(1 + \tilde{f}_3)(1 + \tilde{f}_4)]. \end{aligned} \tag{C7}$$

We evaluate the statistical factors in C_{22}.

$$\begin{aligned} [(1 + \tilde{f})(1 + \tilde{f}_2)\tilde{f}_3\tilde{f}_4 - \tilde{f}\tilde{f}_2(1 + \tilde{f}_3)(1 + \tilde{f}_4)] &= (ee^2 - e^3e^4)\tilde{f}\tilde{f}_2\tilde{f}_3\tilde{f}_4 \\ &= \left(e^{\beta(\tilde{\varepsilon}_{\tilde{\boldsymbol{p}}} + \tilde{\varepsilon}_{\tilde{\boldsymbol{p}}_2} - 2\tilde{\mu})} - e^{\beta(\tilde{\varepsilon}_{\tilde{\boldsymbol{p}}_3} + \tilde{\varepsilon}_{\tilde{\boldsymbol{p}}_4} - 2\tilde{\mu})}\right)\tilde{f}\tilde{f}_2\tilde{f}_3\tilde{f}_4. \end{aligned} \tag{C8}$$

From the δ-term in (C7) $\delta(\tilde{\varepsilon}_{\tilde{\boldsymbol{p}}} + \tilde{\varepsilon}_{\tilde{\boldsymbol{p}}_2} - \tilde{\varepsilon}_{\tilde{\boldsymbol{p}}_3} - \tilde{\varepsilon}_{\tilde{\boldsymbol{p}}_4})$, we see that the condition $\tilde{\varepsilon}_{\tilde{\boldsymbol{p}}} + \tilde{\varepsilon}_{\tilde{\boldsymbol{p}}_2} = \tilde{\varepsilon}_{\tilde{\boldsymbol{p}}_3} + \tilde{\varepsilon}_{\tilde{\boldsymbol{p}}_4}$ applies. We can therefore conclude that the statistical factors cancel and that the collision integral

$$C_{22}[\tilde{f}] = 0. \tag{C9}$$

However, the first collision integral is nonzero in the local equilibrium.

$$\begin{aligned} C_{12}[\tilde{f}] = \frac{2g^2\rho}{(2\pi)^2\hbar^4} \int \mathrm{d}\tilde{\boldsymbol{p}}_1 \int \mathrm{d}\tilde{\boldsymbol{p}}_2 \int \mathrm{d}\tilde{\boldsymbol{p}}_3 \delta(m\boldsymbol{v}_c + \tilde{\boldsymbol{p}}_1 - \tilde{\boldsymbol{p}}_2 - \tilde{\boldsymbol{p}}_3) \\ \times \delta(\varepsilon_{\tilde{\boldsymbol{p}}_c} + \tilde{\varepsilon}_{\tilde{\boldsymbol{p}}_1} - \tilde{\varepsilon}_{\tilde{\boldsymbol{p}}_2} - \tilde{\varepsilon}_{\tilde{\boldsymbol{p}}_3})[\delta(\tilde{\boldsymbol{p}}_c - \tilde{\boldsymbol{p}}_1) - \delta(\tilde{\boldsymbol{p}}_c - \tilde{\boldsymbol{p}}_2) - \delta(\tilde{\boldsymbol{p}}_c - \tilde{\boldsymbol{p}}_3)] \\ \times [(1 + \tilde{f}_1)\tilde{f}_2\tilde{f}_3 - \tilde{f}_1(1 + \tilde{f}_2)(1 + \tilde{f}_3)] \end{aligned} \tag{C10}$$

We evaluate the statistical factors and use the identity of the distribution function from (C6)

$$\begin{aligned} &[(1 + \tilde{f}_1)\tilde{f}_2\tilde{f}_3 - \tilde{f}_1(1 + \tilde{f}_2)(1 + \tilde{f}_3)] \\ &\qquad = (1 + \tilde{f}_1)\tilde{f}_2\tilde{f}_3 - (1 + \tilde{f}_1)\tilde{f}_2\tilde{f}_3 e^{-\beta[\tilde{\varepsilon}_{\tilde{\boldsymbol{p}}_1} - \tilde{\mu}] - [\tilde{\varepsilon}_{\tilde{\boldsymbol{p}}_2} - \tilde{\mu}] - [\tilde{\varepsilon}_{\tilde{\boldsymbol{p}}_3} - \tilde{\mu}]} \\ &\qquad = (1 + \tilde{f}_1)\tilde{f}_2\tilde{f}_3\left(1 - e^{-\beta[\tilde{\varepsilon}_{\tilde{\boldsymbol{p}}_1} - \tilde{\varepsilon}_{\tilde{\boldsymbol{p}}_2} - \tilde{\varepsilon}_{\tilde{\boldsymbol{p}}_3} + \tilde{\mu}]}\right) \\ &\qquad = (1 + \tilde{f}_1)\tilde{f}_2\tilde{f}_3\left(1 - e^{\beta[\varepsilon_{\tilde{\boldsymbol{p}}_c} - \tilde{\mu}]}\right), \end{aligned} \tag{C11}$$

where we in the final step where we've used the condition from the delta-term in $C_{12}[\tilde{f}]$ $\varepsilon_{\tilde{\boldsymbol{p}}_c} + \tilde{\varepsilon}_{\tilde{\boldsymbol{p}}_1} = \tilde{\varepsilon}_{\tilde{\boldsymbol{p}}_2} + \tilde{\varepsilon}_{\tilde{\boldsymbol{p}}_3}$. By Taylor-expanding the exponential, we find the final value of

the first collision integral to be

$$
\begin{aligned}
C_{12}[\tilde{f}] = & \frac{2g^2\rho}{(2\pi)^2\hbar^4}\int \mathrm{d}\tilde{\boldsymbol{p}}_1 \int \mathrm{d}\tilde{\boldsymbol{p}}_2 \int \mathrm{d}\tilde{\boldsymbol{p}}_3 \delta(m\boldsymbol{v}_c + \tilde{\boldsymbol{p}}_1 - \tilde{\boldsymbol{p}}_2 - \tilde{\boldsymbol{p}}_3) \\
& \times \delta(\varepsilon_{\tilde{\boldsymbol{p}}_c} + \tilde{\varepsilon}_{\tilde{\boldsymbol{p}}_1} - \tilde{\varepsilon}_{\tilde{\boldsymbol{p}}_2} - \tilde{\varepsilon}_{\tilde{\boldsymbol{p}}_3})[\delta(\tilde{\boldsymbol{p}}_c - \tilde{\boldsymbol{p}}_1) - \delta(\tilde{\boldsymbol{p}}_c - \tilde{\boldsymbol{p}}_2) - \delta(\tilde{\boldsymbol{p}}_c - \tilde{\boldsymbol{p}}_3)] \\
& \times (1 + \tilde{f}_1)\tilde{f}_2\tilde{f}_3(-\beta[\varepsilon_{\tilde{\boldsymbol{p}}_c} - \tilde{\mu}]) \\
= & \frac{2g^2\rho}{(2\pi)^2\hbar^4 k_B T}(\tilde{\mu} - m(\boldsymbol{v}_c - \boldsymbol{v}_n)^2/2 - \mu_c) \int \mathrm{d}\tilde{\boldsymbol{p}}_1 \int \mathrm{d}\tilde{\boldsymbol{p}}_2 \int \mathrm{d}\tilde{\boldsymbol{p}}_3 \\
& \times \delta(m\boldsymbol{v}_c + \tilde{\boldsymbol{p}}_1 - \tilde{\boldsymbol{p}}_2 - \tilde{\boldsymbol{p}}_3)\delta(\varepsilon_{\tilde{\boldsymbol{p}}_c} + \tilde{\varepsilon}_{\tilde{\boldsymbol{p}}_1} - \tilde{\varepsilon}_{\tilde{\boldsymbol{p}}_2} - \tilde{\varepsilon}_{\tilde{\boldsymbol{p}}_3}) \\
& \times [\delta(\tilde{\boldsymbol{p}}_c - \tilde{\boldsymbol{p}}_1) - \delta(\tilde{\boldsymbol{p}}_c - \tilde{\boldsymbol{p}}_2) - \delta(\tilde{\boldsymbol{p}}_c - \tilde{\boldsymbol{p}}_3)](1 + \tilde{f}_1)\tilde{f}_2\tilde{f}_3,
\end{aligned}
\tag{C12}
$$

where we've set $\beta = 1/k_B T$ and rewritten $\varepsilon_{\tilde{\boldsymbol{p}}_c} = \mu_c + \frac{1}{2}m(\boldsymbol{v}_c - \boldsymbol{v}_n)^2$.

Bibliography

[1] A. E. Varegg, "Parametric Pumping of Antiferromagnetic Magnons", *NTNU*, Project Assignment, (2018).

[2] A. S. Borovik-Romanov and S. K. Sinha, "Spin Waves and Magnetic Excitations", *Modern Problems in Condensed Matter Physics*, vol. 22.1, North Holland, Amsterdam, (1988).

[3] F. Dalfovo, S. Giorgini, L. P. Pitaevskii, and S. Stringari, "Theory of Bose-Einstein condensation in trapped gases", *Rev. Mod. Phys.*, 71, 463 (1999).

[4] T. Nikuni, M. Oshikawa, A. Oosawa, and H. Tanaka, "Bose-Einstein Condensation of Dilute Magnons in $\mathrm{TlCuCl_3}$", *Phys. Rev. Lett.*, 84, 5868 (2000).

[5] C. Rüegg, N. Cavadini, A. Furrer, H. U. Gudel, K. Kramer, H. Mutka, A. Wildes, K. Habicht, and P. Vorderwisch, "Bose–Einstein condensation of the triplet states in the magnetic insulator $\mathrm{TlCuCl_3}$", *Nature (London)*, 423, 62 (2003).

[6] T. Radu, H. Wilhelm, V. Yushankhai, D. Kovrizhin, R. Coldea, Z. Tylczynski, T. Lühmann, and F. Steglich, "Bose-Einstein Condensation of Magnons in $\mathrm{Cs_2CuCl_4}$", *Phys. Rev. Lett.*, 95, 127202 (2005).

[7] S. O. Demokritov, V. E. Demidov, O. Dzyapko, G. A. Melkov, A. A. Serga, B. Hillebrands, and A. N. Slavin, "Bose–Einstein condensation of quasi-equilibrium magnons at room temperature under pumping", *Nature (London)*, 443, 430 (2006).

[8] J. Kasprzak, M. Richard, S. Kundermann, A. Baas, P. Jeam-brun, J. M. J. Keeling, F. M. Marchetti, M. H. Szymanska, R. Andre, J. L. Staehli, V. Savona, P. B. Littlewood, B. Deveaud, and L. S. Dang, "Bose–Einstein condensation of exciton polaritons", *Nature (London)*, 443, 409 (2006).

[9] R. Balili, V. Hartwell, D. Snoke, L. Pfeiffer, and K. West, "Bose-Einstein Condensation of Microcavity Polaritons in a Trap", *Science*, vol. 316, 1007 (2007).

[10] J. Klaers, J. Schmitt, F. Vewinger, and M. Weitz, "Bose–Einstein condensation of photons in an optical microcavity", *Nature (London)*, 468, 545 (2010).

[11] Y. M. Bunkov, E. M. Alakshin, R. R. Gazizulin, A. V. Klochkov, V. V. Kuzmin, T. R. Safin, and M. S. Tagirov, "Discovery of the classical Bose-Einstein condensation of magnons in solid antiferromagnets", *JETP Lett.*, 94, 68 (2011).

[12] S. N. Bose, "Plancks Gesetz und Lichtquantenhypothese", *Zeitschrift für Physik*, vol. 26, Issue 1, (1924).

[13] A. Einstein, "Quantentheorie des einatomigen idealen Gases - Part I", *Sber. Preuss. Akad. Wiss.*, 22, (1924).

[14] A. Einstein, "Quantentheorie des einatomigen idealen Gases - Part II", *Sber. Preuss. Akad. Wiss.*, 1, (1925).

[15] S. A. Bender, R. A. Duine, and Y. Tserkovnyak, "Electronic Pumping of Quasiequilibrium Bose-Einstein-Condensed Magnons", *Phys. Rev. Lett.*, 108, 246601 (2012).

[16] S. A. Bender, R. A. Duine, A. Brataas, and Y. Tserkovnyak, "Dynamic phase diagram of dc-pumped magnon condensates", *Phys. Rev. B*, 90, 094409 (2014).

[17] E. L. Fjærbu, N. Rohling, and A. Brataas, "Electrically driven Bose-Einstein condensation of magnons in antiferromagnets", *Phys. Rev. B*, 95, 144408 (2017).

[18] E. B. Sonin, "Phase fixation, excitonic and spin superfluidity of electron-hole pairs and antiferromagnetic chromium", *Solid State Commun.*, vol. 25, 253 (1978).

[19] E. B. Sonin, "Spin currents and spin superfluidity", *Adv. Phys.*, vol. 59, 181 (2010).

[20] Y. M. Bunkov, E. M. Alakshin, R. R. Gazizulin, A. V. Klochkov, V. V. Kuzmin, V. S. L'vov, and M. S. Tagirov, "High-T_c Spin Superfluidity in Antiferromagnets", *Phys. Rev. Lett.*, 108, 177002 (2012).

[21] W. Chen and M. Sigrist, "Spin superfluidity in coplanar multiferroics", *Phys. Rev. B*, 89, 024511 (2014).

[22] S. Takei and Y. Tserkovnyak, "Superfluid Spin Transport Through Easy-Plane Ferromagnetic Insulators", *Phys. Rev. Lett.*, 112, 227201 (2014).

[23] S. Takei, B. I. Halperin, A. Yacoby, and Y. Tserkovnyak, "Superfluid spin transport through antiferromagnetic insulators", *Phys. Rev. B*, 90, 094408 (2014).

[24] H. Skarsvåg, C. Holmqvist, and A. Brataas, "Spin Superfluidity and Long-Range Transport in Thin-Film Ferromagnets", *Phys. Rev. Lett.*, 115, 237201 (2015).

[25] B. Flebus, S. A. Bender, Y. Tserkovnyak, and R. A. Duine, "Two-Fluid Theory for Spin Superfluidity in Magnetic Insulators", *Phys. Rev. Lett.*, 116, 117201 (2016).

[26] S. Takei and Y. Tserkovnyak, "Nonlocal Magnetoresistance Mediated by Spin Superfluidity", *Phys. Rev. Lett.*, 115, 156604 (2015).

[27] C. Sun, T. Nattermann, and V. L. Pokrovsky, "Unconventional Superfluidity in Yttrium Iron Garnet Films", *Phys. Rev. Lett.*, 116, 257205 (2016).

[28] L. J. Cornelissen, J. Liu, J. B. Youssef, R. A. Duine, and B. J. van Wees, "Long-distance transport of magnon spin information in a magnetic insulator at room temperature", *Nat. Phys.*, 11(12):1022-1026 (2015).

[29] T. Brächer, P. Pirro, and B. Hillebrands, "Parallel pumping for magnon spintronics: Amplification and manipulation of magnon spin currents on the micron-scale", *Phys. Rep.*, vol. 699, (2017).

[30] V E. Demidov, S. Urazhdin, A. B. Rinkevich, G. Reiss, and S. O. Demokritov, "Spin Hall controlled magnonic microwaveguides", *Appl. Phys. Lett.*, 104, 152402 (2014).

[31] V. E. Demidov, S. Urazhdin, E. R. J. Edwards, M. D. Stiles, R. D. McMichael, and S. O. Demokritov, "Control of Magnetic Fluctuations by Spin Current", *Phys. Rev. Lett.*, 107, 107204 (2011).

[32] O. Gladii, M. Collet, K. Garcia-Hernandez, C. Cheng, S. Xavier, P. Bortolotti, V. Cros, Y. Henry, J.-V. Kim, A. Anane, and M. Bailleul, "Spin wave amplification using the spin Hall effect in permalloy/platinum bilayers", *Appl. Phys. Lett.*, 108, 202407 (2016).

[33] K. An, D. R. Birt, C.-F. Pai, K. Olsson, D. C. Ralph, R. A. Buhrman, and X. Li, "Control of propagating spin waves via spin transfer torque in a metallic bilayer waveguide", *Phys. Rev. B*, 89, 140405(R) (2014).

[34] S. M. Rezende, R. L. Rodríguez-Suárez, and A. Azevedo, "Diffusive magnonic spin transport in antiferromagnetic insulators", *Phys. Rev. B*, 93, 054412 (2016).

[35] J. O. Fjærestad, *Magnetism*, (lecture note in the course "TFY4210 – Quantum Theory of Many-Particle Systems", NTNU, Trondheim, Norway, (2012). Link: http://folk.ntnu.no/johnof/magnetism-2012.pdf

[36] P. A. M. Dirac, "On the Theory of Quantum Mechanics", *Proceedings of the Royal Society of London, Series A*, 112, 762 (1926).

[37] B. D. Cullity and C. D. Graham, *Introduction to Magnetic Materials*, John Wiley Sons, Hoboken, USA, (2005).

[38] S. O. Demokritov and A. N. Slavin, *Magnonics – From Fundamentals to Applications*, Springer Verlag, Berlin / Heidelberg, Germany, (2013).

[39] J. Stöhr and H. C. Siegmann, *Magnetism From Fundamentals to Nanoscale Dynamics*, Springer, New York USA, (2006).

[40] P. Samarasekara and U. Saparamadu, "Easy axis orientation of Barium hexa-ferrite films as explained by spin reorientation.", *Georgian Electronic Scientific Journals Phys.*, 1(9), 10-15, (2013).

[41] C. Abert, L. Exl, F. Bruckner, A. Drews and D. Suess, "magnum.fe: A micromagnetic finite-element simulation code based on FEniCS.", *Journal of Magnetism and Magnetic Materials*, 345, 29-35, (2013).

[42] R. Keesman, M. Raaijmakers, A. E. Baerends, G. T. Barkema and R. A. Duine, “Skyrmions in square-lattice antiferromagnets”, *Phys. Rev. B*, vol. 94, 5, Aug. (2016).

[43] N. J. Turro, *Magnetic Interactions and Magnetic Couplings*, (lecture note in the course "Modern Molecular Photochemistry"). University of Columbia, New York, USA, (1999). Link: http://www.columbia.edu/itc/chemistry/photochem/spin/08.pdf

[44] F. Bloch, “Zur Theorie des Ferromagnetismus”, *Zeitschrift für Physik*, vol. 61, Issue 3–4, (1930).

[45] R. K. Srivastava and J. Ashok, *Chapter 7 – Statistical Mechanics*, PHI Learning Pvt. Ltd., New Delhi, India, (2005).

[46] Y. Zhang, “High wave vector spin waves in ultrathin Fe films on W(110) studied by spin-polarized electron energy loss spectroscopy”, *Martin-Luther-Universität*, Dissertation, (2008).

[47] R. M. White, *Quantum Theory of Magnetism*, 3rd ed. Springer-Verlag, Berlin, (2007).

[48] C. Timm, *Theory of Magnetism*, Technische Universität, Dresden, Germany, (2009).

[49] G. Toulouse, A. Pekalski, and J. Przystawa, (lecture notes in Physics. 115.), *Modern Trends in the Theory of Condensed Matter – The frustration model*, Springer Verlag, Berlin / Heidelberg, Germany, (1980).

[50] H. P. J. Wijn, *Ferromagnetism*, Springer-Verlag, Berlin, (1966).

[51] R. E. Troncoso, *Notes concerning AFM-condensate of magnons at finite temperature* Universidad Técnica Federico Santa María, Valparaíso, Chile (May 15, 2017).

[52] A. Griffin, T. Nikuni and E. Zaremba, *Bose-Condensed Gases at Finite Temperatures*, Cambridge University Press, New York USA, (2009).

[53] N. N. Bogoliubov, “On the theory of superfluidity”, *J. Phys. USSR*, vol. 11, 1 (1947).

[54] S. T. Beliaev, “Application of the Methods of Quantum Field Theory to a System of Bosons”, *Sov. Phys. JETP*, vol. 7, 2 (1958).

[55] S. T. Beliaev, “Energy-Spectrum of a Non-ideal Bose Gas”, *Sov. Phys. JETP*, vol. 7, 2 (1958).

[56] J. Gavoret and P. Nozières, “Structure of the perturbation expansion for the bose liquid at zero temperature”, *Ann. Phys.*, vol. 28, 3 (1964).

[57] P. C. Hohenberg and P. C. Martin, “Microscopic theory of superfluid helium”, *Ann. Phys.*, vol. 34, 2 (1965).

[58] N. N. Bogoliubov, Lectures on Quantum Statistics, Gordon and Breach, New York, (1970).

[59] K. Huang, *Statistical Mechanics*, 2nd ed., J. Wiley, New York, (1987).

[60] L. Boltzmann, *Wissenschaftliche Abhandlungen*, vol.II, F. Hasenöhrl, Leipzig, (1909).

[61] E. P. Gross, "Structure of a quantized vortex in boson systems", *Il Nuovo Cimento*, vol. 20, 3 (1961).

[62] L. P. Pitaevskii, "Vortex Lines in an Imperfect Bose Gas", *Sov. Phys. JETP*, vol. 13, 2 (1961).

[63] J. Rogel-Salazar, "The Gross-Pitaevskii Equation and Bose-Einstein condensates", *ArXiv e-prints* (2013), arXiv:1301.2073v1 [cond-mat.quant-gas].

[64] O. Dzyapko, I. Lisenkov, P. Nowik-Boltyk, V. E. Demidov, S. O. Demokritov, B. Koene, A. Kirilyuk, T. Rasing, V. Tiberevich and A. Slavin, "Magnon-magnon interactions in a room-temperature magnonic Bose-Einstein condensate", *Phys. Rev. B*, 96, 064438 (2017).

[65] O. Dzyapko, "Magnon Kinetics in Quasi-Equilibrium under Parametric Pumping Leading to Bose-Einstein Condensation", *Westfälische Wilhelms-Universität (WWU)*, Abschlussarbeit, (2010).

[66] S. Giorgini, L. P. Pitaevskii and S. Stringari, "Thermodynamics of a Trapped Bose-Condensed Gas", *J. Low. Temp. Phys.*, vol. 109, 1-2, (1997).

[67] E. Zaremba, T. Nikuni and A. Griffin, "Two-Fluid Hydrodynamics in Trapped Bose Gases and in Superfluid Helium", *J. Low Temp. Phys.*, 116, 227 (1999).

[68] R. A. Duine, A. Brataas, S. A. Bender and Y. Tserkovnyak, "Spintronics and Magnon Bose-Einstein Condensation", *ArXiv e-prints* (2015), arXiv:1505.01329v1 [cond-mat.mes-hall].

[69] N. P. Proukakis, K. Burnett and H. T. C. Stoof, "Microscopic treatment of binary interactions in the nonequilibrium dynamics of partially Bose-condensed trapped gases", *Phys. Rev. A*, 57, 1230 (1998).

[70] H. T. C. Stoof, "Coherent versus incoherent dynamics during Bose-Einstein condensation in atomic gases", *J. Low. Temp. Phys.*, 114, 1-2 (1999).

[71] R. Walser, J. Williams, J. Cooper and M. Holland, "A Kinetic Theory of a Weakly Interacting Bosonic Gas", *Phys. Rev. A.*, vol. 59, 3878 (1999).

[72] T. R. Kirkpatrick and J. R. Dorfman, "Transport coefficients in a dilute but condensed Bose gas", *Low Temp. Phys.*, 58, 301; 58, 399 (1985).

[73] L. P. Kadanoff and G. Baym, *Quantum Statistical Mechanics*, W. A. Benjamin, New York, (1962).

[74] J. Barak, S. M. Rezende, A. R. King and V. Jaccarino, "Parallel-pumping studies of magnon damping in $\mathrm{MnF_2}$", *Phys. Rev. B*, vol. 21, Nr. 7, (1980).

[75] J. Barak, V. Jaccarino and S. M. Rezende, "The magnetic anisotropy of MnF_2 at 0K", *Journal of Magnetism and Magnetic Materials*, 9, 323-332, (1978).

[76] O. Nikotin, P. A. Lindgård and O. W. Dietrich, "Magnon dispersion relation and exchange interactions in MnF_2", *J. Phys. C (Solid St. Phys.)*, ser. 2, vol. 2, (1969).

[77] V. A. Mutailamov, A. K. Murtazaev and M. A. Magomedov, "Critical Properties of the Models of Small Magnetic Particles of the Antiferromagnet MnF_2", *Journal of Experimental and Theoretical Physics*, vol. 118, 6, 904-908, (2014).

[78] S. M. Rezende, R. L. Rodríguez-Suárez and A. Azevedo, "Theory of the spin Seebeck effect in antiferromagnets", *Phys. Rev. B*, 93, 014425 (2016).

[79] H. Yamazaki, "Parallel Pumping of Spin-Waves in an Orthorhombic Antiferromagnet", *Journal of the Physical Society of Japan*, vol. 32, 5, (1972).

[80] A. H. MacDonald and M. Tsoi, "Antiferromagnetic metal spintronics", *Phil. Trans. R. Soc. A*, 369, 3098 (2011).

[81] M. T. Hutchings and E. J. Samuelsen, "Measurement of Spin-Wave Dispersion in NiO by Inelastic Neutron Scattering and Its Relation to Magnetic Properties", *Phys. Rev. B*, 6, 3447, (1972).

[82] K. Persson, *The Materials Project*, (2019). [Online]. Available: https://materialsproject.org/materials/mp-715434/

[83] Q. Liu, H. Y. Yuan, K. Xia and Z. Yuan, "Mode-dependent damping in metallic antiferromagnets due to intersublattice spin pumping", *Phys. Rev. Materials*, 1, 3447, 061401(R), (2017).

[84] A. Kamra, R. E. Troncoso, W. Belzig and A. Brataas, "Gilbert damping phenomenology for two-sublattice magnets", *ArXiv e-prints* (2018), arXiv:1808.04385v2 [cond-mat.mtrl-sci].

[85] M. P. Ross, "Spin Dynamics in an Antiferromagnet", *Technische Universität München*, Diploma thesis, (2013).

[86] Z. Wang, S. Kovalev, N. Awari, M. Chen, S. Germanskiy, B. Green, J.-C. Deinert, T. Kampfrath, J. Milano and M. Gensch, "Magnetic field dependence of antiferromagnetic resonance in NiO", *Appl. Phys. Lett.*, 112, 252404 (2018).

[87] F. Pereira dos Santos, J. Léonard, J. Wang, C. J. Barrelet, F. Perales, E. Rasel, C. S. Unnikrishnan, M. Leduc and C. Cohen-Tannoudji, "Bose-Einstein condensation of metastable helium", *Phys. Rev. Lett.*, 86, 3459 (2001).

[88] S. Moal, M. Portier, J. Kim, J. Dugué, U. D. Rapol, M. Leduc and C. Cohen-Tannoudji, "Accurate Determination of the Scattering Length of Metastable Helium Atoms Using Dark Resonances between Atoms and Exotic Molecules", *Phys. Rev. Lett.*, 96, 023203 (2006).

[89] J. Achleitner, “Magnetization and magnon excitation energies of the magnetic semiconductors EuTe and EuO on the basis of the renormalized spin wave theory”, *ArXiv e-prints* (2011), arXiv:1103.1831v1 [cond-mat.mtrl-sci].

[90] M. B. Jungfleisch, W. Zhang, and A. Hoffmann, “Perspectives of antiferromagnetic spintronics”, *Physics Letters A*, vol. 382, (2018).

NTNU
Norwegian University of
Science and Technology